



UvA-DARE (Digital Academic Repository)

Homogeneous catalyzed hydrogenation : first-principles computational studies in the gas phase and in solution

Handgraaf, J-W.

Publication date

2003

Document Version

Final published version

[Link to publication](#)

Citation for published version (APA):

Handgraaf, J-W. (2003). *Homogeneous catalyzed hydrogenation : first-principles computational studies in the gas phase and in solution*.

General rights

It is not permitted to download or to forward/distribute the text or part of it without the consent of the author(s) and/or copyright holder(s), other than for strictly personal, individual use, unless the work is under an open content license (like Creative Commons).

Disclaimer/Complaints regulations

If you believe that digital publication of certain material infringes any of your rights or (privacy) interests, please let the Library know, stating your reasons. In case of a legitimate complaint, the Library will make the material inaccessible and/or remove it from the website. Please Ask the Library: <https://uba.uva.nl/en/contact>, or a letter to: Library of the University of Amsterdam, Secretariat, Singel 425, 1012 WP Amsterdam, The Netherlands. You will be contacted as soon as possible.

Homogeneous Catalyzed Hydrogenation

First-Principles Computational Studies in the Gas Phase and in Solution

ACADEMISCH PROEFSCHRIFT

ter verkrijging van de graad van doctor
aan de Universiteit van Amsterdam
op gezag van de Rector Magnificus
prof. mr. P. F. van der Heijden
ten overstaan van een door het college voor promoties ingestelde
commissie, in het openbaar te verdedigen in de Aula der Universiteit

op woensdag 29 oktober 2003, te 10.00 uur

door **Jan-Willem Handgraaf**
geboren te Alkmaar

Promotor:

- prof. dr. B. Smit

Co-promotor:

- dr. E. J. Meijer

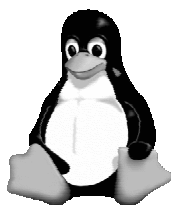
Overige leden:

- prof. dr. E. J. Baerends
- prof. dr. E. E. Drent
- prof. dr. M. Sprik
- prof. dr. P. W. N. M. van Leeuwen
- dr. J. N. H. Reek

Faculteit:

- Faculteit der Natuurwetenschappen, Wiskunde & Informatica

The research reported in this thesis was carried out at the Department of Chemical Engineering, Faculty of Science, University of Amsterdam (Nieuwe Achtergracht 166, 1018 WV, Amsterdam, The Netherlands) and at the Department of Chemistry, University of Cambridge (Lensfield Road, Cambridge, CB2 1EW, UK). Financial support was provided by NWO (Dutch Science Foundation) through PIONIER. The Dutch Foundation of Computer Facilities (NCF) is kindly acknowledged for the use of supercomputer facilities.



OpenDX

- This document was prepared using \LaTeX on a PC running Linux.
- Graphics were made with Gnuplot, gOpenMol, Grace, OpenDx and VMD.
- Printed by Ponsen & Looijen bv, Wageningen.

"A man of genius makes no mistakes; his errors are volitional and are the portals of discovery."

James Joyce (1882–1941)

Contents

1	General Introduction	1
1.1	Homogeneous Catalysis	1
1.1.1	Asymmetric Catalysis	2
1.1.2	The Role of the Solvent	8
1.2	Theory	9
1.2.1	Electronic Structure	9
1.2.2	Molecular Dynamics	11
1.2.3	The Car-Parrinello Approach	12
1.2.4	Special Techniques	13
1.3	Computer Simulations	14
1.4	Scope of this Thesis	15
2	Structural, Dynamic, and Electronic Properties of Liquid Methanol	19
2.1	Introduction	20
2.2	Methods and Validation	20
2.3	Liquid	22
2.3.1	Structure	22
2.3.2	Dynamics	23
2.3.3	Electronic properties	27
2.4	Conclusions	32
3	Iridium(I) versus Ruthenium(II): Catalyzed Transfer Hydrogenation of Ketones	33
3.1	Introduction	34
3.2	Models	34
3.3	Methods and Validation	35
3.4	Results	38
3.4.1	Catalyst Structure and Substrate Coordination	38
3.4.2	Mechanism of Transfer Hydrogenation	39
3.4.3	Iridium(I) versus Ruthenium(II)	44
3.5	Discussion	45
3.6	Summary	47
4	Ruthenium Catalyzed Transfer Hydrogenation of Ketones in Methanol Solution	49
4.1	Introduction	50
4.2	Model and Methods	51
4.3	Thermochemistry	54
4.4	Mechanism: Structural and Electronic Changes	57
4.5	Spontaneous Reaction	61
4.6	Summary and Conclusions	63

5	Directing Rhodium Catalyzed Hydrogenation via the Substrate Polarity	65
5.1	Introduction	66
5.2	Methods	68
5.3	Hydrides	68
5.4	Substrate polarity	70
5.5	Hydrometalation	70
5.6	Discussion	74
5.7	Conclusions	76
6	Concluding Remarks	77
	Bibliography	81
	Summary	89
	Samenvatting voor Iedereen	95
	Curriculum Vitae	99
	Publications	101
	Acknowledgments	103

Chapter 1

General Introduction

1.1 Homogeneous Catalysis

The Oxford Advanced Learner's Dictionary of Current English translates homogeneous to "formed of parts of the same kind" and heterogeneous to "made up of different kinds". In the language of chemistry this means in one phase and in two or more phases, respectively. In living matter essentially all chemical processes take place in an aqueous surrounding and are thus homogeneous in nature. Due to the high level of complexity of these usually coupled processes, or cascades, we are far from detailed understanding of all the molecular transformations that occur in living matter. Even more so with heterogeneous systems, *viz.* industrial plants, where only after tedious optimization of all regulating factors using pilot plants, one obtains a profitable and properly operating system.

The same dictionary translates catalysis to "the process of aiding or speeding up a chemical process by a substance that does not itself undergo any change". A more chemically sane definition is found at www.catalysis.org: "an acceleration of the rate of a process or reaction, brought about by a catalyst, usually present in small managed quantities and unaffected at the end of the reaction. A catalyst permits reactions or processes to take place more effectively or under milder conditions than would otherwise be possible". Again, in living matter all most all chemical transformations are catalyzed, in this case by enzymes. These transformations can be very precise in terms of chemoselectivity, regioselectivity, and even stereoselectivity. Moreover, they take place at room temperature and at ambient pressure. On the contrary, chemical transformations in laboratory or industry predominantly require elevated temperatures and high pressures, and are certainly not as selective as the transformations in living matter. Here, one should keep in mind that nature had four billion years to optimize processes via natural selection, while chemistry had only the last couple of hundred years at its disposal. It is clear that in this period science has made substantial progress, but before it will arrive at the level of nature, still a tremendous amount of work has to be done.

Transition metals play a crucial role in homogeneous catalysis, both in biological and chemical processes. A 2002 survey of the Periodic Table of Elements by Fluck and Heumann [1] reported that manganese (Mn), iron (Fe), copper (Cu), zinc (Zn) and molybdenum (Mo) are essential to humans, and that vanadium (V), chromium (Cr), cobalt (Co), and nickel (Ni) are essential to at least one biological species. In chemistry also a wide variety of transition metals are used. Especially, the late transition metals, such as ruthenium (Ru), rhodium (Rh), palladium (Pd), iridium (Ir) and platinum (Pt), are particularly suited to perform homogeneous catalyzed reactions.

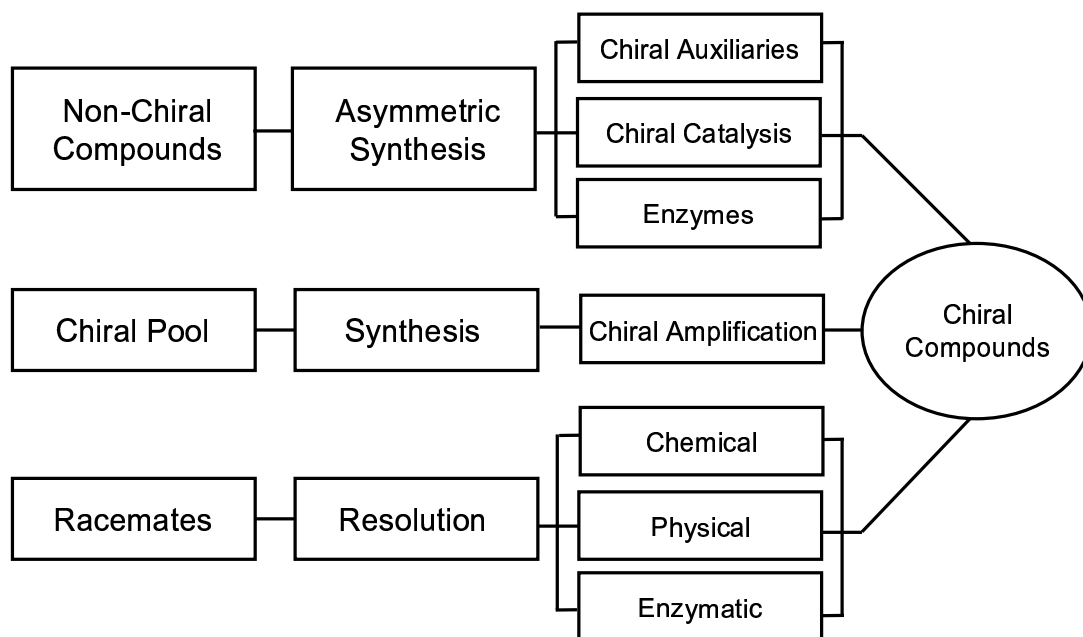


Figure 1.1: Methods for producing chiral compounds.

1.1.1 Asymmetric Catalysis

One of the most important applications of homogeneous catalysis is the synthesis of homochiral compounds. Synthetic chemists have discovered over the years a variety of methods to synthesize optically pure compounds. There are three basic routes for the production of homochiral compounds (Fig. 1.1). Starting from racemates, the use of chiral resolving agents is the simplest route. However, in many cases more than 50% of the product will be wasted [2]. Another route is to use a chiral pool of starting materials. A problem with this method is that often quite a number of chemical transformations are necessary to get useful starting materials. The most ambitious technique is to synthesize homochiral compounds from non-chiral starting materials using asymmetric synthesis, which has extensively been applied in both laboratory and industry over the past two decades [3,4]. However, only after an often time-demanding empirical screening of chiral ligands in combination with the right choice of substrate, one obtains a high enantiomeric excess (e.e.), see *e.g.* Ref. [5]. Since the introduction of combinatorial chemistry several thousand ligands can be screened simultaneously. Although this technique can be very effective in obtaining high-quality and selective catalysts, a detailed understanding of asymmetric catalysis is of fundamental interest and a prerequisite for rational improvement.

Catalytic Hydrogenation

Hydrogenation reactions are of the utmost importance in all fields of chemistry, where they are used to reduce unsaturated compounds. Also in biological processes numerous examples exist of reactions involving hydrogen. Probably the most well-known is the interconversion of nicotinamide adenine dinucleotide (NAD^+) to the complementary reduced compound (NADH H^+), that in turn boosts the energy production in a living cell.

In the mid-sixties of the last century Osborn and Wilkinson discovered the rhodium complex $[\text{Rh}(\text{PPh}_3)_3\text{Cl}]$, which was able to catalytically hydrogenate unhindered alkenes in solution

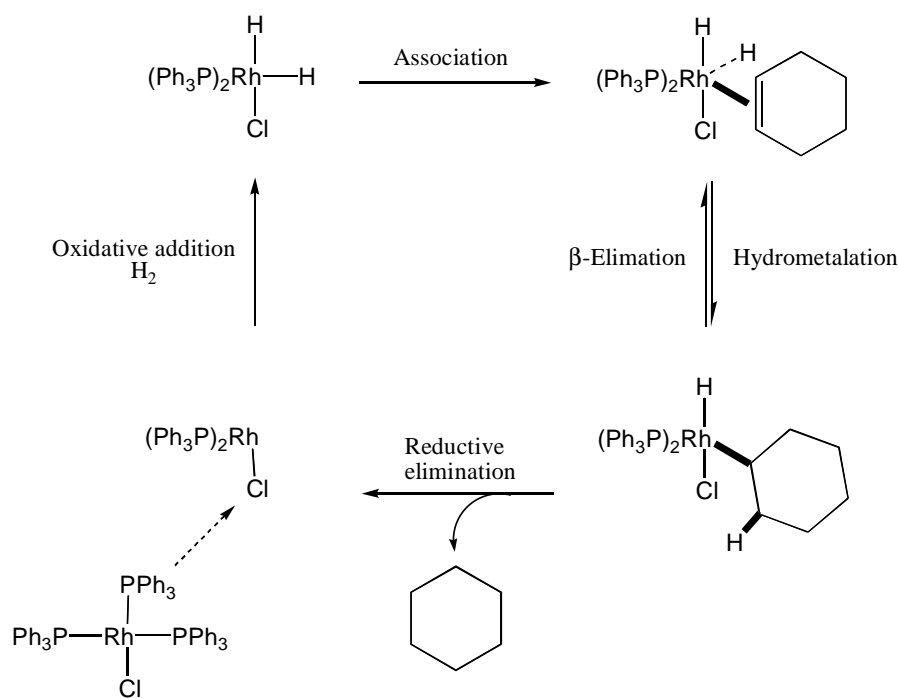


Figure 1.2: Proposed elementary steps in the Rh-catalyzed homogeneous hydrogenation of a non-functionalized alkene (dihydride route).

using molecular hydrogen [6]. However, it was not known whether catalytic asymmetric hydrogenation was feasible. A breakthrough came in 1968 when Knowles* showed that a chiral catalyst, based on this rhodium complex, could transfer chirality to a non-chiral substrate resulting in a chiral product with one of the enantiomers in excess [8]. Based on this earlier work Knowles and coworkers developed in 1974 an industrial synthesis of the rare amino acid L-DOPA which had proved useful in the treatment of Parkinson's disease.

One of the earlier attempts to study in detail the mechanism of transition metal catalyzed hydrogenation reactions was done in the 70s and 80s by Halpern and coworkers [9–11]. They proposed a generic catalytic cycle involving four elementary steps, cf. Fig. 1.2. In first instance the 16-electron $[\text{Rh}(\text{PPh}_3)_3\text{Cl}]$ complex, *i.e.* the precursor, loses one PPh_3 (triphenylphosphine) ligand. The resulting 14-electron coordinatively unsaturated $[\text{Rh}(\text{PPh}_3)_2\text{Cl}]$ complex activates H_2 via oxidative addition. The formed 16-electron hydrogenated complex is still coordinatively unsaturated and therefore is able to activate an alkene in a similar manner as H_2 . The intramolecular insertion of the metal-bound hydride to the coordinating alkene (hydrometalation) is the key step and leads to the formation of the metal-alkyl complex. Since this hydrometalation step is also the rate-limiting step, the mechanism is assigned to the so-called "dihydride route" [10, 12].

In the case of functionalized alkenes the mechanism can differ from the one depicted in Fig. 1.2. The pioneering work in this field was also done by Halpern and coworkers who studied the mechanism of a model reaction in which the Rh-catalyzed hydrogenation of an enamide

*Recipient of the 2001 Nobel Prize in Chemistry, see his Nobel lecture [7].

yields a phenylalanine derivative [13]. Based on the characterization of the catalyst-substrate adduct in the hydrogenation of the enamide using 1,2-bis(diphenylphosphino-ethane)rhodium as catalyst [14] an "unsaturated route" (Fig. 1.3) was put forward by Halpern [11]. Here, solvent molecules, *S*, in the catalyst precursor are displaced by the enamide to form a chelate-Rh complex in which the olefinic bond and the carbonyl oxygen interact with the Rh center. Hence, contrary to the dihydride route, the unsaturated route involves the coordination of the functionalized alkene as a bidentate ligand, *prior* to oxidative addition of molecular hydrogen. This mechanism was both verified by kinetic experiments [15] and more recently by density-functional-theory (DFT) based calculations [16]. Furthermore, Halpern and coworkers investigated the origin of the stereoselectivity of the Rh-catalyzed hydrogenation of this pro-chiral enamide [10, 11, 14, 15]. Based on the unsaturated route (Fig. 1.3) they proposed a mechanism where the absolute stereoselectivity is controlled when the pro-chiral enamide binds to the square-planar Rh-complex to give a mixture of two diastereomers, cf. Fig. 1.4. The two diastereomers are in rapid equilibrium in solution. Subsequent oxidative addition of molecular hydrogen fixes then the stereochemistry. Although one of the diastereomers is more stable in solution (major) its barrier for oxidative addition of molecular hydrogen is higher, and hence, the less stable diastereomer (minor) gives the preferred chiral product. In this way they could explain the origin of the stereoselectivity via the unsaturated route. This was recently verified by the DFT calculations of Landis and Feldgus [17]. Moreover, using the unsaturated route, they could also explain the unusual enantioreversing effect of the α -substituent of the enamide [18]. This effect, experimentally found by Burk *et al.* [19], is the complete reversal of the enantioselection if the α -substituent is changed from carboxyl (*i.e.* the COOMe-group in Fig. 1.4) to *tert*-butyl. However, in contradiction to the results of Landis and Feldgus, Gridnev *et al.* [20, 21] showed that this dramatic effect in enantioselection could also be explained via the dihydride route.

In recent years the low-temperature NMR studies of Brown and coworkers [22–24] and Gridnev and coworkers [20, 21, 25, 26] showed that a Rh dihydride complex is stable in solution and can be used to directly hydrogenate substrates. These experiments also showed that the discrimination between the dihydride and the unsaturated route is very subtle, and possibly both routes are accessible during the catalytic hydrogenation.

A drawback of catalytic hydrogenation is the use of molecular hydrogen as hydrogen source. This often requires high hydrogen pressures and dedicated equipment in order to keep a sufficient concentration of molecular hydrogen in solution. A way to circumvent this is to use an alternative hydrogen source as discussed in the next section.

Transfer Hydrogenation

Saturation of olefinic and carbonyl double bonds may be achieved by using various hydrogen donors other than molecular hydrogen. Common hydrogen donors are 2-propanol and an azeotropic mixture of formic acid and triethylamine [27]. Fig. 1.5 shows schematically the mechanism of transition metal catalyzed transfer hydrogenation. The 16-electron metal complex is generated from a catalyst precursor, usually the corresponding metal halide, using a strong inorganic base. This 16-electron metal complex reacts with the solvent (hydrogen donor), giving the 18-electron metal-hydride complex, which in turn reacts with the unsaturated substrate (hydrogen acceptor). During the reaction the hydrogen donor is oxidized and the substrate is reduced. As denoted by the double arrows, the transfer hydrogenation is an equilibrium reaction which in certain cases can lead to an unfavorable conversion of the substrate. This can be remedied by using a large excess of the hydrogen donor, or by removing the oxidized by-product. Since dehydrogenation of formic acid is an irreversible and exothermic process, this usually overwhelms

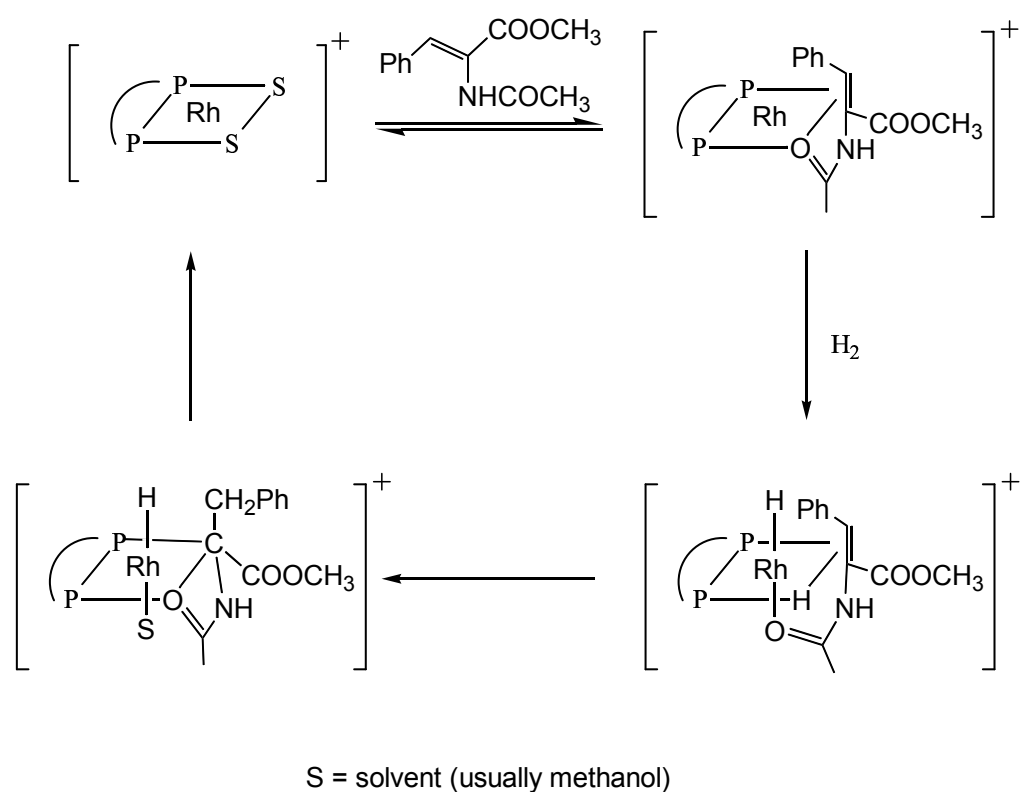


Figure 1.3: Mechanism of Rh-catalyzed homogeneous hydrogenation of an enamide (unsaturated route).

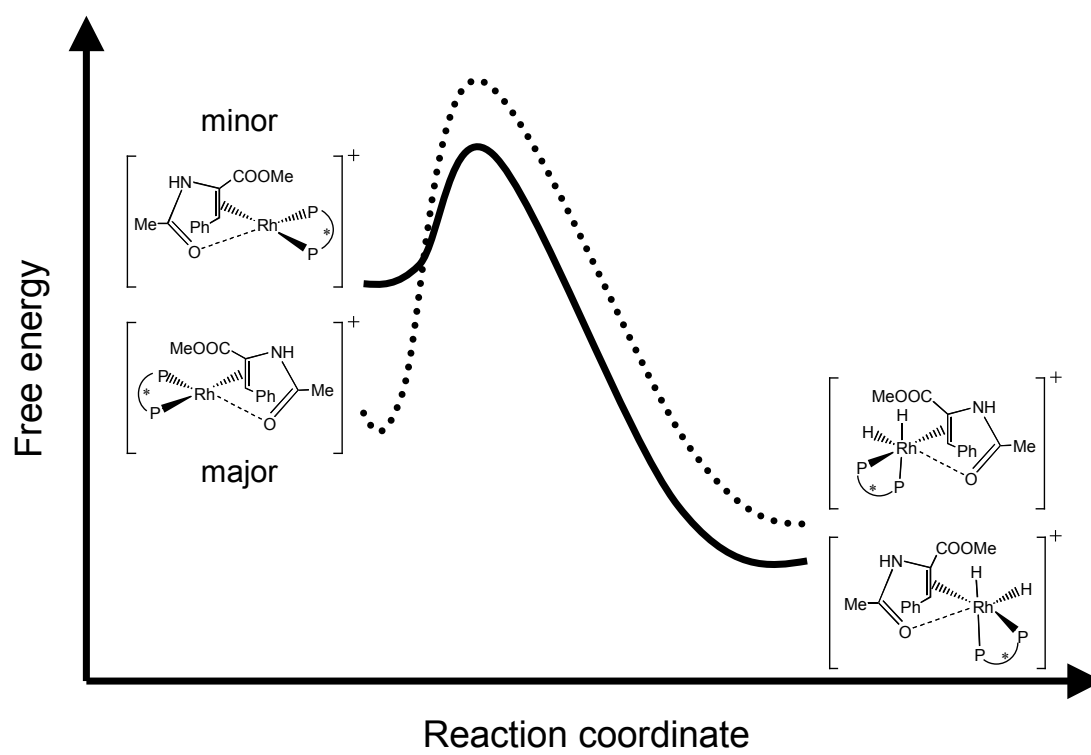


Figure 1.4: Proposed reaction profile of the two Rh-dihydride diastereomer intermediates.

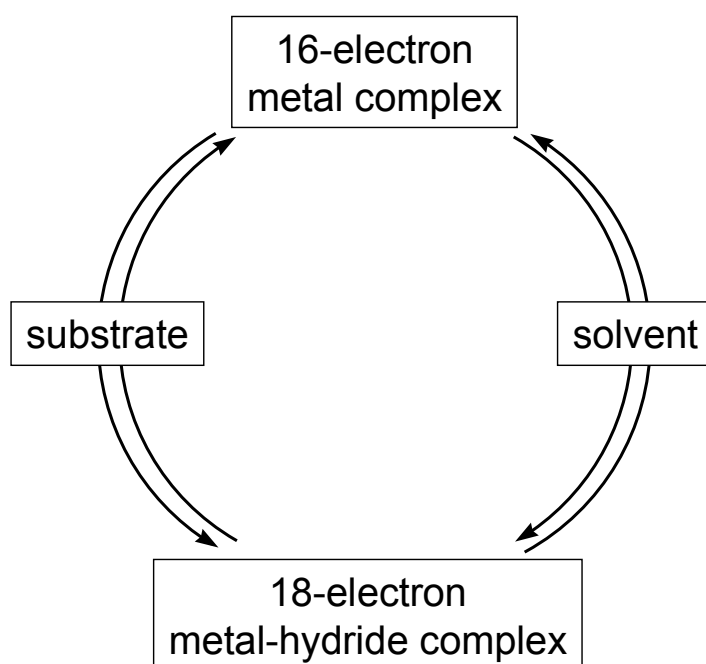


Figure 1.5: Schematic representation of the mechanism of transition metal catalyzed transfer hydrogenation.

the energetic requirement of the reduction process, and should only be used when unfavorable energetic balances are expected [27]. Overall, the use of a hydrogen source other than molecular hydrogen is experimentally much more convenient as it can be operated at room temperature and ambient pressures.

In recent years a lot of research has been devoted to the elucidation of the mechanism of the transition metal catalyzed transfer hydrogenation. In this field, Noyori[†] coworkers performed ground-breaking research with their detailed study of the Ru-catalyzed transfer hydrogenation of pro-chiral ketones [29]. Mechanistically, the metal-catalyzed transfer hydrogenation can be divided in three main categories, see Fig. 1.6. Besides the direct transfer of an α -hydrogen of a solvent alcohol molecule to the carbonyl carbon of a ketone (Meerwein-Ponndorf-Verley reduction [30]) and the migratory insertion of a coordinated ketone into a metal-hydride bond, Noyori and coworkers proposed a novel mechanism where a proton of the ligand and the metal-bound hydride are transferred simultaneously to the ketone [5], *i.e.* a metal-ligand bifunctional mechanism [29]. From DFT computational studies [31–33] it is now well-established that for the Ru-catalyzed transfer hydrogenation of ketones using an aminoalcohol ligand this mechanism is energetically favorable over the other mechanisms. There is also evidence that for the Rh-catalyzed transfer hydrogenation this is the preferred mechanistic pathway [34]. However, these computational studies were performed in the gas phase. One can imagine that the solvent plays an important role in the homogeneous metal-catalyzed hydrogenations reactions, as will be shown in the following section.

[†]Recipient of the 2001 Nobel Prize in Chemistry, see his Nobel lecture [28].

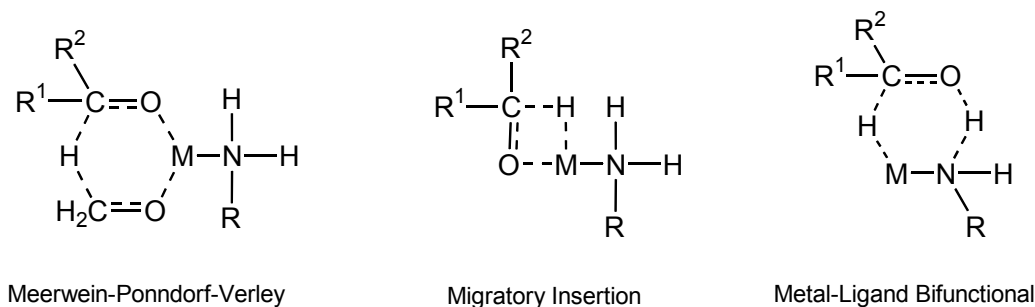


Figure 1.6: Three different mechanistic alternatives for metal-catalyzed transfer hydrogenation.

Table 1.1: Rhodium-catalyzed hydrogenation of ethyl-2-(benzoyloxy)crotonate in different solvents, taken from Ref. [35].

solvent	conversion	% e.e.
MeOH	100	97.0
2-PrOH	100	99.3
CF ₃ CH ₂ OH	60	98.0
EtOAc	60	90.0
THF	80	96.5
C ₆ H ₆	0	-
CH ₂ Cl ₂	100	99.8

1.1.2 The Role of the Solvent

As an example, Table 1.1 shows the conversion and e.e. of the Rh-catalyzed hydrogenation of a pro-chiral α -(acyloxy)acrylate in different solvents [35]. As shown, high enantioselectivities can be obtained in all solvents, except for ethyl acetate. In contrast, the relative reaction rates are significantly affected by the solvent type. Complete conversions are obtained for the small polar protic solvents methanol and 2-propanol, whereas for the more acidic 1,1,1-trifluoroethanol the conversion is reduced to 60%. The polar aprotic solvents ethyl acetate and tetrahydrofuran also give reduced conversions. The reaction is even inhibited if benzene is used as solvent, caused by the formation of an inactive benzene-catalyst adduct. From this example it is evident that a solvent should not be considered as a macroscopic continuum characterized only by physical constants such as density, dielectric constant, index of refraction *etc.*, but as a discontinuum consisting of individual, mutually interacting solvent molecules. This certainly holds for the hydrogen-bonding solvents commonly used in hydrogenation reactions, since molecules in these solvents have the tendency to form strong hydrogen bonds with the catalyst and substrate.

The transfer hydrogenation is commonly conducted in small polar protic solvents. Noyori and Hashiguchi showed that formic acid gives in general higher conversions than 2-propanol [5], although as mentioned before, dehydrogenation of formic acid is highly exothermic which possibly leads to an unfavorable energy balance. This makes 2-propanol the solvent of choice. In addition, according to their relative oxidation potentials, secondary alcohols are better hydrogen

donors than primary ones [27].

Most reactions are done in solution, and it is therefore important to recognize some of the ways in which a solvent can affect the course and rates of reactions. Fortunately, it is possible to study the effect of the solvent in a quantitative way by performing "experiments" with the computer. The theory we need to study reactions in solution with the computer is described in the next sections.

1.2 Theory

In order to investigate the structure, energetics and dynamics of transition metal catalyzed reactions in solution with computational methods we need an accurate description of the electronic structure including those of the chemical transformations. For the nuclear motions we will see that molecular dynamics (MD) or Monte Carlo (MC) techniques are sufficient as long as the forces acting on the nuclei are obtained from electronic structure calculations. In essence, we need a theory that does not rely on empirically, predetermined interactions such as in classical force fields, but one which computes the interactions directly from first principles.

1.2.1 Electronic Structure

At the beginning of the twentieth century, experimental evidence suggested that atomic particles were also wave-like in nature. For example, electrons were found to give diffraction patterns when passed through a double slit in a way similar to light waves. Therefore, it was reasonable to assume that a wave equation could explain this strange behavior of atomic particles. To this end Schrödinger postulated in 1926 the following equation

$$\mathcal{H}\Psi = E\Psi, \quad (1.1)$$

where \mathcal{H} is the Hamiltonian of a given system, Ψ the corresponding wavefunction representing the state of the electrons and nuclei, and E the energy. Although in principle there exists an exact solution to this equation, in a practical calculation it is very difficult to obtain. The reason for this is the inherent complicated, many-body nature of the wavefunction that depends on all electronic and nuclear degrees of freedom. As the electronic mass is much smaller than that of the nuclei one can assume the electrons to respond instantaneously to the displacement of the nuclei. This allows to decouple the electronic and nuclear system (Born-Oppenheimer approximation [36]) and if one in addition considers the nuclei to be classical particles one can describe the system by the Schrödinger equation for the electrons only with the nuclei giving an external field depending of their fixed positions. As an additional assumption one can neglect electronic excitations and consider only the electronic ground state. In general this approximate approach provides an accurate description for many chemical reaction processes. However, while a classical nuclei/ground-state Born-Oppenheimer approximation simplifies the computational effort considerably, it is still a formidable challenge to obtain accurate solutions to Eq. 1.1. For an overview of the different approaches see *e.g.* Ref. [37].

In 1964 Hohenberg and Kohn[‡] revolutionized the field of quantum mechanics by proving that there exists a universal functional, only depending on the density of a system, from which in principle all ground-state properties of the system can be known [38]. In the following we restrict ourselves to a system of electrons. Hohenberg and Kohn defined this universal functional as

$$E_{\text{HK}}[\rho] \equiv \langle \Phi | \mathcal{H}_e | \Phi \rangle, \quad (1.2)$$

[‡]Recipient of the 1998 Nobel Prize in Chemistry.

where \mathcal{H}_e is the Hamiltonian of the electronic system and Φ the corresponding electronic wavefunction. For a given external potential $v(\mathbf{r})$ the energy functional of the system is then defined as

$$E_v[\rho] = \int v(\mathbf{r})\rho(\mathbf{r})d\mathbf{r} + F_{\text{HK}}[\rho], \quad (1.3)$$

and $F_{\text{HK}}[\rho]$ as

$$F_{\text{HK}}[\rho] = T[\rho] + V_{ee}[\rho], \quad (1.4)$$

where $T[\rho]$ is the kinetic-energy functional and $V_{ee}[\rho]$ is the functional of the electronic interaction energy. For the ground-state $\rho(\mathbf{r})$ Hohenberg and Kohn showed that $E_v[\rho]$ is the exact ground-state energy E_0 . In practice, the major benefit of this theory is that *not* the Schrödinger equation with the unknown wavefunction has to be solved, but just an equation containing a functional depending on the density, which in itself depends only on three spatial coordinates. However, all difficulty is now shifted towards the functionals which only known to an approximate level [39].

Kohn and Sham [40] invented an ingenious indirect approach to the kinetic-energy functional $T[\rho]$. Thereby they turned density functional theory into a practical tool for rigorous calculations. With the introduction of one-electron orbitals they defined the kinetic-energy functional as

$$T_s[\rho] = \sum_{i=1}^N \langle \psi_i | -\frac{1}{2} \nabla^2 | \psi_i \rangle, \quad (1.5)$$

where N is the number of electrons, s denotes the spin dependency, and the density ρ is obtained as the sum of the densities of the one-electron orbitals:

$$\rho(\mathbf{r}) = \sum_{i=1}^N \sum_s |\psi_i(\mathbf{r}, s)|^2. \quad (1.6)$$

Although $T_s[\rho]$ is not equal to the exact $T[\rho]$, in most cases it will approach $T[\rho]$ to a high accuracy [39]. The complete functional in the Kohn-Sham approach is given as

$$F_{\text{KS}}[\rho] = T_s[\rho] + J[\rho] + E_{\text{XC}}[\rho], \quad (1.7)$$

where the electronic interaction energy $V_{ee}[\rho]$ is split up in a classical Coulomb term $J[\rho]$ and a non-classical *exchange-correlation* term E_{XC} , containing all the quantum effects. Note that E_{XC} also contains the small difference between $T[\rho]$ and $T_s[\rho]$. Unfortunately, E_{XC} is unknown and has to be approximated. In the last 15 years a whole range of good approximations to E_{XC} have been developed [41]. We will return to this shortly. Solutions to the ground-state energy problem can be obtained by solving the N independent one-electron equations

$$[-\frac{1}{2} \nabla^2 + v_{\text{eff}}(\mathbf{r})] \psi_i = \epsilon_i \psi_i \quad (1.8)$$

where $v_{\text{eff}}(\mathbf{r})$ is the Kohn-Sham effective potential defined as

$$v_{\text{eff}}(\mathbf{r}) = v(\mathbf{r}) + \int \frac{\rho(\mathbf{r}')}{|\mathbf{r} - \mathbf{r}'|} + \frac{\delta E_{\text{XC}}[\rho]}{\delta \rho(\mathbf{r})}. \quad (1.9)$$

Since $v_{\text{eff}}(\mathbf{r})$ depends on $\rho(\mathbf{r})$ Eqs. 1.8 and 1.6 have to be solved self-consistently. One begins with a guessed $\rho(\mathbf{r})$, constructs $v_{\text{eff}}(\mathbf{r})$ from Eq. 1.9, and then finds a new $\rho(\mathbf{r})$ from Eqs. 1.8 and

1.6. It is stressed that these equations apply to a system of *non-interacting* electrons moving in the effective potential.

The first attempts to approximate E_{XC} were based on the local density approximation (LDA). In this approximation the results obtained by accurate numerical calculation of the homogeneous electron gas are used as input. Although LDA works quite well for bulk and surface properties in solid-state physics, it fails to accurately describe chemical properties for which an accuracy of 1-2 kcal/mol is needed. This prompted the development of new exchange-correlation functionals that not only depend on the density (Eq. 1.9), but also on the *gradient* of the density, the so-called generalized gradient-corrected functionals. Nowadays, a whole range of these type of functionals exist [41]. The most commonly used are Becke's gradient correction to the exchange [42], the Lee-Yang-Parr correction to the correlation [43], and the Perdew-Wang corrections to the exchange and correlation [44]. Also the so-called hybrid functionals [41], which mix in exact Hartree-Fock exchange, are becoming more and more popular. The choice of functional is highly dependent on the property or system under study [45,46], and no functional is perfect in all cases. Hence, the development and improvement of exchange-correlation functionals remains the focus of much current research.

1.2.2 Molecular Dynamics

Now that we have established a first-principles theory to describe the electronic structure, we have to go one step further, and let the nuclei[§] move in time. Molecular dynamics is a simulation technique that is particularly well-suited to perform this task [47,48]. Here, the motion of the nuclei is determined using a finite-time step propagation of Newton's equation of motion. This is of course only valid as long as the electronic subsystem remains in the ground state, *i.e.* there is no overlap between the electronic and nuclear energy spectrum.

The most expensive (*i.e.* time-consuming) part of almost all molecular dynamics simulations is the computations of the forces on the nuclei, and since in our case we use a first-principles method to describe the internuclear interactions, this is by far the most expensive part. In molecular dynamics the force on a particle is simply the gradient of the energy with respect to its position. Hence, when using Kohn-Sham formulation of density functional theory, the force on nucleus I can be given as

$$\mathbf{F}_I = -\nabla_I \min \{E_v(\rho)\}. \quad (1.10)$$

Here 'min' denotes that we have to take the minimum of the energy functional with respect to a set of one-electron orbitals $\{\psi_i\}$. In addition, these orbitals are constrained to remain orthonormal. The orthonormality ensures that the total electronic wavefunction, Φ , remains a single Slater determinant. In this way, the electronic structure minimization problem (wavefunction optimization) is solved every time step, using for example Eqs. 1.6 and 1.8, for a fixed set of nuclear positions, *i.e.*. This is referred to as Born-Oppenheimer molecular dynamics.

At the heart of every molecular dynamics program lies the algorithm which integrates Newton's equations of motion. Quite a number of different algorithms exist in the literature [48]. Since Newton's equations of motion are time reversible, also the algorithm we choose should be. An algorithm that is time reversible and often used is the velocity Verlet algorithm [49]. In this algorithm the position of a nucleus \mathbf{R}_I is updated as

$$\mathbf{R}_I(t + \Delta t) = \mathbf{R}_I(t) + \mathbf{v}_I(t)\Delta t + \frac{\mathbf{F}_I(t)}{2M_I}\Delta t^2, \quad (1.11)$$

[§]In a classical force-field simulation the nuclei are the atoms.

and its velocity \mathbf{v}_I as

$$\mathbf{v}_I(t + \Delta t) = \mathbf{v}_I(t) + \frac{\mathbf{F}_I(t + \Delta t) + \mathbf{F}_I(t)}{2M_I} \Delta t. \quad (1.12)$$

Note that in this algorithm the new velocities are computed only after the new positions are computed and, from these, the new forces. A crucial parameter is the time step Δt which should be small enough in order not to cause a drift in the total energy that is a constant of motion. However, it should also be as large as possible in order to speed up the calculation. In addition, one should also keep in mind that Born-Oppenheimer molecular dynamics requires a rather high convergence on the wavefunction optimization in order to conserve the total energy [50].

1.2.3 The Car-Parrinello Approach

At the beginning of the 1980s there were no computational resources to perform Born-Oppenheimer molecular dynamics, hence there was an urgent need for a computationally less expensive way to perform first-principles molecular dynamics simulations. In 1985 Car and Parrinello published a letter where they presented a scheme in which molecular dynamics is unified with density functional theory in a very efficient way [51]. According to a 2003 survey of the "Web of Science" this letter has been cited almost 3000(!) times. Their basic idea was to introduce a fictitious dynamics for the electrons. To this end they postulated the following type of Lagrangian's

$$\mathcal{L}_{CP} = \sum_I \frac{1}{2} M_I \dot{\mathbf{R}}_I^2 + \sum_i \frac{1}{2} \mu \langle \dot{\psi}_i | \dot{\psi}_i \rangle - E_v(\rho) + \sum_{i,j} \Lambda_{ij} (\langle \psi_i | \psi_j \rangle - \delta_{ij}). \quad (1.13)$$

Here μ is the fictitious mass associated with the orbital degrees of freedom. The latter constitute the coefficients of the plane-wave[¶] basis set used to describe the Kohn-Sham orbitals. The corresponding equations of motions are defined as

$$M_I \ddot{\mathbf{R}}_I = -\nabla_I \{E_v(\rho)\} \quad (1.14)$$

$$\mu \ddot{\psi}_i = -\mathcal{H}_e \psi_i + \sum_j \Lambda_{ij} \psi_j. \quad (1.15)$$

In Eq. 1.14 there is no need to minimize the total electronic energy. This is a great advantage over Born-Oppenheimer dynamics and, depending on the system under study, speeds up the calculation by a factor of roughly ten [50]. Note that in Eq. 1.15 an additional fictitious kinetic energy term appears, associated with the orbital degrees of freedom.

The Car-Parrinello approach yields an accurate approximation of the nuclear trajectory in the Born-Oppenheimer approximation. This is caused by the fact that the electronic and nuclear dynamics are decoupled due to a non-overlapping frequency spectrum. This ensures that the electronic kinetic energy remains approximately constant. As the total energy is a constant of motion, this in turn implies that the total energy minus the electronic kinetic energy, *i.e.* the sum of the electronic energy $E_v(\rho)$ and the nuclei kinetic energy, is an approximate constant of motion as is required for the true nuclear trajectory. This adiabaticity can be tuned by choosing the electronic mass μ properly as to set the electronic frequency spectrum.

[¶]For an explanation of plane waves see the next section.

1.2.4 Special Techniques

Here we discuss briefly some techniques that we need to perform a first-principles simulations. As we want to study a reaction in solution, we have to mimic the solvent as best as possible. In principle, we could take the system large as possible to reduce surface effects. However this is computationally far too demanding. A way to circumvent these problems is to use periodic boundary conditions. This is done by taking a computationally feasible simulation box and implicitly copy it in all directions to infinity. In this way we are able to simulate a solvent, albeit approximately. However, experience has shown that with already 32 solvent molecules using the periodic boundary conditions, one is able to simulate the first and a large part of the second solvation shell of small solutes accurately, see *e.g.* Refs. [52–54].

As indicated previously we are able to describe the total wavefunction of the system by introducing the one-electron orbitals $\{\psi_i\}$. However, we are still not there, since it is not *a priori* known what these orbitals look like, hence we have to expand them in some sort of basis functions. In general a linear combination of simple analytic functions

$$\psi_i(\mathbf{r}) = \sum_{\nu} c_{i\nu} f_{\nu}(\mathbf{r}; \{\mathbf{R}_i\}) \quad (1.16)$$

is used. In addition, these functions should also describe the periodicity of the system. This naturally suggests to use plane waves as the generic basis set in order to expand the periodic part of the orbitals. Plane waves are defined as

$$f_{\mathbf{G}}^{\text{PW}}(\mathbf{r}) = N e^{i\mathbf{G}\mathbf{r}}, \quad (1.17)$$

where the normalization is simply given by $N = 1/\sqrt{\Omega}$ and \mathbf{G} denotes a vector in reciprocal space that satisfies the specific periodic boundary conditions; Ω is the volume of the periodically repeated box. The quality of the basis set is directly related to the number of \mathbf{G} -vectors that are included. Hence, larger basis sets will give more accurate results, but will also make the simulation more expensive. In practice, the size of the basis set is chosen so as to converge structural properties and binding energies within a certain small value.

Nowadays, it is still computationally very demanding to perform first-principles simulations. For a typical system of 32 methanol molecules one would have to solve the electronic structure problem for a system of 576 electrons every molecular dynamics time step. A particular problem appearing when using a plane-wave expansion of the Kohn-Sham orbitals is related to the oscillating structure of the core electronic states. Describing these states accurately requires a large plane-wave basis set. Fortunately this can be circumvented by exploiting the fact that the electrons in the core region can be considered chemically inert. Only the valence electrons are chemically active. When using atomic pseudopotentials [55–57] the presence of the core-electrons is incorporated in a modified electron-nucleus potential, and only the valence electrons are explicitly accounted for. The pseudopotentials are constructed such that they reproduce the all-electron electronic structure outside the core region. The reduction of number of electronic states in the pseudopotential scheme comes with the complication that it requires separate potentials for different angular momenta of the valence electrons. To exemplify things the valence ($l = 0$) all-electron- and pseudowavefunction of the gold atom are shown in Fig. 1.7. The wiggles in the core region of the all-electron wavefunction are clearly visible and from a certain value, that defines the core radius, the pseudowavefunction is equal to the all-electron wavefunction. This is of course required as we want a correct description of the valence states of the atom. Since for the pseudowavefunction the core wiggles are absent a smaller plane-wave basis set can be used. In general, the generated atomic pseudopotentials should be tested thoroughly for the specific conditions of the system under consideration, before a large scale calculation is started.

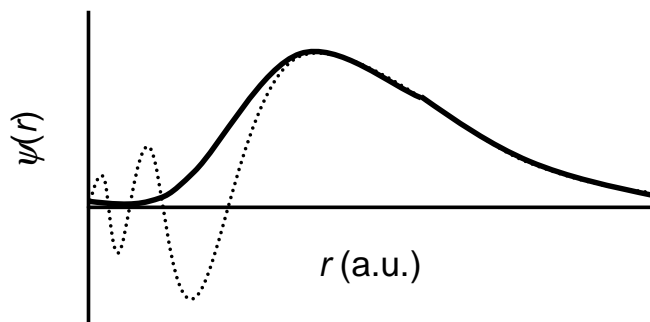


Figure 1.7: Valence wavefunction ($l = 0$) for the gold atom. Dashed curve corresponds to the all-electron atom and the solid curve to the pseudo atom. Taken from Ref. [55].

1.3 Computer Simulations

Computer simulations are in many respects very similar to real experiments. When we perform a real experiment, we proceed as follows. We prepare a sample of the material that we wish to study. We connect this sample to a measuring instrument (*e.g.* thermometer, manometer, or viscosimeter), and we measure the property of interest during a certain time interval. In a computer simulation we follow exactly the same approach. First we prepare a sample: we select a model system consisting of N molecules and we solve Newton's equations of motion for this system until the properties under study are equilibrated. Then the actual measurement is performed. In fact, some of the most common mistakes that can be made when performing a computer experiment are very similar to the mistakes that can be made in real experiments. For example, the sample is not prepared correctly, the measurement is too short, the system undergoes an irreversible change during the experiment, or we do not measure what we think to measure.

An important aspect of a computer simulation is the hardware needed to actually run the simulation. Computer hardware is available in a tremendous amount of varieties, from relatively cheap, small-scale PC clusters to very expensive, massive super computers. Some of the simulations presented in this thesis were performed on our own Beowulf cluster [58] currently consisting of close to 200 PC's running Linux as an operating system. The major part of the simulations were performed on the Dutch national supercomputer Teras, located at SARA (Stichting Academisch Rekencentrum Amsterdam) [59]. This machine is a 1024-CPU (Central Processor Unit) system consisting of two 512-CPU SGI (Silicon Graphics, Inc.) Origin 3800 systems.

Another important aspect of a computer simulation is the software program which should be able to run on the chosen hardware system. To this end programming languages like FORTRAN (FORmula TRANslator), C, and C++ were developed. These languages are platform independent, so given a suitable compiler one should be able to run the program on any hardware type. Almost all simulations in this thesis were performed with the CPMD program [60], and a small part with the atomic-orbital based ADF program [61]. The foundation of both programs is density functional theory, and whereas the former is more suited to perform molecular dynamics simulations, from the latter a wide range of molecular properties can be obtained.

Nowadays, one of the bottleneck of first-principles molecular dynamics simulations remains the amount of physical memory needed to perform a simulation. For a relatively small system of 32 methanol molecules one already needs approximately 2.7 Gigabyte, so one cannot do this calculation on, lets say, a single PC. Moreover, if you would have a PC capable of doing such a calculation, it would still take many months, because the CPU is simply too slow. To overcome these problems special communication software has been developed which makes it possible to run a simulation on more than one PC. In other words one runs the simulation in *parallel*. A message passing interface (MPI) takes care of the communications between the processors, also called "nodes", and distributes the total workload of a calculation over the nodes. In this way a typical first-principles molecular dynamics simulation is feasible, although it still requires several weeks with the current computer hardware and software available.

The final point that we want to mention is the use of 3D graphics in computer simulations, which are obviously very well-suited to promote and "sell" your results. Furthermore, 3D graphics can also give a better insight in the problem under study. As an example, Fig. 1.8 shows 3D-molecular graphics of the electronic charge distribution of the highest occupied and lowest unoccupied molecular orbital (HOMO and LUMO) of a 32-molecule liquid methanol system. From the images it is immediately clear that the LUMO is more diffuse than the HOMO, and that they do not overlap. As a second example, Fig. 1.9 shows a 3D-molecular graphics of the HOMO and LUMO of fulvic acid. This acid is commonly found in humic deposits, and supposedly will be the human health drug of the 21st century [62]. Numerous reported claims of effective treatment ranging from anaemia to yeast infection. From the images it is obvious where the chemically active sides of this large molecule are located. These images were rendered with OpenDx [63] which uses the visualization toolkit (VTK) [64]. This toolkit allows you to import multidimensional data, write a visualization program with predefined tools and render a 3D image. And whereas the newest PCs have more memory and faster CPUs, they generally have also more advanced and faster graphical cards. This allows one to look with the computer at a problem using real-time rendering! This is possible because these graphics cards often have support for OpenGL hardware acceleration [65], which can speed up the image-rendering process by orders of magnitude. Finally, a specific application of computer graphics in molecular dynamics simulations is the possibility to make movies, which clearly helps to investigate and understand the problem under study. Sadly, with the current technology is difficult to put a movie in a thesis, although it has been done recently using the old technique of "flip over of pages" [66].

1.4 Scope of this Thesis

As it stands, this thesis deals with a variety of different research themes. About four years ago, at the start of my Ph.D., the main idea was to study a reaction in solution using the Car-Parrinello technique. In collaboration with Joost Reek of the Research Group Homogeneous Catalysis of the University of Amsterdam we initially performed DFT calculations of a model system of the Ru-catalyzed transfer hydrogenation of ketones in the gas phase using the ADF package, in order to unravel the reaction mechanism. The results of this gas-phase study are not incorporated in this thesis, in stead they can be found in the thesis of Daniëlle Petra [69] and in a separate publication [32]. This proved to be a very interesting research area, and we decided to extend it towards a study in solution using an atomistic model of the solvent, since this has never been done, and moreover, we expected a substantial influence of the solvent. This was not an easy task, as we had to check quite a number of things before we could commence with the study of the solvated reaction. First of all, we had to check whether the CPMD program accurately describes the chosen solvent, *i.e.* methanol. With a few exceptions the CPMD program had

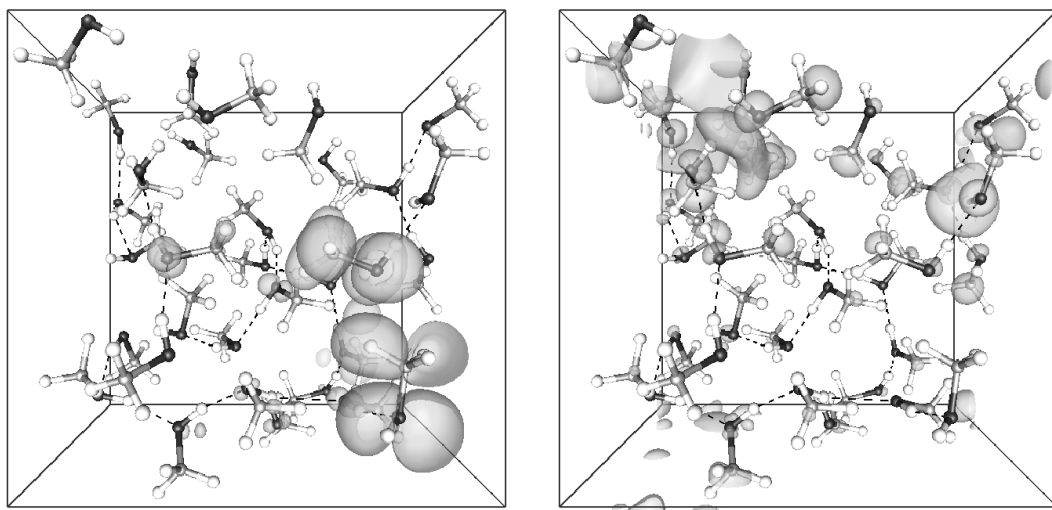


Figure 1.8: 3D-isocontour plots of the electronic charge distribution of the HOMO (left) and LUMO (right) of a 32-molecule methanol liquid system [67].

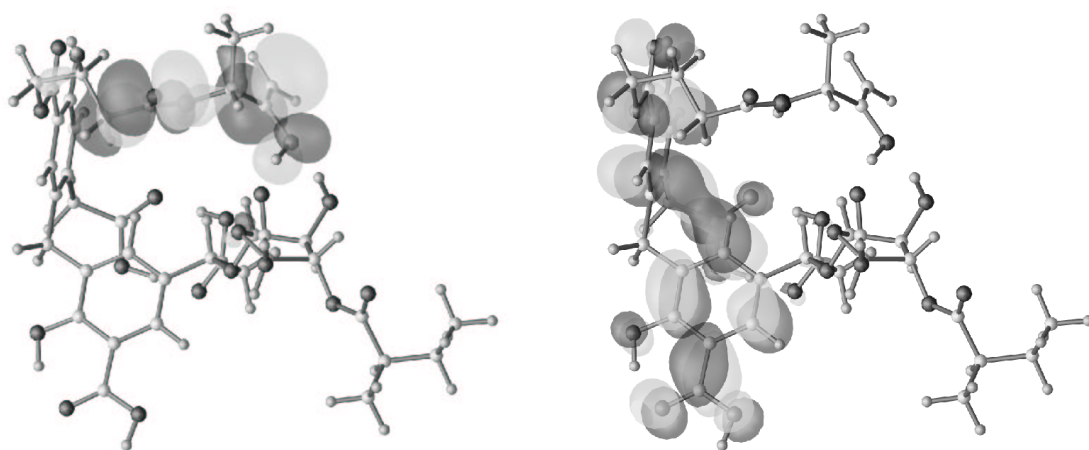


Figure 1.9: 3D-isocontour plots of the HOMO (left) and LUMO (right) of fulvic acid [68].

only been used to study reactions in aqueous environment. An additional advantage of a first-principles molecular dynamics study of liquid methanol is that also the underlying electronic structure and related properties can be studied. All the more, because both from experiments and classical simulations a lot of controversy exist in the literature about the structure of liquid methanol. The results of our first-principles molecular dynamics study of liquid methanol are discussed in Chapter 2.

Secondly, we had to design and test a pseudopotential for Ru. After some preliminary testing, it became evident that not only the valence states of Ru had to be included in the pseudopotential, but also the semicore states in order to get accurate structures and energies. The Ru semicore pseudopotential was thoroughly tested against benchmark ADF calculations. Subsequently, the gas-phase study of an extended model system of the Ru-catalyzed transfer hydrogenation of ketones was repeated and compared against other computational study available in the literature. In addition, experimental work performed by Daniëlle Petra indicated that the mechanism for the Ir-catalyzed transfer hydrogenation of ketones possibly differed, hence we decided to investigate this in more detail with DFT and make the comparison with Ru. And whereas the Ru-catalyzed transfer hydrogenation of ketones was by now quite thoroughly investigated by us and others, the Ir-catalyzed transfer hydrogenation of ketones had not be studied computationally at all. The results of the comparison between Ir and Ru are presented in Chapter 3.

Having investigated the liquid and studied the ketone transfer hydrogenation in the gas phase, we could finally commence with the first-principles molecular dynamics study of the reaction in solution. In first instance we used a system containing the Ru-catalyst and 64 methanol molecules to model the reaction in solution. However, this proved to be computationally too demanding.^{||} Hence, we decreased the number of solvent molecules to 40 to make the calculation feasible. The results of the study of the Ru-catalyzed transfer hydrogenation of ketones in solution are presented in chapter 4.

The final chapter deals with a somewhat different subject: a computational study of the Rh-catalyzed hydrogenation of functionalized alkenes in the gas phase. During my Ph.D. I spend six weeks in Cambridge (UK) under supervision of Michiel Sprik. There I worked with Jinquan Yu and Jonathan Spencer on this subject. In the 1990s they proposed a model where the mode of coordination of the alkene to the catalyst determines the enantioselective outcome of the hydrogenation. Using well-chosen functionalized alkenes they were able to direct the mode of coordination, and hence the enantioselectivity. However, these were experimental findings and required computational backup.

^{||}With this system a first-principles molecular dynamics run of 2.1 ps took approximately two weeks using 64 Teras-nodes in parallel.

Chapter 2

Structural, Dynamic, and Electronic Properties of Liquid Methanol from First Principles*

Jan-Willem Handgraaf, Titus S. van Erp, and Evert Jan Meijer

Department of Chemical Engineering, University of Amsterdam,
Nieuwe Achtergracht 166, 1018 WV Amsterdam, The Netherlands

Abstract

We present a density-functional-theory based molecular dynamics study of the structural, dynamic, and electronic properties of liquid methanol under ambient conditions. The calculated radial distribution functions involving the oxygen and hydroxyl hydrogen show a pronounced hydrogen bonding and compare well with recent neutron diffraction data. We observe that in line with infrared spectroscopic data, the hydroxyl stretching mode is significantly red-shifted in the liquid, whereas the hydroxyl bending mode shows a blue-shift. A substantial enhancement of the molecular dipole moment is accompanied by significant fluctuations due to thermal motion. We compute a value of 33 for the relative permittivity, identical to the experimental value. Our results provide valuable data for improvement of empirical potentials.

*This chapter is adapted from *Chem. Phys. Lett.* **2003**, 367, 617-624 and from a paper in preparation.

2.1 Introduction

Liquid methanol is of fundamental interest in natural sciences and of significant importance in technical and industrial applications. The liquid phase of the simplest alcohol has been widely studied, both experimentally and theoretically. Among the alcohols, methanol is the closest analog to water. The characteristic hydroxyl group allows methanol to form hydrogen bonds that dominate the structural and dynamical behavior of the liquid phase. The methyl group does not participate in the hydrogen bonding and constitutes the distinction with water. This difference is apparent in the microscopic structure of the liquid, with water having a tetrahedral-like coordination, whereas for methanol experiments and molecular simulations suggest a local structure consisting of chains, rings, or small clusters.

The precise quantification of the microscopic structural and dynamical picture of liquid methanol has been a long-time subject in both experimental and molecular simulation studies. Recently, a series of state-of-the-art studies have been reported. Among these are the neutron diffraction (ND) experiments of Refs. [70, 71]. Simulation studies include work based on empirical force fields [72, 73], mixed empirical and *ab initio* interactions [74, 75], and a full *ab initio* molecular dynamics study [76]. The recent ND experiments have provided a detailed microscopic picture of the structure of liquid methanol, including the pair distribution functions among all atoms. Yet, some of these distribution functions are still subject to some uncertainty as they are obtained indirectly.

Molecular simulation provides a complementary approach to study the microscopic behavior of liquids. Most molecular simulation studies of liquid methanol are based on empirical force-field potentials that are designed to reproduce a selection of experimental data. Obviously, molecular simulations based on these potentials do not provide a picture completely independent of experiment. Moreover, the reliability of the results at conditions that are significantly different from those where the potential was designed for, may be questionable. Density-functional-theory (DFT) based molecular dynamics (MD) simulation such as the Car-Parrinello molecular dynamics method [51], where the interactions are calculated by accurate electronic structure calculations, provides a route to overcome these limitations. This has been demonstrated in studies of liquid water [77–79] and aqueous solvation [52, 80, 81]. Important advantages of DFT-MD over force-field MD are that it intrinsically incorporates polarization, that it accounts for the intra-molecular motion and therefore allows for a direct comparison with spectroscopy of intra-molecular vibrations, and that it yields detailed information on the electronic properties, such as the energy levels of electronic states and the charge distribution. In a broader chemical perspective it is important to note that DFT-MD is capable of the study of chemical reactions in solution, where force-field MD would fail completely as it cannot account for the change in chemical bonding.

Here, we report a DFT-MD study of liquid methanol that addresses the liquid structure, the inter- and intra-molecular dynamics, and the electronic charge distribution.

2.2 Methods and Validation

Electronic structure calculations are performed using the Kohn-Sham formulation of DFT. We employed the gradient-corrected BLYP functional [42, 43]. The choice for the BLYP functional was guided by its good description of the structure and dynamics of water [78] where hydrogen bonds are, as in liquid methanol, the dominant interactions. Furthermore, it has been shown that DFT-BLYP gives a proper description of solvation of methanol in water [52].

The DFT based MD simulations are performed with the Car-Parrinello method [50, 51] using the CPMD package [82]. Semi-local norm-conserving Martins-Troullier pseudopotentials [57]

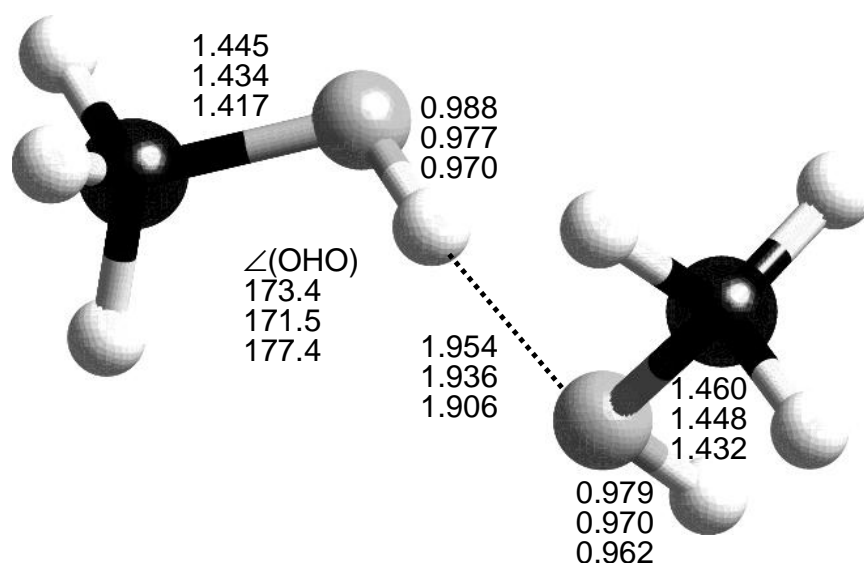


Figure 2.1: Optimized geometry of the methanol dimer. Selected distances (Å) and angles (degrees) are given for three computational methods: CPMD-BLYP (top, this work), ADF-BLYP [83] (second, this work) and are within 0.01 Å of the B3LYP result.

are used to restrict the number of electronic states to those of the valence electrons. The pseudopotential cut-off radii were taken to be 0.50, 1.11 and 1.23 a.u., for H, O, and C, respectively. The electronic states are expanded in a plane-wave basis with a cut-off of 70 Ry yielding energies and geometries converged within 0.01 Å and 1 kJ/mol, respectively. Vibrational frequencies are converged within 1 %, except for C-O and O-H stretch modes that are underestimated by 3 % and 5 % compared to the basis-set limit values [52].

To validate our computational approach we compared results for the gas-phase monomer and hydrogen-bonded dimer against state-of-the-art atomic-orbital DFT calculations obtained with ADF [83],[†] and against the B3LYP and MP2 calculations of Ref. [84]. The CPMD-BLYP calculations were performed using a cubic box with an edge of 12.9 Å, with the interactions among the periodic images eliminated by a screening technique [85]. Results for geometry and complexation energy of the dimer are given in Fig. 2.1 and Table 2.1. Deviations among CPMD and ADF are 1 kJ/mol for the complexation energy, smaller than 0.01 Å for the intra-molecular bonds, and smaller than 0.02 Å for the hydrogen bond. This indicates a state-of-the-art accuracy for the numerical methods employed in CPMD. Compared to the MP2 and B3LYP results, the BLYP bond lengths are slightly longer, with deviations up to 0.03 and 0.05 Å for the intra- and inter-molecular bond lengths respectively. Differences among BLYP, B3LYP, and MP2 complexation energies are within acceptable limits, with the BLYP energies smaller by 2-4 kJ/mol. The deviations are similar to the comparison between BLYP [78] and MP2[‡] for the water dimer and the water-methanol dimer [52, 87]. We obtained a zero-Kelvin association enthalpy $\Delta H^0(0)$ of 10.6 kJ/mol using the B3LYP zero-point energy of Ref. [84]. This is in reasonable agreement with the experimental value of 13.2(4) kJ/mol. The calculated hydrogen bond length ($r_{O\dots O} = 2.94$ Å, $r_{H\dots O} = 1.95$ Å) is in good agreement with the experimental values of $r_{O\dots O} = 2.98(2)$ Å and $r_{H\dots O} = 1.96(2)$ Å of Refs. [88] and [89], respectively.

[†]Kohn-Sham orbitals are expanded in an even-tempered, all-electron Slater type basis set augmented with 2p and 3d polarization functions for H and 3d and 4f polarization functions for C and O.

[‡]MP2 limit estimate. See for example [86].

Table 2.1: Complexation energies (kJ/mol) of the methanol dimer shown in Fig. 2.1. Numbers are bare values without zero-point energy corrections and without entropy contributions.

CPMD-BLYP	ADF-BLYP ^a	B3LYP ^b	MP2 ^c
16.4	17.3	20.6	18.4

^a Refs. [83]

^b B3LYP/6-311+G(3df,2p) method. B3LYP/6-311+G(d,p) optimized geometries, taken from Ref. [87].

^c G2(MP2) method. MP2(full)/6-311+G(d,p) optimized geometries, taken from Ref. [87].

Current gradient corrected functionals such as BLYP do not account for dispersion forces. For methanol this could be important as attraction to the methyl group is fully due to the dispersion force. To estimate the effect of the absence of the dispersion we computed the BLYP binding energy of two dimer configurations that are sensitive to this: one with methyl groups approaching (M-M) and the other with the methyl and hydroxyl group approaching each other (M-OH). State-of-the-art MP2 calculations [90] incorporate to a good approximation the dispersion force and were taken as reference. The dimer configurations were taken from Ref. [90] and chosen such that the carbon-carbon (M-M dimer) and carbon-oxygen (M-OH dimer) distances were close to the peak position of their atom-atom distribution function in the liquid state.[§] The comparison yields for the M-M dimer values for the binding energy of 2.3 kJ/mol and -2.0 kJ/mol for BLYP and MP2, respectively. For the M-OH dimer these values are -1.2 kJ/mol and -4.9 kJ/mol, respectively. The too-repulsive nature of the BLYP interaction is consistent with DFT calculations of dispersion dominated systems [91,92]. However, the magnitude of the deviation is much smaller than the hydrogen-bond interaction and of the same order of magnitude as the error in the latter. It can therefore be argued that for a study of liquid methanol on the accuracy level of BLYP, neglecting the dispersion interaction is acceptable.

In Ref. [52] van Erp and Meijer showed that for the gas-phase monomer CPMD-BLYP vibrational frequencies are in excellent agreement with ADF results and, compared to experiment, underestimate almost all modes by approximately 10%, a known feature of the BLYP functional. Overall, we conclude that our level theory is satisfactory in comparison with experimental and other theoretical gas-phase data.

2.3 Liquid

Liquid methanol was modeled by 64 molecules in a periodic cubic box with an edge of 16.3 \AA , reproducing the experimental density of 0.791 g/cm^3 at 293 K [93]. In order to estimate finite-size effects we compare the results of the 64-molecule system with a smaller 32-molecule system in a periodic cubic box of a size corresponding to the same density. The temperature was fixed at 293 K using the Nosé-Hoover thermostat [94]. The fictitious mass associated with the plane-wave coefficients is chosen at 700 a.u., which allowed for a time step in the numerical integration of the equations-of-motion of 0.121 fs. The system was equilibrated for 1 ps from an initial configuration obtained from a force-field simulation. Subsequently, we gathered statistical averages from a 10 ps trajectory.

2.3.1 Structure

In Fig. 2.2 we have plotted the most characteristic atom-atom radial distribution functions (RDFs), *i.e.* the hydrogen bonding O-O, O-H_O, and H_O-H_O RDF and the C-O, C-C, and C-H RDF for

[§]Configurations from Ref. [90]. M-M dimer: geometry M with $r_{\text{CC}} = 3.75 \text{ \AA}$. M-OH dimer: geometry I with $r_{\text{CO}} = 3.50 \text{ \AA}$. Both monomers in the dimer are kept fixed to their isolated geometries.

the 64 and 32-molecule system. For comparison we also plotted results of recent ND experiments [70] and the peak positions obtained using Haughney's empirical potential [72], the latter being considered one of the most accurate empirical force fields to date.

The pronounced structure in the first three RDFs are a clear indication of the presence of hydrogen bonds. Comparison with the experimental data shows that the positions of the first peaks match within the statistical error for the O-O and O-H₂O RDFs and is slightly smaller (≈ 0.1 Å) for the H₂O-H₂O RDF. For the 64-molecule system the height of the first peak of the O-O RDF is in good agreement with the ND result. Both the first peak of the O-H₂O and the H₂O-H₂O RDF of the 64-molecule system are approximately 10% higher than the ND results. Similar discrepancies with respect to ND experiments are reported for the O-H₂O and the H₂O-H₂O RDF of liquid water [79]. Nuclear quantum effects, which are in both cases neglected, could be a possible explanation for these discrepancies, since these effects tend to soften the structure of a liquid [95]. Comparing the results for the 64- and 32-molecule system we see that all hydrogen-bonding RDFs show a less pronounced structure for the smaller system. This holds in particular for the RDFs involving the oxygens where the height of the first peaks is reduced by a significant amount. It suggests, not surprisingly, that 32-molecule system is too small for an accurate description of the local structure. Comparison of our DFT-BLYP results with force field results [72], that yield slightly higher peak values for the O-O and O-H₂O RDFs, suggests that the Haughney potential performs quite well.

The number of H-bonds as calculated by integrating the O-H₂O and O-O RDFs of the 64-molecule system up to the first minimum, and using the geometrical criterion of Ref. [72], yields values of 2.0, 2.0, and 1.6, respectively. This is in good agreement with the experimental ND results of Ref. [70] yielding 1.8 and 1.9 obtained by integrating the O-H₂O and O-O RDFs. Applying the geometrical criterion to the Hughes force-field simulation [72] yields a slightly higher value of 1.9. The hydrogen bonding in the liquid phase is accompanied by an elongation of the O-H₂O bond of 0.15 Å. Direct comparison with the experimental results for this change in the geometry of the methanol molecule is rather difficult due to the large scatter in the reported values. However, similar change in the geometry is observed in the DFT-MD study of liquid methanol reported in Ref. [76] and in *ab initio* studies of small methanol clusters [84].

The calculated C-O RDF in Fig. 2.2 is in good agreement with the ND result, with the overall shape well reproduced, but the first peak somewhat less pronounced than in the ND result. This is consistent with the underestimation of the BLYP binding energy of the M-OH dimer in a configuration with the C-O distance at the RDF peak position (see section 2.2). This is due to the absence of the dispersion interaction in BLYP. However, the absence of the dispersion interaction clearly does not lead to a completely distorted C-O positional correlation. The comparison of the calculated C-C RDF with the ND result shows a more dramatic effect of the absence of dispersion. Interestingly, in case of the C-H RDF we see somewhat more structure than the ND result as indicated by the more pronounced maxima and minima.

In general, the RDFs computed for the 64-molecule system show more structure and are in better agreement with the ND results than the ones obtained for the 32-molecule system. However, the disagreement as shown is rather small and it is concluded that already with a 32-molecule system a good description of the first and part of the second solvation shell for small solutes is feasible.

2.3.2 Dynamics

The time scale of the present simulation (10 ps) allows for an analysis of the short-time dynamics of liquid methanol. Figure 2.3 shows the Fourier transform of the velocity auto-correlation function (VACF) of all atoms and the VACF of the hydroxyl hydrogen for the 64-molecule sys-

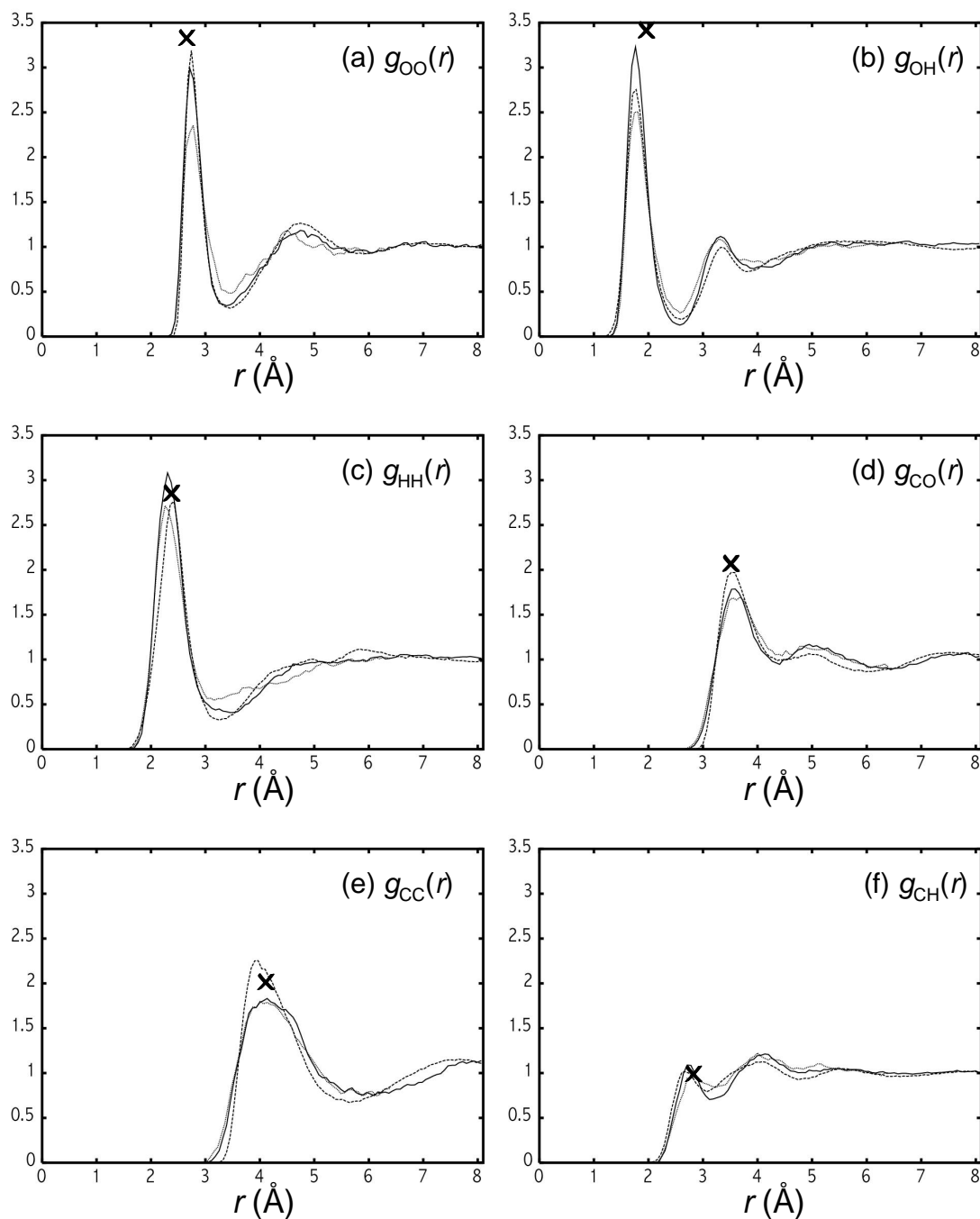


Figure 2.2: Calculated hydrogen-bonding, C-O, C-C and C-H radial distribution functions (solid line for the 64-molecule system, dotted line for the 32-molecule system). Dashed line indicate neutron diffraction results of Ref. [70]. Crosses indicate the position of the first peak of the RDFs obtained by Haughney *et al.* using an empirical force field [72].

tem. For comparison we also plotted the calculated monomer spectrum obtained from a 12 ps trajectory of a single isolated methanol molecule. The three distinct peaks in the all-atom spectrum of the liquid correspond to the CH₃ stretch modes (2800 cm⁻¹), CH₃ deformation and OH bend modes (1400 cm⁻¹), and the CH₃ rocking modes (1050 cm⁻¹). Note that the distinction between the degenerate and symmetric modes of the CH₃ stretch and CH₃ deformation cannot be made. The broad peak at 3150 cm⁻¹ is associated with the OH stretch and the small peak at 900 cm⁻¹ belongs to the CO stretch. From the power spectrum of the hydroxyl hydrogen we see that the liquid OH stretch mode has red-shifted by approximately 200 cm⁻¹ and broadened compared to the gas phase. In contrast, the OH bend, which is now not screened by the CH₃ deformation modes, is blue-shifted by approximately 70 cm⁻¹. The modes associated with the CH₃ group hardly show a shift when going from the gas phase monomer to the liquid. The observed shifts and broadening are characteristic for hydrogen-bonded liquids and are also observed in the spectrum of water [77] and hydrated methanol [52]. The calculated shifts compare reasonably well with experimental infrared data [96] that yield shifts of -354 cm⁻¹ and +78 cm⁻¹ for the OH stretch and OH bend. The calculated positions and shifts of the modes match within statistical errors with those of methanol in aqueous solution [52] determined using the same computational approach. This indicates that the intra-molecular dynamics of methanol is affected in a similar way by an aqueous environment and a methanol environment. A clear feature is the appearance of a broad band at approximately 650 cm⁻¹ in liquid which is not seen in the gas-phase monomer spectrum. This band is found experimentally at 655 cm⁻¹ and assigned to the OH torsion [96,97]. The gas-phase value is around 300 cm⁻¹ [96]. Clearly, the OH torsion is blue-shifted and broadened in the liquid. This should be attributed to the coupling of the torsion with the intermolecular motions. The same phenomena was also recently found in an *ab initio* study by Bouř who compared the IR spectra of a single methanol molecule with a cluster of 120 molecules [98]. The features below 300 cm⁻¹ in the VACFs of the liquid and the monomer are due to coupled rotational-translational modes [99].

We further considered the reorientational correlation function defined as [72,100]

$$C_2(t) = \langle P_2[\cos\theta(t)] \rangle \quad (2.1)$$

where P_2 is the $l = 2$ Legendre polynomial and $\theta(t)$ is the angle through which a molecule-fixed vector rotates in time t . The calculated function for the O-H₂O bond vector of methanol for the 64-molecule system is plotted in Fig. 2.4. At short times there is an oscillation of the type characteristic for strong intermolecular association. This can be linked to a librational motion of the methanol molecule in the potential energy well provided by the hydrogen bond in which the hydroxyl group takes part. At longer correlation times it shows the typical Debye-like, exponential decay. Although our simulation time is short, we obtain an integral correlation time τ_2 of 5-8 ps in line with the value of 5 ps from NMR spectroscopy [101]. Recently, Bakker and coworkers [102] obtained from an IR spectroscopic study 1.1-7.2 ps for the time constant of equilibration of the O-H₂O-stretch vibration, where they argue that the relatively large spread is due to two different processes: a relatively quick motion in the hydrogen-bond stretch coordinate (~ 1 ps) and a slower motion in the hydrogen-bond bending coordinate (~ 7 ps), *i.e.* reorientational rotational correlation, in close agreement with our result.

The diffusion constant D is a key measure of the collective dynamics. In view of the limited length of the calculated trajectory we can only provide a rough estimate. From the mean square displacement of the oxygen atoms we obtained $D = 2.6 \pm 0.9 \times 10^{-9} \text{ m}^2/\text{s}$, in agreement with the experimental value of $2.42 \pm 0.05 \times 10^{-9} \text{ m}^2/\text{s}$ [103].

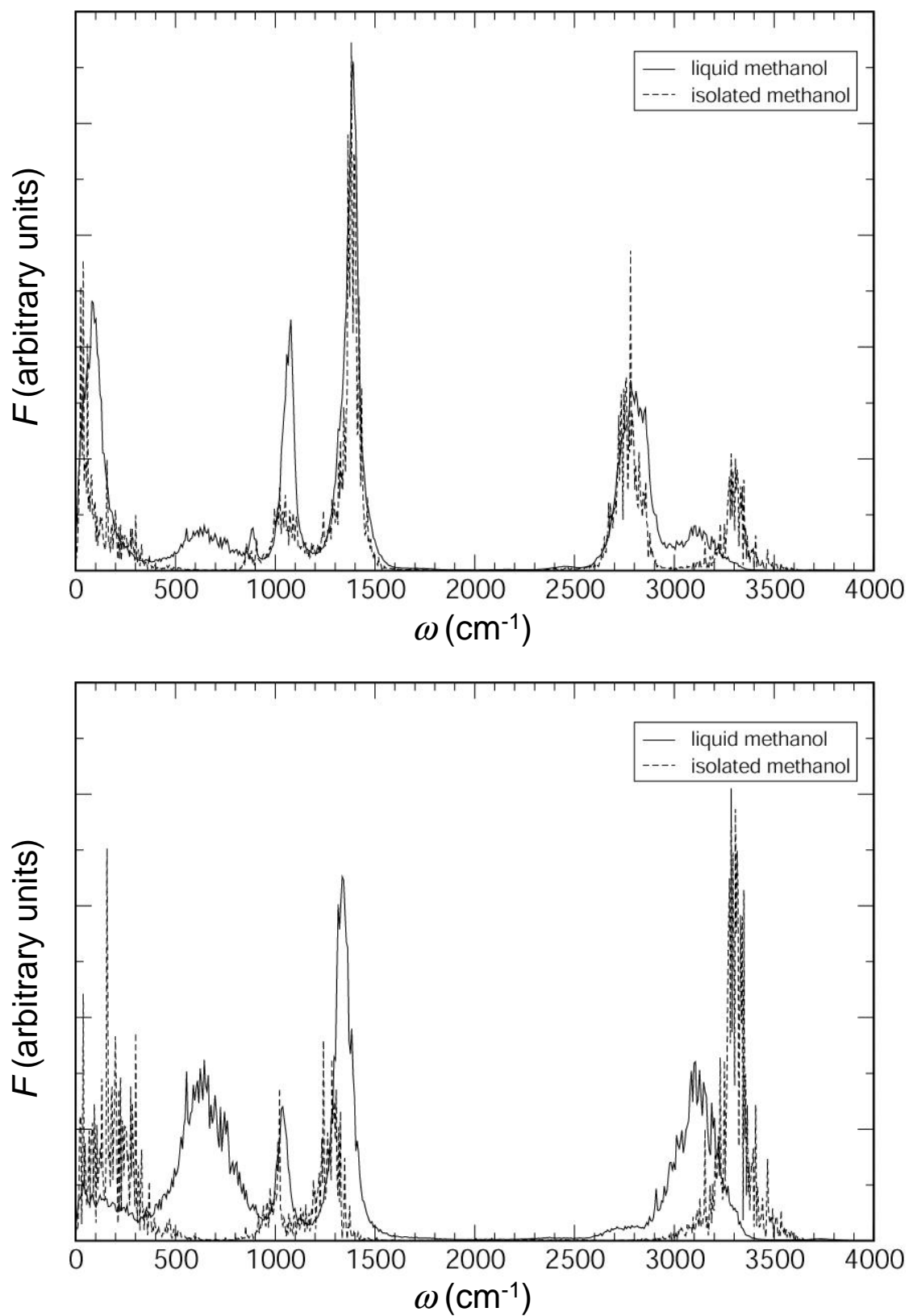


Figure 2.3: Calculated power spectrum of all atoms (top) and the hydroxyl hydrogen (bottom) of liquid methanol (64-molecule system) (solid line) and an isolated methanol molecule (dashed line) at $T = 293$ K.

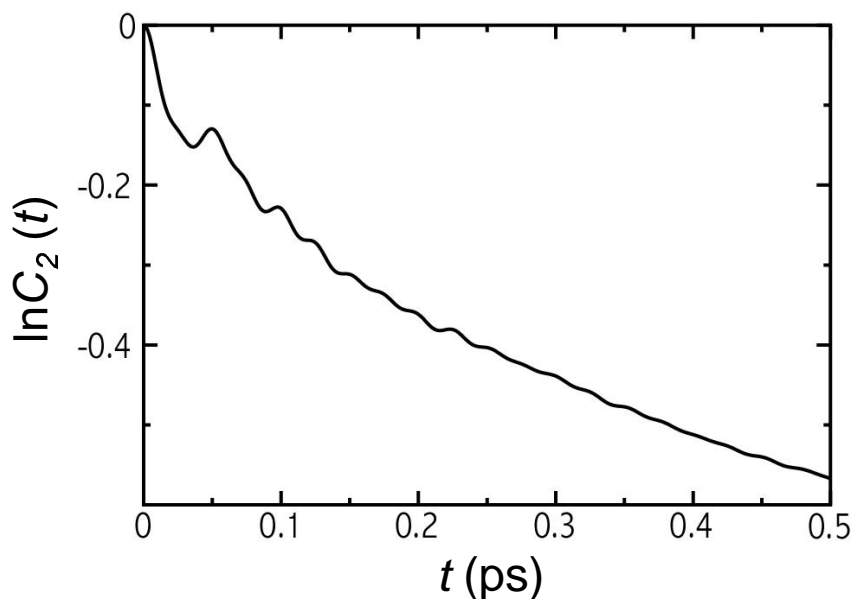


Figure 2.4: The $l = 2$ reorientational correlation function for the O-H_O bond vector of methanol for the 64-molecule system.

2.3.3 Electronic properties

As the electronic structure is an intrinsic part of a CPMD simulation, detailed information on the electronic charge distribution is obtained. To quantify the charge distribution we used the method of maximally localized Wannier functions that transforms the Kohn-Sham orbitals into Wannier functions. The centers of these functions (WFC) may be assigned to common chemical functionality such as being associated with an electron bonding- or lone-pair (LP) [104,105]. Since we use the pseudopotential approach, we explicitly consider 14 electrons per methanol molecule, the carbon and oxygen 1s core electrons being essentially inert with respect to the bonding properties. Due to spin degeneracy we therefore need to consider seven doubly occupied WFCs. Fig. 2.5 shows schematically the positions of the WFCs of the methanol molecule in the gas phase. Here, the sticks represent the bonds, whereas the balls indicate the positions of the WFCs. Bonding WFCs are situated along the three C-H bonds, one C-O bond, and one O-H bond, and the two lone-pair WFCs are located on top of the oxygen atom.

We calculated the positions of the WFCs for the monomer, the dimer, and 6 independent configurations of the 32- and 64-molecule system. Table 2.2 lists the (average) distances of the WFCs associated with the oxygen electrons. Most notably is the small but significant shift of 0.028 Å for the OH bond WFC towards the oxygen atom when going from the monomer to the 64-molecule system. At the same time, one of the LP WFCs shifts away from the oxygen by 0.025 Å. These changes should be considered a manifestation of the hydrogen bonding and the induced polarization among the dipolar methanol molecules in the liquid state. Similar effects are found for the 32-molecule system. The positions (not reported) of the three WFCs located at the carbon methyl-hydrogen bonds do not change in going from the gas-phase monomer to the condensed phase, and hence are not involved in intermolecular bonding. To quantify the change in the charge distribution in a single number we calculated the molecular dipole moment assuming the electronic charge to be distributed as point charges located on the WFCs.

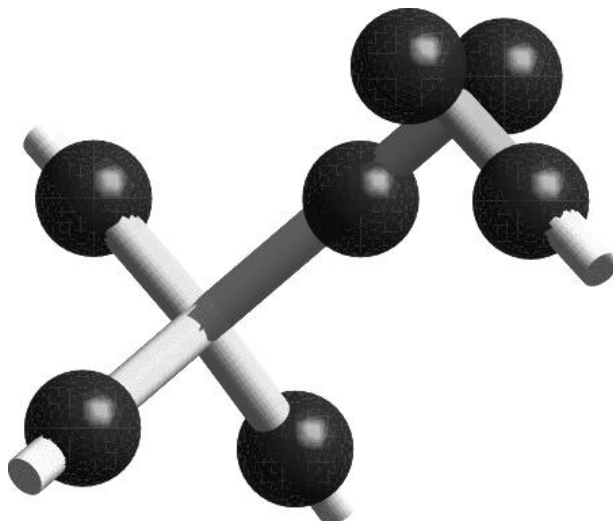


Figure 2.5: Methanol molecule in the gas phase. The sticks represent bonds while the balls indicate the positions of the WFCs.

For liquid water it has been shown that such a partitioning of the charges over the molecules yields a unique assignment of the WFCs over distinct molecules [79]. From Table 2.3, that lists the values for the monomer, dimer, and the 32- and 64-molecule system, we observe a significant enhancement of the dipole moment going from the monomer via the dimer to the liquid. A comparable liquid-state value of 2.39 D has been observed in a coupled empirical and *ab initio* MP2 study [74]. Note that the value of the dipole moment is somewhat larger than in the Haughney [72] (2.33 D) or AMBER [106] (2.2 D) force field. A second important feature of the electronic charge distribution in the liquid is its fluctuating character due to the thermally driven configurational changes. In Fig. 2.6 we have plotted the calculated distribution of the dipole moments in the 64-molecule system. It shows that the distribution is asymmetric and that there is a significant variation ranging from 1.7 D to 3.5 D. The 32-molecule system gives essentially the same distribution (not plotted) with a slight shift of the maximum to smaller values, in line with the computed averaged dipole moment of the 32- and 64-molecule system given in Table 2.3. This indicates that the polarization of the electronic charge cloud of molecule in the liquid is dominated by local interactions between first-neighbor, hydrogen-bonded molecules.

We have also computed (see Fig. 2.7) the dipole-dipole orientation correlation function, $c(r)$ and the distance-dependent Kirkwood function $G(r)$ defined as [79]

$$c(r_i) = \langle \cos\gamma \rangle_{r_i}, \quad (2.2)$$

$$G(r) = 1 + \sum_{r_i \leq r} N_{r_i} c(r_i), \quad (2.3)$$

where $\langle \cos\gamma \rangle_{r_i}$ indicates the average value of the cosine of the angle between the dipole moment of a reference molecule and those of the N_{r_i} molecule whose distance from the reference molecule is between r_i and $r_i + dr$. $G(r)$ reflects the degree of correlation between the orientation

Table 2.2: Electronic charge distribution in terms of Wannier function centers. $d(\text{LP})$ denotes the average distances between a lone pair WFC and the O nucleus. $d(\text{OH})$ and $d(\text{OC})$ denote the (average) distances between the covalent WFC along the O–H bond and the O–C bond with the O nucleus, respectively. All distances are given in Å. Statistical errors for the liquid data are around 0.002.

	$d(\text{LP})$	$d(\text{LP})$	$d(\text{OH})$	$d(\text{OC})$
Monomer	0.305	0.305	0.533	0.562
Dimer	0.316	0.306	0.522	0.561
Liquid (32)	0.328	0.309	0.509	0.561
Liquid (64)	0.330	0.308	0.505	0.560

Table 2.3: Dipole moment. Experimental value is given in parentheses. Data for the liquid phase were obtained by averaging over 6 configurations of the MD simulation. Statistical errors are in the order of some units in the last digit.

	μ (D)
Monomer	1.73 (1.69 ^a)
Dimer	2.03
Liquid (32)	2.54
Liquid (64)	2.59

^aMicrowave study, ref. [107].

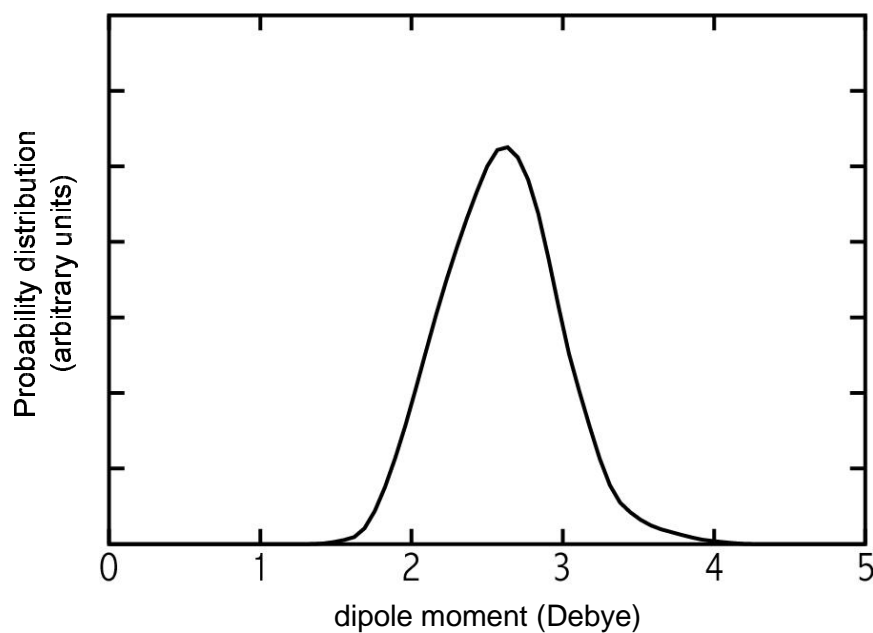


Figure 2.6: Distribution of the molecular dipole moment in liquid methanol, obtained from 6 independent configurations of the 64-molecule system.

of neighboring molecules: $G(r) = 1$ implies no correlation; $G(r) > 1$ when molecular dipole moments tend to orient themselves parallel to each other; and $G(r) < 1$ when molecular dipole moments tend to orient themselves in opposite directions.

The pronounced first peak in $c(r_i)$ at 2.6 Å is a clear indication of the alignment of the dipole moment among first neighbors. Contrary to liquid water [79] there is also a second peak at 4.7 Å. Moreover there is also a distinct minimum between 3.6 and 4.2 Å where $c(r_i)$ is negative, *i.e.* molecules tend to have antiparallel dipoles. By treating the methanol molecules as point dipoles (centered on the oxygen atoms) we obtain the average dipole-dipole interaction energy, at a distance corresponding to the position of the first peak of $c(r_i)$, of 15.7 kJ/mol. In the same way we compute for the gas phase dimer a value of 8.5 kJ/mol indicating that the dipole-dipole interaction energy is roughly doubled in the liquid phase. The computed $G(r)$ is nowhere smaller than 1 and gives a similar picture in comparison to $c(r_i)$ with a distinct peak at 3.0 Å and a broad band in the range 4.7-7.1 Å. Finally $G(r)$ reaches a value of 1.7, somewhat smaller than the value of 1.9 found for liquid water [79]. The overall structure of $c(r_i)$ and $G(r)$ with only two clear maxima can be rationalized by the formation of rather short hydrogen-bonded chains of molecules consistent with the value of 5.5 ± 1.0 molecules per chain found by Soper and coworkers [70].

Another important electronic property of a polar liquid is its relative permittivity, commonly used to describe in averaged manner solvent effects in quantum chemistry packages. Assuming that the system is isotropic [108, 109] the relative permittivity of liquid methanol is given by

$$\epsilon = \epsilon_\infty + \frac{y}{3} G_k, \quad (2.4)$$

where ϵ_∞ is the relative permittivity at optical frequencies, $y = \rho \mu^2 / k_B T \epsilon_0$ with ρ the molecular number density, μ the molecular dipole moment, and G_k the finite system Kirkwood correlation factor that accounts for the correlations of the total dipole moment and is given by

$$G_k = \frac{\langle \mathbf{M}(t) \rangle^2}{N \mu^2}, \quad (2.5)$$

where \mathbf{M} is the total dipole moment of the system and N the number of molecules in the system. The computation of \mathbf{M} is in the case of liquids non-trivial as special techniques are needed to correctly describe the polarization in periodic systems [110]. This methodology has proven to work successfully in recent calculations of the IR absorption spectrum of liquid water [111] and aqueous uracil [54]. Once ϵ has been obtained from Eq. 2.4, the Kirkwood factor g_k , which describes orientational correlations in an infinite sample, may be obtained by means of the relationship

$$g_k = \frac{(2\epsilon + \epsilon_\infty)}{3\epsilon} G_k. \quad (2.6)$$

In this way, using the experimental value of 1.85 for ϵ_∞ [112] we obtain for the 64-molecule system a value for the relative permittivity of 33, identical to the experimental value [113], and in agreement with the force-field simulations of Svishchev and Kusalik who report a value of 31.5 [114]. For g_k we compute a value 2.09, underestimating the experimental value of 2.94 [113]. This underestimation indicates that there must be a residual correlation in the orientations of the molecules in different chains. The fact that we do not find this in our simulation is most likely a finite size effect. Kusalik *et al.* [115] showed that even a system of 108 methanol molecules still exhibits finite size effects.

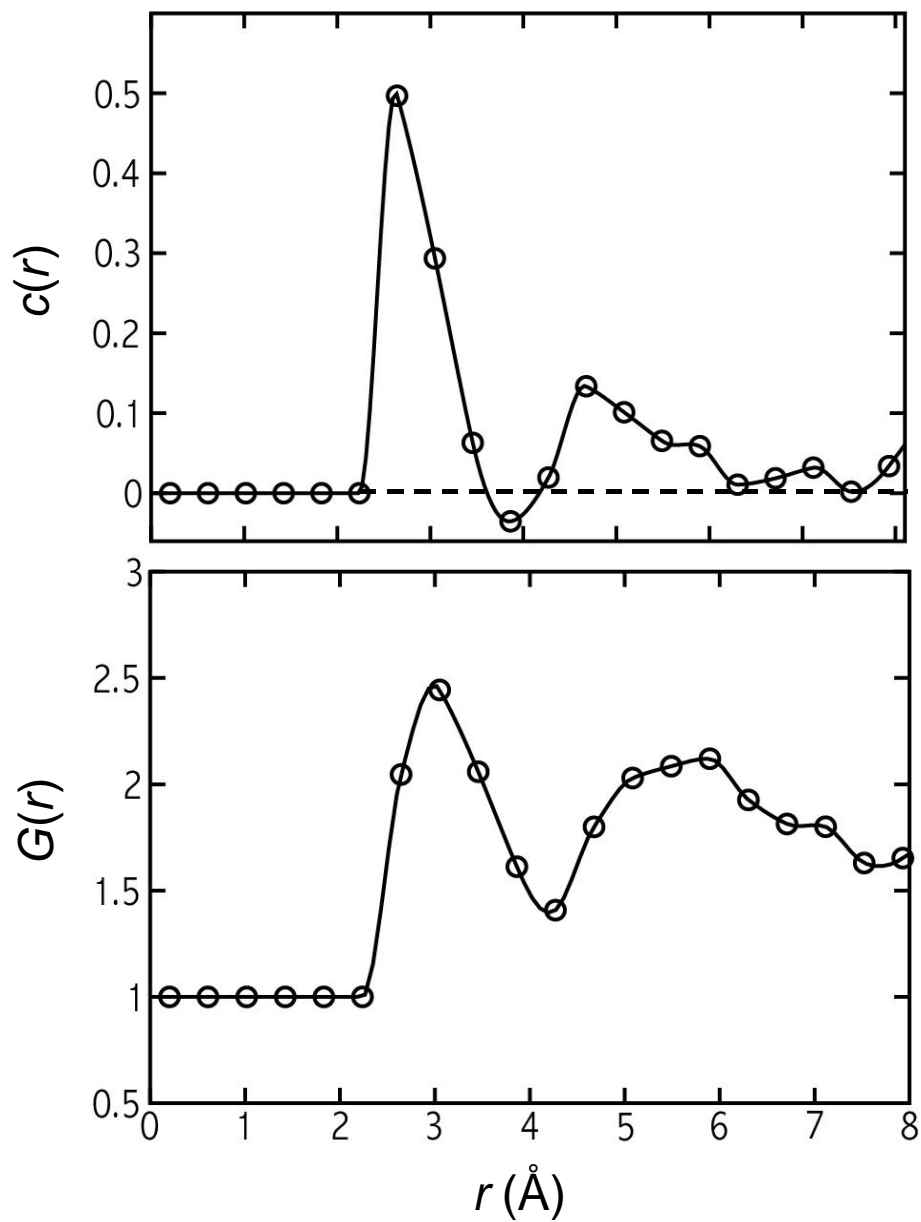


Figure 2.7: Dipole-dipole orientation correlation function $c(r)$ (top) and Kirkwood $G(r)$ function (bottom) in liquid methanol, obtained from 6 independent configurations of the 64-molecule system. The lines are a guide to the eye.

2.4 Conclusions

We have demonstrated that *ab initio* MD is a valuable approach to study the structural, dynamic, and electronic properties of liquid methanol. The calculated pair distribution functions involving the hydroxyl hydrogens correlate well with recent state-of-the-art neutron diffraction experiments of Soper and co-workers and the empirical force-field simulations of Haughney *et al.*, although there is still some discrepancy in the height of the first peak of the O-H₂O RDF. Results for the dimer binding energies, the carbon-oxygen RDF and the carbon-carbon RDF suggest that the absence of the dispersion interaction is noticeable but has no major impact. Comparing the vibrational spectra of the liquid phase against that of the gas phase monomer shows a significant red shift of the O-H stretch accompanied by a smaller blue shift of the O-H bend mode, in reasonable agreement with experimental observations with the O-H shift somewhat underestimated in our calculation. We quantified the electronic charge distribution using a Wannier function center decomposition. A small but measurable shift of the positions of the Wannier function centers when going from the gas-phase to the liquid is accompanied by a substantial enhancement of the dipole moment. Moreover we have found that in the liquid the molecular dipole moment fluctuates significantly with variations up to half the average magnitude. The latter suggest that the assumption made in empirical potentials using a fixed dipole moment is a strong simplification. Observed correlations among dipole moments indicates that short hydrogen-bonded chains are formed in the liquid. The computed relative permittivity is identical to the experimental value, indicating that our first-principles simulation gives an accurate description of the polarization of liquid methanol. The present results may be considered valuable data for improvement of empirical potentials for the study of liquid methanol.

Acknowledgements

We are grateful to A. K. Soper for providing us data of the RDFs of Ref. [70].

Chapter 3

Iridium(I) versus Ruthenium(II). A Computational Study of the Transition Metal Catalyzed Transfer Hydrogenation of Ketones*

Jan-Willem Handgraaf,[†] Joost N. H. Reek,[‡] and Evert Jan Meijer[†]

[†]Department of Chemical Engineering, University of Amsterdam,
Nieuwe Achtergracht 166, 1018 WV Amsterdam, The Netherlands

[‡]Institute of Molecular Chemistry, University of Amsterdam,
Nieuwe Achtergracht 166, 1018 WV Amsterdam, The Netherlands

Abstract

We present a density-functional-theory based computational study comparing simplified models for the ruthenium(II)- and iridium(I)-catalyzed transfer hydrogenation of ketones. For the ruthenium compound our results confirm earlier findings that the hydrogenation involves a ruthenium-hydride and occurs via a concerted hydrogen transfer mechanism with no direct ruthenium-ketone binding along the reaction path. In contrast, for the iridium compound our calculations suggest that the reaction proceeds via direct hydrogen transfer between simultaneously coordinated ketone and alcohol. We find that for both metal-complexes the formation of a very stable metal-alkoxide complex plays an important role. For the ruthenium-catalyzed reaction it constitutes a resting state that takes no active part in the transfer hydrogenation, while for the iridium-catalyzed reaction it is an important intermediate along the reaction path.

*This chapter is adapted from *Organometallics* 2003, 22, 3150-3157.

3.1 Introduction

One of the most fundamental transformations in synthetic chemistry is the asymmetric reduction of C=O and C=N bonds forming stereospecific centers in molecules [4]. In this field, Noyori *et al.* initiated significant progress by introducing well-designed chiral ruthenium compounds that catalyze transfer hydrogenation from 2-propanol to pro-chiral ketones with a high enantioselectivity [116]. Subsequently, various other chiral compounds with a ruthenium(II) [5, 32, 116–137] (Ru), rhodium(I) [138–148] (Rh), or iridium(I) [140, 144, 145, 147, 149–153] (Ir) catalytic metal center have been designed that shown both a high yield and a high enantioselectivity under relatively mild conditions. For example, in Ru-catalyzed reactions, that have been studied in detail, a high enantioselectivity is in particular induced by chiral aminoalcohol and *N*-tosylated diamine-based ligands yielding an enantiomeric excess (e.e.) of up to 99% [5, 32, 118]. Excellent reviews on this subject can be found in the literature [27, 29].

To date it is still a formidable challenge to obtain experimentally direct and accurate insight in the mechanistic pathways of chemical reactions. The most important limitation is the fact that key intermediates often have a very short lifetime. Obviously this holds also for the transition metal catalyzed reactions of the type as addressed in the present paper. Computational studies do not suffer from these limitations and provide therefore a valuable complementary approach to study these reactions. In order to unravel the underlying mechanistic reaction pathway of the metal-catalyzed transfer hydrogenation reactions a number of computational studies of simplified Ru and Rh model complexes have been performed [31–34, 154]. In these studies mainly three types of mechanisms were considered (Fig. 3.1): (I) concerted transfer of the proton of the amine ligand and the metal coordinated hydride to the pro-chiral ketone, referred to by Noyori as the metal-ligand bifunctional mechanism [155]; (II) migratory insertion of the pro-chiral ketone into the metal-hydride bond; (III) direct transfer of the α -hydrogen of the metal-alkoxide complex to the pro-chiral ketone, commonly known as the Meerwein-Ponndorf-Verley reduction [30, 156]. For a Ru-complex with an aminoalcohol ligand Noyori and co-workers [33], Alonso *et al.* [31], and Petra *et al.* [32], have recently found that the transfer hydrogenation via mechanism (I) is energetically favorable compared to the other two mechanisms. Guiral *et al.* [34] showed for a Rh-complex with a primary ligand that hydrogen transfer prefers mechanism (I) over a mechanism first proposed by Gladiali *et al.* which is very similar to (II) [157]. However, they found that for a Rh-complex bearing a tertiary diamine ligand mechanism (III) is also possible.

To our knowledge computational studies of Ir-catalyzed hydrogen transfer are still absent. However, in view of the good performance of Ir compounds as illustrated by the 92 % e.e. in the reduction of acetophenone using a *N*-(*p*-tolylsulfonyl)-1,2-diphenylethylenediamine ligand [151], and the 97 % e.e. obtained with aminosulfide ligands in the reduction of aryl-alkyl ketones as reported by Petra *et al.* [153], there is an obvious need for further clarification of Ir-catalyzed hydrogen transfer by computational methods.

Here, we report a density functional theory (DFT) study of the Ir-catalyzed transfer hydrogenation of ketones and compare this directly to the well characterized Ru-catalyzed transfer hydrogenation. Reaction paths for the above mentioned mechanisms including all important transition states (TSs) are computed. The results are mutually compared and put in perspective in a qualitative comparison with experimental results.

3.2 Models

Fig. 3.2 shows the simplified catalytic cycle of asymmetric transfer hydrogenation of ketones [33, 155]. A 16-electron complex is generated from a catalyst precursor, typically the corre-

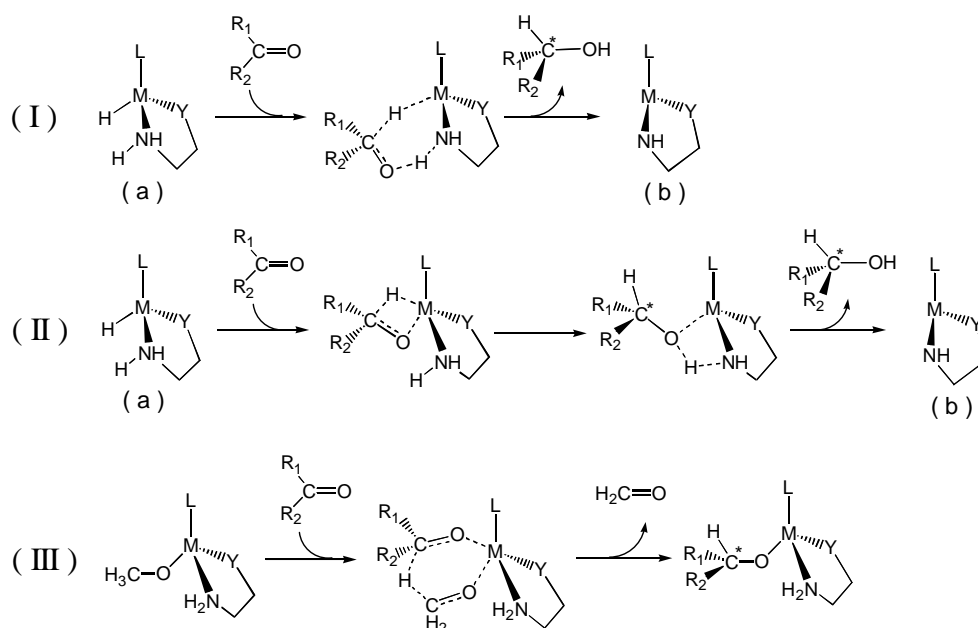


Figure 3.1: Mechanistic alternatives for transition metal catalyzed asymmetric hydrogen transfer. (I) Concerted hydrogen transfer, (II) migratory insertion, and (III) direct hydrogen transfer. M = transition metal, L = arene or olefin, and Y = nitrogen, oxygen or sulfur. (a) denotes the 18-electron metal-hydride complex and (b) the 16-electron metal-complex, see further section 'Models'.

sponding metal halide, using an inorganic base such as KOH, NaOH, or K₂CO₃. In a typical experiment 2-propanol acts both as solvent and hydrogen donor. It first reacts with the 16-electron complex to form the 18-electron metal-hydride complex. This in turn reacts with a pro-chiral ketone to form a chiral secondary alcohol. In the case of Ru both the 16- and the 18-electron complex have been isolated and the crystal structure has been elucidated [122]. In the present computational studies we considered a simplified form of a well-performing Ru-arene-aminoalcohol compound [121], similar to that of Noyori and coworkers [33], with a stabilizing benzene ligand and an aminoethanol ligand (Fig. 3.3a,d). For the Ir catalyst we considered two simplified models: one with an aminoethanol (Fig. 3.3b,e) ligand and a second with a 2-aminoethylmethylsulfide ligand (Fig. 3.3c,f), both of them with an additional stabilizing cycloocta-1,5-dienyl (COD) ligand. The chiral analogues of the model aminosulfide ligand yield active catalysts with relatively high e.e. (80 % e.e. at 82 % conversion for the reduction of acetophenone), whereas the Ir compounds with aminoalcohol ligands show much lower activity [153]. Experimental work by Petra *et al.* [153] suggests that in the active catalyst COD is η⁴-coordinated to Ir. Crystal structures [149] of an analogous Ir catalyst show also coordination of COD in η⁴-mode. Calculations by Bernard *et al.* [142] found COD η⁴-coordinated in a isoelectronic Rh-complex, supporting the observation by Petra *et al.* For the transfer hydrogenation we consider a symmetric model reaction with methanol being the hydrogen donor and formaldehyde representing the ketone.

3.3 Methods and Validation

We performed DFT based electronic structure calculations using the BLYP functional, that combines a gradient correction term for the exchange energy as proposed by Becke [42] with a correction for the correlation energy due to Lee, Yang, and Parr [43]. The pseudopotential method is

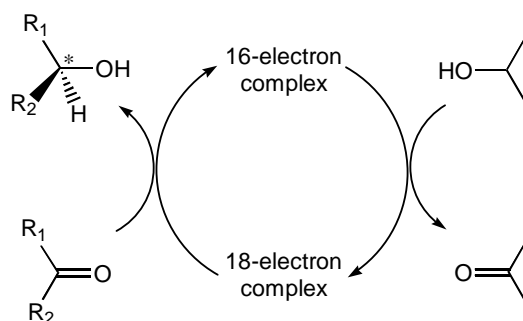


Figure 3.2: Transition metal catalyzed asymmetric transfer hydrogenation of ketones.

used to restrict the number of electronic states to those of the valence electrons. The interaction with the core electrons is taken into account using semi-local norm-conserving Martins-Troullier pseudopotentials [57]. The Ru and Ir pseudopotentials were of the semi-core type including the highest s - and p -shell electrons as valence electrons. They were generated using ionized configurations (Ru^+ and Ir^{2+}) with the electrons treated relativistically in the scalar approximation. The pseudopotential cut-off radii for C, N, O, and H were 1.23, 1.12, 1.10, and 0.50 a.u., respectively. In case of Ru the radii of the s , p , and d pseudopotentials were 1.10, 1.20, and 1.24 a.u., respectively. For Ir these values were 1.13, 1.15, and 1.28 a.u. The electronic states were expanded in a plane-wave basis including waves up to an energy of 70 Ry. Calculations are performed in a cubic periodic box of edge 13.0 Å. Test calculations showed that with this setup structural properties are converged within 0.01 Å and 0.02 Å for the intra- and intermolecular bonds, respectively. Energies are converged within 0.25 kcal/mol. All calculations are performed with the CPMD package [82].

We validated the numerical accuracy of our computational approach against benchmark calculations performed with the state-of-the-art atomic-orbital based ADF package [83] by calculating properties of Ru and Ir hexacarbonyls.[†] Table 3.1 lists the optimized bond lengths and the first bond dissociation energy (FBDE). This corresponds to the energy change upon removing one of the carbonyl ligands from the metal hexacarbonyl. To our knowledge no experimental structural data are available. With respect to the bond lengths the agreement between the CPMD and ADF results is excellent with a maximum deviation of 0.01 Å, but most deviations within 0.005 Å. Also the FBDEs are in good agreement. This indicates state-of-the-art accuracy of the numerical methods employed in CPMD.

[†]Kohn-Sham orbitals are expanded in a triple- ζ basis set augmented with $3d$ and $4f$ polarization functions for C and O, $5p$ and $4f$ for Ru, and $6p$ and $5f$ for Ir. Cores were kept frozen.

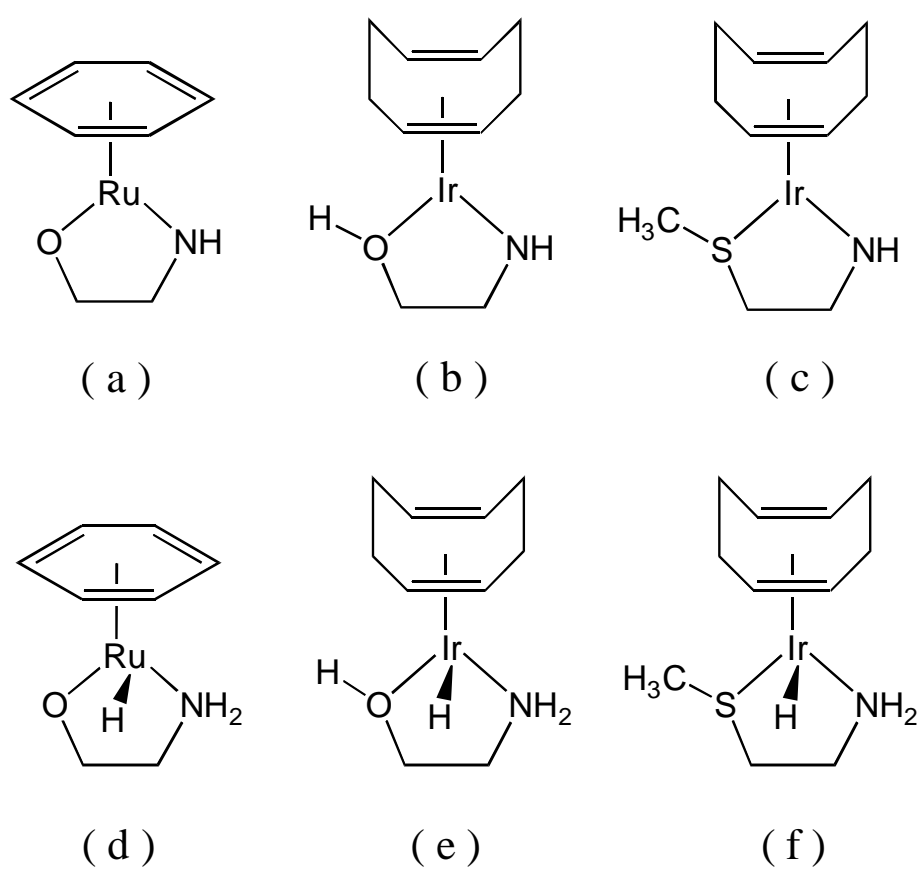


Figure 3.3: Schematic structures of the 16- (top) and 18-electron (bottom) Ru- and Ir-complexes.

Table 3.1: Optimized bond lengths (Å) and first bond dissociation energy (FBDE) (kcal/mol) of ruthenium(II) and iridium(I) hexacarbonyl.

		$r(\text{M}-\text{C})$	$r(\text{C}-\text{O})$	FBDE
$[\text{Ru}(\text{CO})_6]^{2+}$	CPMD-BLYP	2.055	1.132	44.8
	ADF-BLYP ^a	2.054	1.129	45.4
$[\text{Ir}(\text{CO})_6]^{3+}$	CPMD-BLYP	2.069	1.127	68.2
	ADF-BLYP ^a	2.080	1.122	68.1

^aScalar-relativistic corrections are included by way of the zero order regular approximation (ZORA) [158].

3.4 Results

Geometrical differences among the Ir-complexes with the aminoethanol and 2-aminoethylmethylsulfide ligands are, for almost all distances, less than 0.1 Å. In the following figures we will therefore only show structures of the complexes with the aminoethanol ligand. Note that all reported energy values (kcal/mol) are with respect to energy of the metal-methoxide complex. In the following we will first present results for the bare catalysts, followed by the possible coordinations of the substrates to the catalyst, and finally present results for the different mechanisms.

3.4.1 Catalyst Structure and Substrate Coordination

Fig. 3.4 shows the optimized structures of the 16-electron and the 18-electron complexes, both important intermediates in the catalytic cycle. The figure reveals some interesting aspects of the binding within the different complexes. Firstly, we observe that the M–N bond distance is ~ 0.3 Å longer for the 18-electron complex compared to the 16-electron complex. This is to be expected since the character of the nitrogen changes from an amide to an amine. The Ru–O bond is also slightly elongated in the 18-electron complex, in contrast to the Ir–O bond which shows a very small decrease. Overall, it is clear that ligand coordination is stronger in the 16-electron Ru and Ir complexes. Secondly, when comparing the Ru- and Ir-complex the oxygen-metal bond is significantly stronger in the Ru-complex. This difference originates from the fact that Ru has a strong, intramolecular-like, σ -bond with the oxygen, whereas Ir forms a bond involving one of the oxygen lone pairs that has a more intermolecular nature. Obviously, this difference originates from the different valence configurations of Ru and Ir atoms, with Ir having one electron more. Thirdly, note that the metal-hydride bond is ~ 1.6 Å for all complexes and similar to that found for the Rh–H bond in the isoelectronic complex $[\text{RhH}(\text{NH}_3)_2(\text{C}_2\text{H}_4)_2]$ [142]. Apparently this bond length is typical for these metal-hydride complexes and indicates a stable metal-hydride coordination. Finally, it is interesting to note the reversal of the O–C–C–N torsion angle of the ligand-backbone from $+53.7^\circ$ for (4) to -58.1° for (5). Hence, the mode of ligand-coordination is also rather different for Ru compared to Ir.

The coordination of methanol and formaldehyde to the 16- and 18-electron Ru- and Ir-complexes are shown in Fig. 3.5. For the coordination of methanol to the 16-electron complexes we have found two types of stable structures. In the first structure, an intermolecular bond is formed between the amide-nitrogen of the 16-electron complex and the hydroxyl group of methanol, (7) and (8), stabilizing the complex with approximately 2 kcal/mol. Note also the further elongation of the Ir–O bond with 0.11 Å, while the Ru–O bond-length remains unchanged. The second structure involves a direct coordination to the metal via a lone pair of the methanol oxygen, (10) and (11). The complexes differ in the metal-oxygen bond lengths. For Ru the oxygen coordination appears relatively weak with a Ru–O bond-length of 2.42 Å, and is accompanied by a short hydrogen bond of 1.65 Å between the hydroxyl hydrogen of

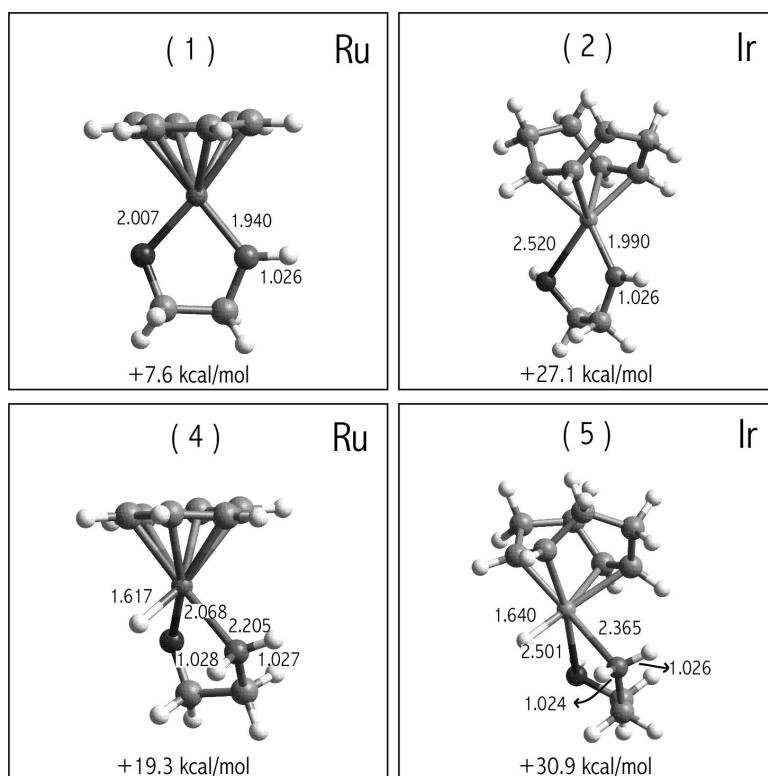


Figure 3.4: Catalyst structure. Optimized geometries of the 16- and 18-electron Ru- and Ir-complexes. Energies are relative to the metal-methoxide complex (21,22).

methanol and the amide-nitrogen. In contrast, for Ir the coordination of the methanol oxygen effectively replaces the coordination of the ligand alcohol oxygen. The Ir–O bond associated with the ligand dissociates without any activation barrier and no methanol-amide hydrogen bond is formed. This shows that the Ir ligand is a clear example of a hemilabile ligand [159], consistent with the observation for the bare catalysts (*supra vide*) that the Ir–O bond is weak. Guiral *et al.* [154] reported a similar de-coordination of one of the Rh–N bonds of the diamine ligand in the electronically equivalent Rh-complex. Comparing the energies relative to methanol dissociation we see that the hydrogen-bonded coordination is stable for both the Ru-complex and the Ir-complexes. The oxygen-metal coordination is even more stable for Ir, but unstable for Ru.

The coordination of formaldehyde to the 18-electron Ru- and Ir-complexes is very similar to that of the hydrogen bonded methanol, with the oxygen of formaldehyde hydrogen-bonded to the amine-nitrogen, see (13) and (14). The complexation energy relative of formaldehyde dissociation is approximately 4 kcal/mol.

3.4.2 Mechanism of Transfer Hydrogenation

Fig. 3.6 shows the structures involved in the formation of the metal-methoxide complex. In Figs. 3.7, 3.8, and 3.9 we show the optimized structures for the concerted hydrogen-bond, migratory insertion and direct transfer mechanisms, respectively. The overall energy profiles are shown in Fig. 3.10. We did not investigate the direct hydrogen transfer mechanism for the Ru-

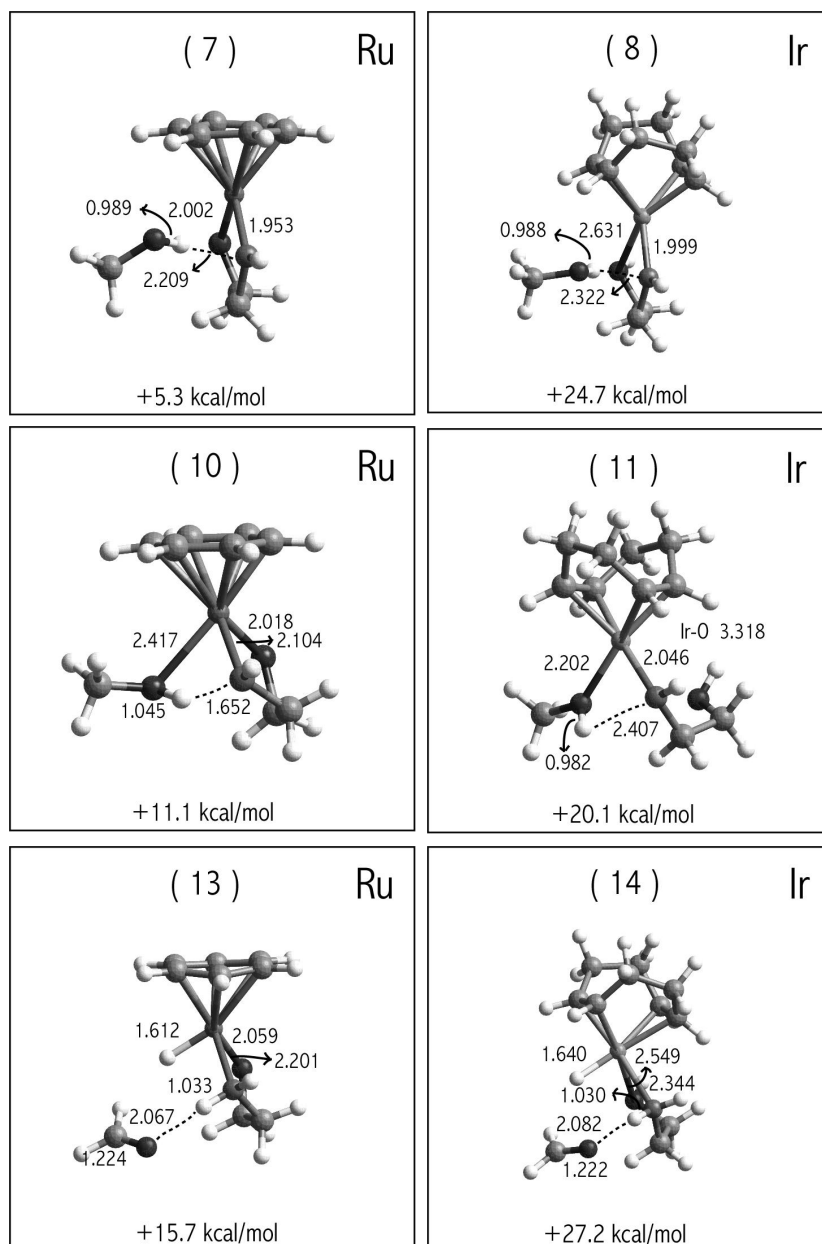


Figure 3.5: Substrate coordination. Optimized geometries of initial coordination of methanol and formaldehyde to the 16- and 18-electron Ru- and Ir-complexes. Energies are relative to the metal-methoxide complex (21,22).

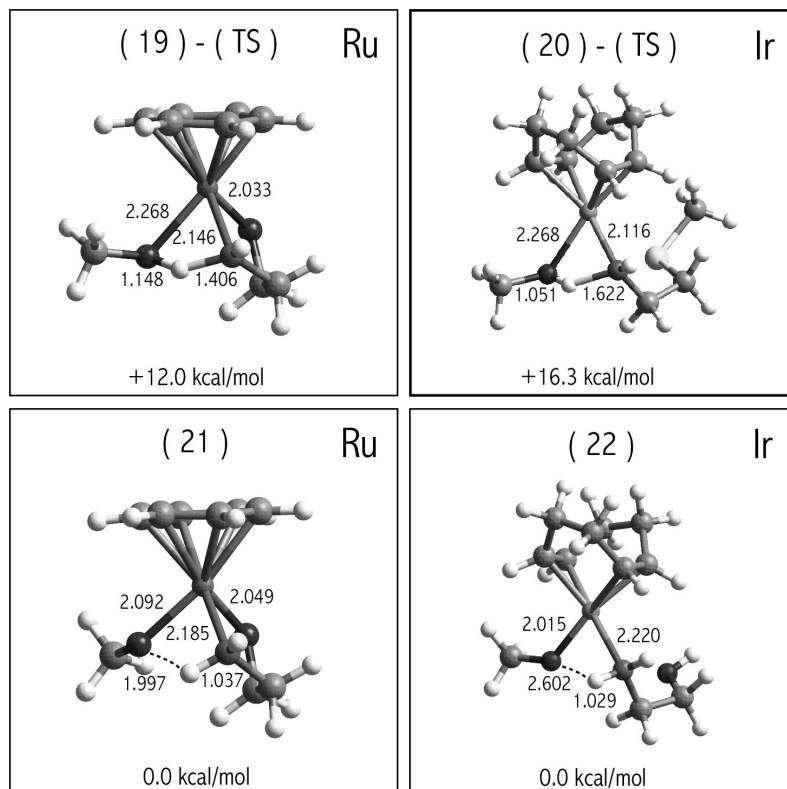


Figure 3.6: Metal methoxides. Structures of formation of the metal-methoxides. Energies are relative to the metal-methoxide complex (21,22,23).

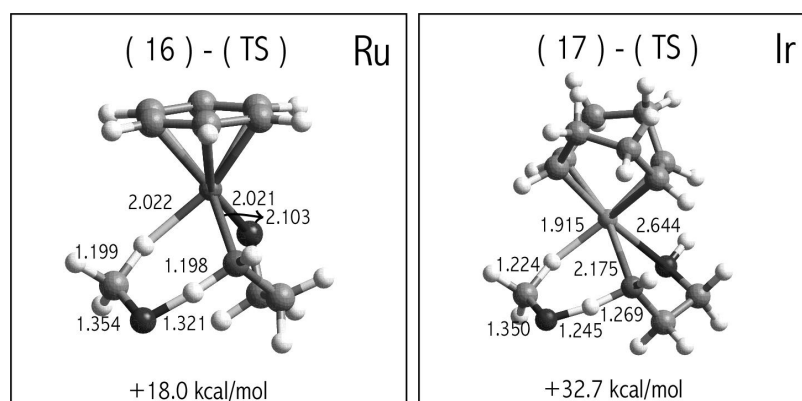


Figure 3.7: Concerted hydrogen transfer. Transition-state structures of the concerted hydrogen transfer (metal-ligand bifunctional mechanism [155]). Energies are relative to the metal-methoxide complex (21,22).

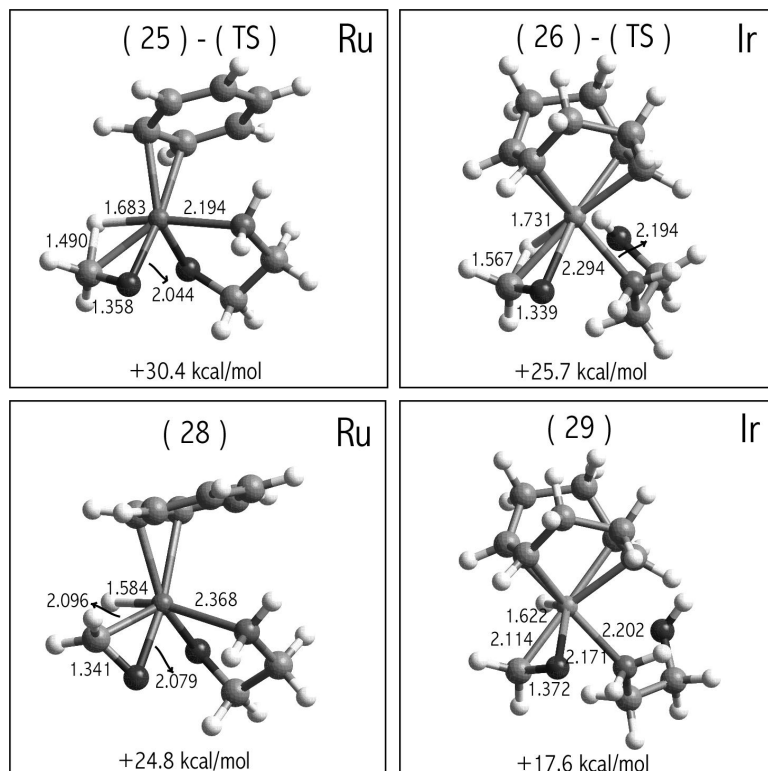


Figure 3.8: Migratory insertion. Optimized structures of the β -elimination/migratory insertion mechanism. Energies are relative to the metal-methoxide complex (21,22).

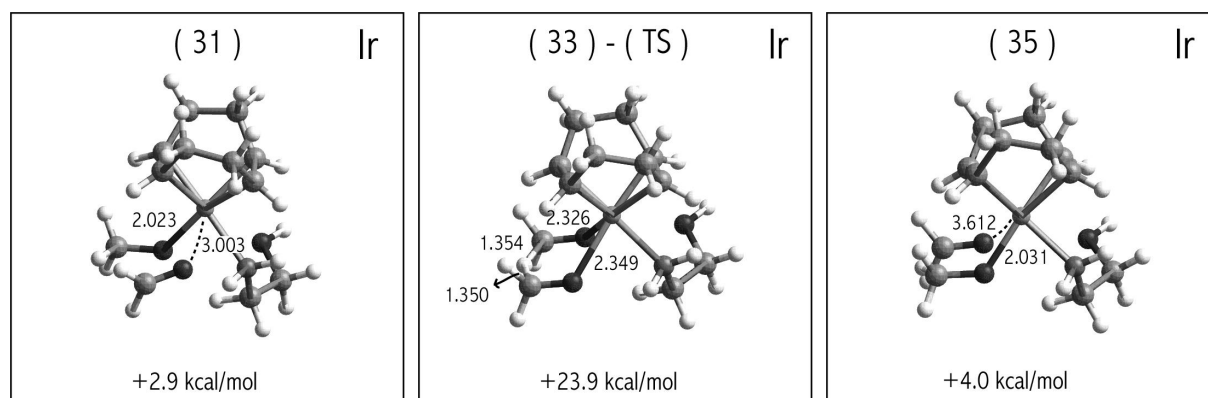


Figure 3.9: Direct hydrogen transfer. Optimized structures of the Ir-catalyzed direct hydrogen transfer mechanism. Energies are relative to the metal-methoxide complex (22).

complex. Alonso *et al.* [31] computed at the B3PW91/6-311+G**^{*}-level a barrier of 30 kcal/mol, and concluded that this mechanism can be excluded.

Concerted transfer of both hydride and proton to the coordinating formaldehyde (Fig. 3.7) is accompanied by a small barrier of 2.3 kcal/mol for the Ru-complex: the TS (16) is only slightly higher in energy than the formaldehyde-associated complex (13). If ZPE corrections are included the barrier is 2.0 kcal/mol. Noyori and coworkers [33] obtained for the same system a barrier of 4.7 kcal/mol.[‡] This result can be considered consistent with our result as differences of a few kcal/mol among different density functionals are common. In general, barriers computed with BLYP are somewhat smaller than those obtained with B3LYP [160]. For the Ir-complexes the barriers are also moderate with a value of 6 kcal/mol for both the aminoethanol ((14)→(17)) and aminosulfide ((15)→(18)) ligands. The reverse reaction, with the methanol transferring its hydrogens to the metal-complex yields reaction barriers of 13 kcal/mol ((7)→(16)), 8 kcal/mol ((8)→(17)), and 13 kcal/mol ((9)→(18)), for the Ru-complex, Ir-aminoalcohol, and Ir-aminosulfide complexes, respectively. Overall, it is clear that the barriers for Ru and Ir-catalyzed concerted transfer of both hydride and proton are modest.

Before describing the migratory insertion and direct transfer mechanisms we first discuss the formation of the metal-methoxide complexes (Fig. 3.6). They are an important intermediate in these mechanisms and obtained via proton transfer from the methanol-coordinated metal-complex. The proton transfer proceeds for the Ru- and Ir-complexes via negligible barriers, yielding very stable metal-methoxide complexes (21), (22), and (23). Note that especially for Ir the formation of the methoxides is highly exothermic with energy differences of at least 20 kcal/mol.

For the Ru-complex the subsequent β -elimination step (Fig. 3.8) from the Ru-methoxide (21) to the formaldehyde-coordinated complex (13), via (24),[§] TS (25), and (28) involves a high energy barrier of 30 kcal/mol. This is caused by electronic saturation of the metal: in structures (25) and (28) the substrate CO coordination to the metal forces a η^6 to η^2 de-coordination of the benzene ligand. Calculations by other groups have shown a similar de-coordination of the benzene ligand [31,33]. The reverse pathway, *i.e.* the hydrogenation of the formaldehyde-coordinated Ru-complex by migratory insertion, (13) →(21), shows an energy barrier of 15 kcal/mol.

Also for both Ir-complexes we see that the β -elimination step (Fig. 3.8) from the methoxide-coordinated complexes (22) and (23) to the formaldehyde-coordinated complexes (14) and (15) proceeds via high energy barriers, with values of 26 and 30 kcal/mol. Again, for the transition states the coordination of the substrate CO bond induces electronic saturation, giving rise to de-coordination of the relatively weakly bound alcohol/sulfide-part of the ligand. Also the locally stable complexes (29) and (30), with formaldehyde coordinated to the metal via its CO π -bond, shows this de-coordination. This de-coordination explains why, in contrast to the Ru-complex, these π -bond coordinated configurations are stable compared to the formaldehyde hydrogen-bonded to the ligand amine group, structures (14) and (15). The reverse migratory insertion pathway hydrogenating the Ir-coordinated formaldehyde, (29)→(22) and (30)→(23), shows energy barriers of 8 and 13 kcal/mol for the Ir-aminoalcohol and Ir-aminosulfide complexes, respectively.

In the direct hydrogen transfer mechanism (see Fig. 3.9) a formaldehyde coordinates to the Ir-methoxide complex, (31) and (32), and subsequently a methyl hydride is exchanged between the facing methoxide and formaldehyde carbon groups. For both Ir-complexes the formaldehyde coordination is accompanied by a slight increase in energy, 1-3 kcal/mol. The subsequent hydride exchange proceeds via a energy barrier of 24/19 kcal/mol for the Ir-aminoalcohol/amino-

[‡]B3LYP/6-311++G(d,p)-level including ZPE corrections.

[§]Configuration (24), not shown in the figures, constitutes a Ru-methoxide complex with an η^2 -coordinated benzene.

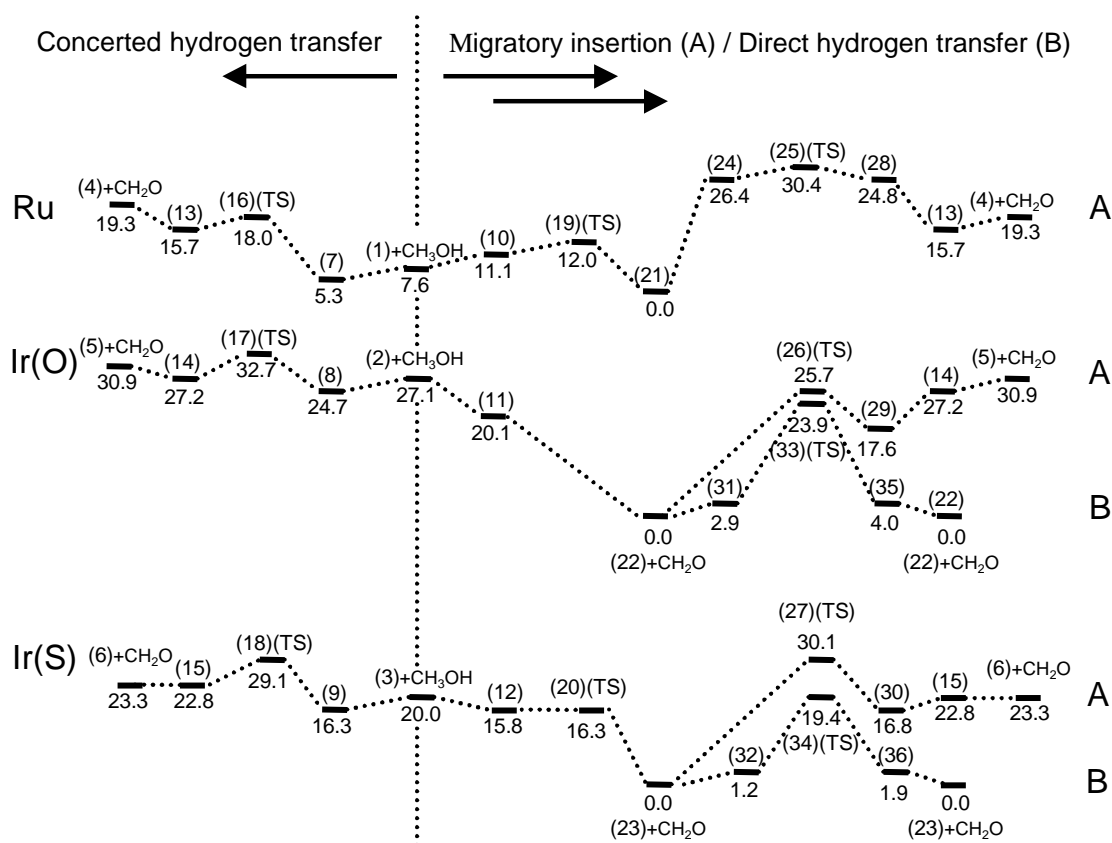


Figure 3.10: Energy profiles for the concerted hydrogen transfer (left), migratory insertion (right, A) and direct hydrogen transfer (right, B). Ir(O) denotes the Ir catalyst with a aminoethanol ligand and Ir(S) that with 2-aminoethylmethylsulfide ligand. The energy profile for Ru-catalyzed direct hydrogen transfer is not calculated, see text. Note that the energy profiles for the direct hydrogen transfer involve the metal-complex, one methanol, and one formaldehyde. Energies in kcal/mol (without ZPE corrections) are relative to the metal-methoxide complex (21,22,23).

sulfide complexes. Note that, as for the β -elimination/migratory-insertion transition state, the relatively weakly bound alcohol/sulfide-part of the ligand is de-coordinated from the Ir in the transition state, again due to electronic saturation.

3.4.3 Iridium(I) versus Ruthenium(II)

Since the Ir atom has a $5d^7 6s^2$ valence electronic configuration, whereas the Ru atom a $4d^8 5s^1$ configuration, it is evident that they are not isoelectronic. Fig. 3.11 shows the 3D-contour plots of the electronic charge density of the highest occupied molecular orbital (HOMO) of the 16-electron and 18-electron complexes, in which the charges on selected atoms, as derived from a fit to the molecular electrostatic potential (ESP) [161] are also given. For the Ru-complexes there is a substantial amount of electron density situated on the ligand, while for the Ir-complexes it is almost exclusively located at the metal center. As noted before, this is due to the difference in bonding of the metal to the oxygen of the ligand, i.e. a strong Ru–O σ -bond and a weak Ir–O bond via one of the lone pairs of oxygen. The charges on the metal give a similar picture with

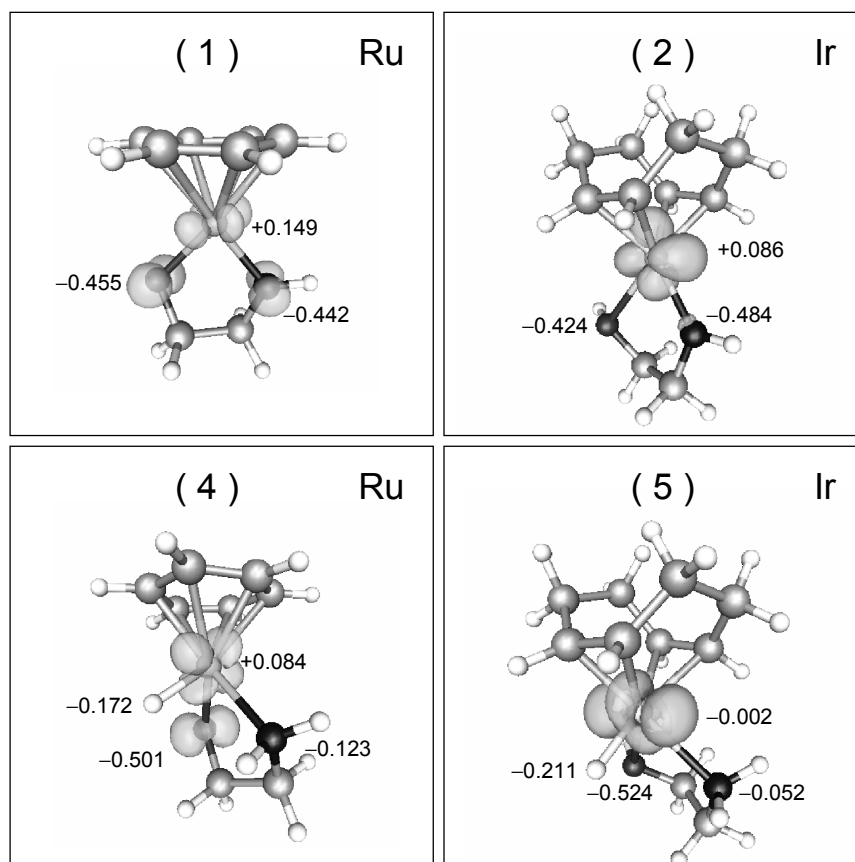


Figure 3.11: 3D-contour plots of the electronic charge density of the highest occupied molecular orbital (HOMO) of the 16-electron (top) and 18-electron (bottom) Ru- and Ir-complexes. Selected atomic charges derived from the molecular electrostatic potential (ESP) are also given.

a more positive charge on Ru compared to Ir. In essence, the Ir atom has closed-shell nature and is not very polarizable, hence the preference for hemilabile ligands as we have found. In contrast, the Ru atom is highly polarizable which leads to strong coordination of the ligand. This could explain the difference we find in the reactivity for the catalyzed hydrogen transfer, since in the case of the Ru-compound, also pointed out by Noyori [155], the ligand actively participates in the mechanism. On the other hand, for the Ir-compound the ligand seems to be more an important spectator and the actual hydrogen transfer occurs at the metal center.

3.5 Discussion

From the calculated energy profiles (Fig. 3.10) it is evident that, at least for the gas-phase model systems considered here, the metal-alkoxide complex comprises an important intermediate in the catalytic cycle. For the Ru-complex the metal-alkoxide complex is stable by at least 5 kcal/mol compared to the other intermediates along the reaction paths. For the Ir-complexes this energy difference is far more pronounced: 17 and 16 kcal/mol for the aminoalcohol- and aminosulfide-coordinated complexes, respectively. Indeed, Noyori and coworkers refer to these stable complexes as 'reservoirs' or 'sinks' [33], and Halpern has pointed out that in the early 80s such

reservoir species may play an important role in stabilizing catalytic systems [11].

The energy profiles of the concerted hydrogen transfer and migratory insertion/ β -elimination mechanism for the Ru-complexes (Fig. 3.10, upper profile) provides a picture that is fully consistent with the B3LYP and MP4 results of Noyori and coworkers [33]. It is also in qualitative agreement with computational studies of other, similar model systems [31, 32]. Comparison of the energy profiles shows that the concerted hydrogen transfer pathway has the lowest transition-state energy with a local barrier of 2 kcal/mol for the hydrogenation of formaldehyde ((13) \rightarrow (16)) and 13 kcal/mol for the de-hydrogenation of methanol ((7) \rightarrow (16)). A direct consequence is that the stable metal-methoxide complex, intermediate involved in the migratory insertion/ β -elimination pathway, is on a non-productive route, and will give rise to a reservoir of inactive catalysts. Note that de-coordination of methanol from the metal-methoxide intermediate involves a reaction barrier of 12 kcal/mol ((21) \rightarrow (19)) that is comparable to the de-hydrogenation barrier (7) \rightarrow (16), and is therefore important to the overall kinetics of the catalytic cycle. The calculations strongly suggest that the methanol de-hydrogenation is the rate-limiting step whereas formaldehyde hydrogenation proceeds relatively easily. Analysis of an experimental study of a Ru-complex with a proper diamine-derivative ligand arrived at the same conclusion [122].

The energy profiles for the Ir-complexes (Fig. 3.10, middle and lower profile) provide a different picture. Comparison of the energy profiles for the aminoalcohol-coordinated Ir-complex shows that the β -elimination ((22) \rightarrow (26)) and direct hydrogen transfer ((22) \rightarrow (33)) are competing mechanisms with transition-state energies at least 6 kcal/mol lower than that of the concerted hydrogen transfer route. However, in the catalytic cycle of the migratory insertion/ β -elimination mechanism the highest energy intermediate state is the 18-electron Ir-complex (5), whereas in the direct hydrogen transfer mechanism this intermediate does not appear, and the highest-energy intermediate state, *i.e.* the 16-electron Ir-complex (2), is 4 kcal/mol lower. Hence, the calculations suggest that the direct hydrogen transfer mechanism is preferred. For the aminosulfide-coordinated Ir-complex the direct hydrogen transfer mechanism ((23) \rightarrow (34)) has by far the lowest transition-state energy with a barrier for hydride exchange ((23) \rightarrow (34) \rightarrow (23)) of 19 kcal/mol. Hence, also for the aminosulfide-coordinated Ir-complex our calculations suggest that the 18-electron Ir-complex does not participate actively in the catalytic cycle.

For both Ir-complexes the methanol de-coordination energy of the Ir-methoxide complexes (22) and (23), with values of 27 and 20 kcal/mol, respectively, is significant and comparable to the energy barrier for the direct hydrogen transfer. They are therefore, as in the Ru-system, important for the kinetics of the full catalytic cycle. For the aminoalcohol-coordinated complex the energy difference between lowest and highest energy intermediate along the reaction path (27 kcal/mol) is significantly higher than that of the aminosulfide-coordinated complex (20 kcal/mol). This indicates a lower activity of the former complex, consistent with experimental observations [153].

The mechanisms for Ru- and Ir-catalyzed transfer hydrogenation suggested by our calculations are consistent with the experimental observation that for Ir-complexes the enantioselective distribution is dominated by the choice of the hydrogen source [153]. In contrast, for Ru-complexes the choice of the hydrogen source does not effect the stereochemical outcome [5].

Comparing the energy profiles of the Ru-complex and Ir-complexes may give an indication why the reaction pathways differ. Taking the isolated methanol and 16-electron metal complexes, structures (1), (2), and (3) as reference we see that the transition-state energies for the concerted hydrogen transfer mechanism show a small spread. In contrast, the transition states of the migratory insertion or direct hydrogen transfer mechanism show significant energy differences between Ru and Ir, with the Ir transition-state energies more than 20 kcal/mol lower. This relative difference in transition-state energies can be qualitatively understood from the

structure of the transition states (25), (26), (27), (33), and (34). Both the migratory insertion and direct hydrogen transfer mechanism require a transition state with a high coordination of the metal. To prevent electronic over-saturation one of the stabilizing ligands has to change coordination. For the Ru-complex this is achieved by η^6 to η^2 partial de-coordination of the strongly bound benzene ligand, whereas for the Ir-complexes the alcohol/sulfide-part of the hemilabile aminoalcohol/aminosulfide ligand de-coordinates. This is not possible in the Ru-complex that has a strongly bound aminoalcohol group. The coordination change of the strongly bound benzene ring is far more destabilizing than the de-coordination of the weakly bound alcohol/sulfide group giving rise to the observed difference in the transition-state energies of more than 20 kcal/mol.

For the Ir-compounds it is not clear how chiral induction is achieved when the aminoalcohol/aminosulfide ligand is partially de-coordinated. However, Noyori and coworkers [162] showed for the ruthenium(II)-catalyzed asymmetric hydrogen transfer that a large part of the chiral induction is *electronic* and not *steric* in nature, caused by the attractive CH/ π interaction between the η^6 -arene and the aromatic substituent in carbonyl substrates. A similar effect can also be envisaged for the iridium(I)-catalyzed transfer since experiments showed that the catalytic performance is far superior for aromatic ketones compared to dialkyl ketones [69, 153]. Further computational studies including pro-chiral substrates should reveal the origin of enantioselection for the iridium(I)-catalyzed transfer hydrogenation.

Another important aspect is the role of the solvent, in particular when interactions between the catalyst and the substrates are strong, as in the present study, where commonly used solvents are 2-propanol or formic acid. Alonso *et al.* [31] showed that incorporating electrostatic effects by a simple polarized continuum model (PCM) has a substantial effect on barrier heights. Moreover, these type of solvents may form strong hydrogen bonds both with the substrate and catalyst. This may also have a large impact on the reactivity of the catalyst. For example, Burk *et al.* [35] showed that the Rh-catalyzed hydrogenation of enol esters in methanol gave 100 % conversion, while benzene as solvent inhibited the reaction completely. The influence of the solvent can be particularly important for hemilabile ligands where there is no rigidly defined catalyst structure, and a solvent molecule can more easily coordinate to the metal or ligand.

3.6 Summary

We have performed a DFT-BLYP based computational study to compare model systems for transfer hydrogenation reactions among alcohols and ketones catalyzed by Ru-aminoalcohol, Ir-aminoalcohol, and Ir-aminosulfide complexes. In this comparison we considered three reaction mechanisms: 1) concerted hydrogen transfer, also known as the metal-ligand bifunctional mechanism [33], 2) migratory insertion, and 3) direct hydrogen transfer. Our results for the Ru-complex system are fully consistent with the results of Noyori and co-workers [33] who studied the same model system using DFT-B3LYP and MP4 computational methods. The calculations suggest that the reaction mechanism for the Ru- and Ir-catalyzed reactions are fundamentally different. For the Ru-complex the reaction proceeds via concerted hydrogen transfer whereas for both the Ir-aminoalcohol and Ir-aminosulfide complexes the reaction proceeds via direct hydrogen transfer between simultaneously coordinated ketone and alcohol. This is consistent with experimental data on the dependence of the enantioselective distribution on the hydrogen source. Comparing the results for the Ir-aminoalcohol and Ir-aminosulfide complexes we found our results to be consistent with the experimental data, with the Ir-aminoalcohol energy profile showing a significantly higher reaction barrier.

Both for the Ru-complex and Ir-complexes the metal-alkoxide complex plays an important role, and is in all cases the most stable complex on the potential energy surface. In the Ru-

catalyzed reaction it is not an intermediate of the reaction mechanism, and therefore gives rise to a reservoir of inactive catalysts. In contrast, for the Ir-catalyzed reaction it is an intermediate along the reaction path.

The calculations suggest that the distinction between reaction mechanism for Ru- and Ir-complexes can be attributed to differences in the nature of the binding of the ligands. The direct hydrogen transfer mechanism, as well as the migratory insertion mechanism, requires partial de-coordination of the ligands. For the Ru-complex this is achieved by a η^6 to η^2 partial de-coordination of the strongly bound benzene ligand, whereas for the Ir-complexes the alcohol/sulfide-part of the hemilabile aminoalcohol/aminosulfide ligand de-coordinates relatively easily. Consequently, the transition state of the Ru-complex is far more destabilized than the transition state in the Ir-catalyzed reaction.

Finally we should mention that computational studies such as presented here, although at the limit of present day capabilities, are still open for significant improvement. The variation in calculated energy profiles among different computational methods, *e.g.* DFT versus MP2 [33], indicates that the underlying electronic structure calculation has an inaccuracy that is not negligible. This should be improved in order to be able to do precise quantitative predictions. Secondly, the role of the solvent, neglected in the present study as well as in most related studies reported in literature, is expected to be significant. This holds in particular for metal-catalyzed transfer hydrogenation in alcohol solutions, where there are relatively large changes in solvation energies due to strong hydrogen bonding among substrate, catalyst, and solvent. This implies that a truly realistic description requires incorporation of solvent molecules.

Chapter 4

Ab Initio Simulation of Ruthenium Catalyzed Transfer Hydrogenation of Ketones in Methanol Solution*

Jan-Willem Handgraaf and Evert Jan Meijer

Department of Chemical Engineering, University of Amsterdam,
Nieuwe Achtergracht 166, 1018 WV Amsterdam, The Netherlands

Abstract

We report the first computational study of a full atomistic model of the ruthenium catalyzed transfer hydrogenation of ketones in methanol solution. Using *ab initio* molecular dynamics techniques we determined the thermodynamics, mechanism, and electronic structure along the reaction path. In order to assess the effect of the solvent quantitatively we make a direct comparison with the gas phase reaction. We find that the energy-profile in solution bears little resemblance with the profile in the gas phase and a distinct solvation barrier is found: the activation barriers in both directions are lowered and the concerted hydride and proton transfer in the gas phase is converted into a sequential mechanism in solution. Our results indicate that besides the metal-ligand bifunctional mechanism, as proposed by Noyori, also a concerted solvent-mediated mechanism is feasible. Our study gives a new perspective of the active role a solvent can have in transition metal catalyzed reactions.

*Paper in preparation.

4.1 Introduction

One of the most fundamental transformations in (bio)chemistry is the asymmetric reduction of C=O and C=N bonds forming stereospecific centers in molecules [4]. In this field, Noyori *et al.* initiated significant progress by introducing well-designed chiral ruthenium (Ru) compounds that catalyze the transfer hydrogenation from 2-propanol to pro-chiral ketones with a high enantioselectivity [116]. In particular, Ru compounds with aminoalcohol- and *N*-tosylated diamine-based ligands perform well with an enantiomeric excess (e.e.) of up to 99% [5,32,118]. Excellent reviews on this subject can be found in the literature [27,29,163].

Obviously, rational improvement of reaction characteristics such as rate and selectivity requires a good understanding of the mechanistic and electronic aspects of the molecular transformation. To date it is still a formidable challenge to obtain experimentally direct and accurate insight in the mechanistic pathways of chemical reactions, although progress has been made in the field of low-temperature NMR spectroscopy, see *e.g.* Ref. [24]. The most important limitation is that key intermediates have often a very short lifetime. Evidently, this holds also for the transition metal catalyzed reactions addressed in the present work. Computational studies do not suffer from these limitations and provide therefore a valuable complementary approach to study these reactions. A number of computational studies of simplified gas phase Ru model complexes have been performed in order to unravel the underlying mechanistic reaction pathway of the catalyzed transfer hydrogenation of ketones [31–33,164]. These studies showed that the preferred mechanistic pathway is the concerted transfer of the proton of the amine ligand and the metal coordinated hydride to the pro-chiral ketone, referred to by Noyori as the metal-ligand bifunctional mechanism [155]. Recent kinetic isotope measurements showed strong support for this mechanism [165].

A serious drawback of these gas-phase computational studies is the neglect of solvent interactions, which can be particularly important for the protic polar solvents, *i.e.* 2-propanol and formic acid, commonly used in the transfer hydrogenation. These kind of solvent molecules may have significant electrostatic and hydrogen bond interactions with the substrate and the ligands of the metal complex. Alonso *et al.* [31] showed that the incorporation of the electrostatic effects of the solvent by a simple polarized continuum model already has a substantial effect on barrier heights of the Ru-catalyzed transfer hydrogenation. Also, specific solute-solvent interactions can increase or decrease the reaction rate, or could give rise to a different reaction mechanism [166].

A powerful approach to study chemical reactions in solution is *ab initio* molecular dynamics (MD), where the interatomic forces are obtained from accurate electronic structure calculations. Examples of recent studies are the acid-catalyzed addition of water to a carbonyl group [167], the ligand substitution of an aqueous *cis*-platin complex [168], and the chemical involvement of solvent water molecules in the Fenton oxidation reaction [169]. Furthermore, this approach can also provide valuable fundamental information on systems that are difficult to access experimentally, such as the transport of the hydroxide ion in aqueous solution [170]. To date, almost all of these studies were in aqueous environment [171]. Recently, we investigated the simplest alcohol, methanol, with *ab initio* MD techniques [172], and showed that the computed structural properties were in close agreement with state-of-the-art neutron diffraction experiments. These results encouraged us to study the Ru-catalyzed transfer hydrogenation of ketones in methanol solution. Such a, computationally challenging, study should provide a more complete picture of transition metal catalyzed transfer hydrogenation.

Here, we present a density-functional-theory (DFT)-based Car-Parrinello MD simulation of a full atomistic model of the Ru-catalyzed ketone hydrogenation in the gas-phase and in a methanol solvent. We determined the thermodynamics along the reaction pathway and, most

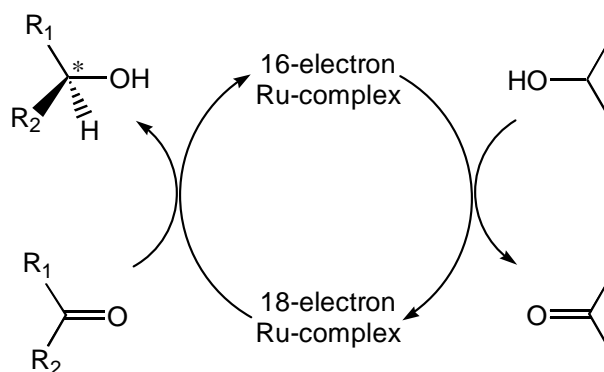


Figure 4.1: Ru-catalyzed asymmetric transfer hydrogenation of ketones.

importantly, for the first time we were able to quantitatively determine the role of the solvent on the reaction mechanism and energetics. This chapter is organized as follows. First we describe the models employed, secondly a short explanation of the computational methods is given, then we present and discuss the results, and we end with the conclusions.

4.2 Model and Methods

Fig. 4.1 shows the simplified Ru-catalyzed cycle of the asymmetric transfer hydrogenation of ketones [33,155]. The 16-electron Ru-complex is generated from a catalyst precursor, typically the corresponding Ru-halide, using an inorganic base such as KOH, NaOH, or K₂CO₃. In a standard experiment 2-propanol acts both as solvent and hydrogen donor. It first reacts with the 16-electron complex to form the 18-electron Ru-hydride complex. This in turn reacts with a pro-chiral ketone to form a chiral secondary alcohol. Both the 16- and the 18-electron complex have been isolated and the crystal structure has been elucidated [122].

In the present computational study we used a simplified form of an experimentally well-performing Ru-arene-aminoalcohol compound [121], similar to that of Noyori and coworkers [33] and Handgraaf *et al.* [164], with a stabilizing benzene ligand and an ethanolamine ligand (Fig. 4.2). We studied a symmetric model reaction with methanol being the hydrogen donor and formaldehyde representing the ketone. For the hydrogenation reaction we only consider the concerted transfer of the proton of the amine ligand and the Ru coordinated hydride to the ketone (Fig. 4.3). For a Ru-complex with an aminoalcohol ligand Alonso *et al.* [31], Noyori and coworkers [33], Petra *et al.* [32] and Handgraaf *et al.* [164] have found recently that this concerted transfer mechanism is energetically favorable over other mechanisms proposed in the literature.

The electronic structure calculations were performed using the Kohn-Sham formulation of DFT. We employed the BLYP functional that combines a gradient correction term for the exchange energy as proposed by Becke [42] with a correction for the correlation energy due to Lee, Yang, and Parr [43]. The choice for BLYP was guided by its good description of the structure and dynamics of liquid methanol [172] where hydrogen bonds are, as in liquid water [78], the

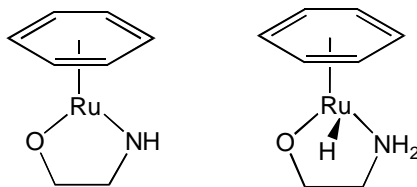


Figure 4.2: Schematic structures of the 16- (left) and 18-electron (right) Ru-complexes.

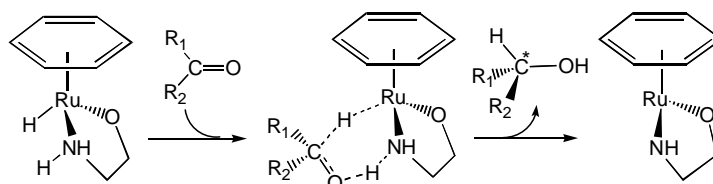


Figure 4.3: Concerted hydrogen transfer (metal-ligand bifunctional mechanism [155]).

dominant interactions.

The DFT-based MD simulations were performed with the Car-Parrinello method [50, 51] using the CPMD package [82]. The pseudopotential method is used to restrict the number of electronic states to those of the valence electrons. The interaction with the core electrons is taken into account using semi-local norm-conserving Martins-Troullier pseudopotentials [57]. The pseudopotential cut-off radii for C, N, O and H were 1.23, 1.12, 1.10 and 0.50 a.u., respectively, both for the $l=s$ and $l=p$ terms. The Ru pseudopotential was of the semi-core type including the highest s - and p -shell electrons as valence electrons. It was generated using an ionized Ru^+ -configuration with the electrons treated relativistic in the scalar approximation. The cut-off radii of the $l=s$, $l=p$ and $l=d$ terms of pseudopotentials were 1.10, 1.20 and 1.24 a.u., respectively. The Kohn-Sham states are expanded in a plane-wave basis including waves up to an energy of 70 Ry. Test calculations showed that with this setup structural properties are converged within 0.01 Å and 0.02 Å for the intra- and intermolecular bonds, respectively. Binding energies are converged within 0.25 kcal/mol. The hydrogen nuclei were treated as classical particles with the mass of the deuterium isotope in order to be able to use a larger time step [77]. In this way, the fictitious mass associated with the plane-wave coefficients is chosen at 1100 a.u., which allowed for a time step in the numerical integration of the equations-of-motion of 0.169 fs, while maintaining adiabatic conditions for the electrons.

We performed calculations of a methanol solvated system consisting of the Ru-complex and 40 methanol molecules in a periodic cubic box with an edge of 14.1 Å. The volume of the box was obtained from a constant pressure and temperature simulation performed at ambient conditions using an empirical force field. In this simulation the Ru-complex was kept fixed as the force field does not describe properly the intramolecular bonds of the complex [173]. For the solvated system the simulations were performed at a temperature of 293 K that was imposed using the

Table 4.1: Free-energy changes (kcal/mol) at $T = 293$ K along the reaction path of the concerted hydrogen transfer in the gas phase (left) and in the methanol solution (right) at different values of the constraint Q . Mean force of constraint is given in 10^{-10} N. Energies are relative to the lowest value in the gas phase and in methanol solution, respectively.

Q^a (Å)	ΔA^b	Q (Å)	$\langle F \rangle^c$	ΔA^b	Q (Å)	$\langle F \rangle^c$	ΔA^b
-3.167	0.4	-3.0	-0.29	0.0	0.3	-1.90	12.0
-2.579	0.0	-1.5	4.76	1.0	1.5	0.85	11.6
-1.599	4.6	-1.3	6.54	2.7			
-0.823	13.9	-1.0	9.14	7.0			
-0.491	14.3	-0.8	2.54	9.5			
-0.228	14.2	-0.7	0.17	9.7			
0.007	12.4	-0.6	2.41	10.5			
0.171	11.6	-0.4	3.11	11.5			
0.680	10.7	-0.1	2.44	13.0			
1.425	9.6	0.1	-0.59	12.2			

^aThis is not a constraint, but simply the difference in distance between r_{C-H} and r_{Ru-H} .

^bValues include estimate for the zero-point energy, see text.

^cStatistical errors are around 0.5×10^{-10} N.

Nosé-Hoover thermostat [94]. From the force field simulation we choose an initial configuration for the *ab initio* MD simulation where one of the methanol molecules is hydrogen-bonded to the nitrogen of the ligand. This molecule was going to serve as the hydrogen donor. For comparison we also performed calculations of a gas-phase Ru-complex and a micro-solvated Ru-complex in a periodic cubic box of $15 \times 13 \times 13 \text{ \AA}^3$, large enough to have negligible interactions among the periodic images. The micro-solvated complex comprises, in addition to the Ru-complex, five methanol molecules hydrogen bonded to the ligand oxygen and to the methanol/formaldehyde substrate.

From the literature we know that the gas-phase barrier for oxidative addition of methanol is larger than 10 kcal/mol, and therefore a rare event on the timescale of *ab initio* MD (≈ 10 ps). To be able to study the reaction by *ab initio* MD, a reactive event must be enforced on the system by imposing a change of a suitable reaction coordinate Q . Here, we choose as reaction coordinate the transfer of the hydride:

$$Q = r_{C-H} - r_{Ru-H}, \quad (4.1)$$

where r_{C-H} is the distance between a hydrogen nucleus and the carbon nucleus of the methyl group of the hydrogen donor and r_{Ru-H} is the distance between the same hydrogen nucleus and the Ru nucleus. Now by changing the value of Q using the constraint MD setup the C-H bond of the donor is gradually broken whereas the Ru-H bond is gradually formed. To impose the constraint a Lagrange multiplier is added to the Car-Parrinello Lagrangian (cf. Eq. 1.13). The value of the Lagrange multiplier is related to the constraint force. The calculation of the free-energy[†] profile $\Delta A(Q)$ is then obtained as [168, 174]

$$\Delta A(Q) = - \int_{Q_0}^Q dQ' \langle \lambda \rangle_{Q'}, \quad (4.2)$$

where $\langle \lambda \rangle_{Q'}$ is the average of the Lagrange multiplier over a MD run with the constraint value fixed to Q' . The actual calculation consisted of 12 constrained MD runs along the reaction path

[†]Helmholtz free energy since the volume is kept constant during the simulation.

with Q -values in the range of -3.0 to 1.5 Å and a typical run time 4 to 5 ps. The free-energy increments were then obtained from the discrete approximation to Eq. 4.2.

The gas-phase finite-temperature free-energy changes[‡] at 293 K were estimated using

$$\Delta A = \Delta E_0 + \Delta E_{\text{ZPE}} + \Delta A_{\text{corr}}, \quad (4.3)$$

where ΔE_0 is the change in electronic energy, ΔE_{ZPE} the change in zero-point vibrational energy and ΔA_{corr} constitutes the change in vibrational, rotational, and translational free energy. Both corrections to ΔE_0 are computed in the classical harmonic approximation [175, 176]. All zero-point energies were calculated using deuterium. We estimated ΔE_{ZPE} of the solvated system by calculating the ZPE of the reacting complex (Ru-complex + substrate) taken from a single configuration of the trajectory at the different values of Q along the reaction path, implying that the zero-point energy corrections of the solvent molecules were neglected.

4.3 Thermochemistry

Table 4.1 lists the free-energy changes of the concerted hydrogen transfer in the gas-phase and in the methanol solution. Fig. 4.4 shows for the solvated system the mean force of constraint Q , and Fig. 4.5 shows the associated free-energy profiles of the gas phase (compare Fig. 3.10) and the solvated system. Fig. 4.6 shows three snapshots of the solvated system at key points along the reaction path. In the following we discuss the reaction path going from methanol to formaldehyde, *i.e.* in the Figs. 4.4 and 4.5 going from right to left. As expected, in the initial phase of the hydride transfer from the methyl C to Ru, $Q = -3.0$ to -1.0 Å (see snapshot), the mean force of constraint increases, yielding an increase of the free energy. Surprisingly, in the range of $Q = -1.0$ to -0.8 Å the constraint force value decreases in magnitude and reaches at $Q = -0.7$ Å (see snapshot) a value of approximately zero. At this point the free energy profile reaches a small plateau. During the MD simulation at $Q = -0.7$ Å the proton associated with the substrate hydroxyl hydrogen transfers back and forth several times between the substrate-oxygen and the nitrogen of the aminoalcohol ligand. However, the proton is bound predominantly to nitrogen. Increasing Q further we find a second positive increase of the force in the range of $Q = -0.7$ to -0.4 Å (see snapshot) yielding a further increase of the free energy. At $Q \approx 0.0$ Å the force changes sign indicating the location of the transition state, which is a formaldehyde coordinated ru-complex, clearly different from the

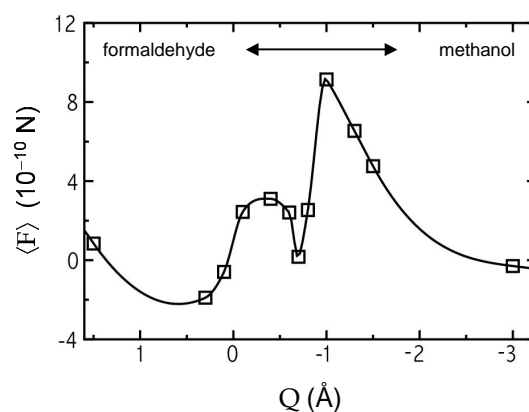


Figure 4.4: Mean force of constraint along the reaction path of the concerted hydrogen transfer in the methanol solution. Statistical errors are around 0.5×10^{-10} N.

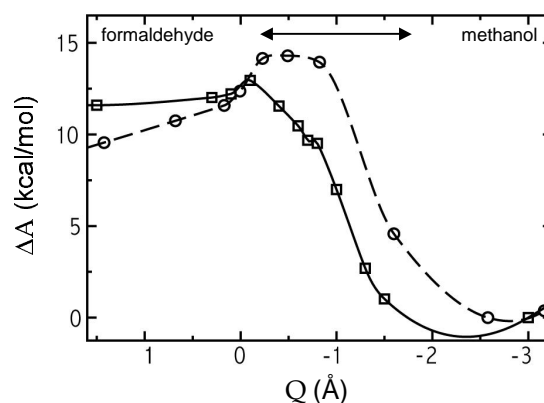


Figure 4.5: Free-energy profiles of the concerted hydrogen transfer in the gas phase (dashed lines, circles) and in the methanol solution (solid lines, squares). Profiles are relative to lowest energy value in the gas phase and in the methanol solution, respectively (cf. Table 4.1).

[‡]Gibbs free-energy changes are in this case equal to the Helmholtz free-energy changes as the number of moles of gas does not change during the reaction.

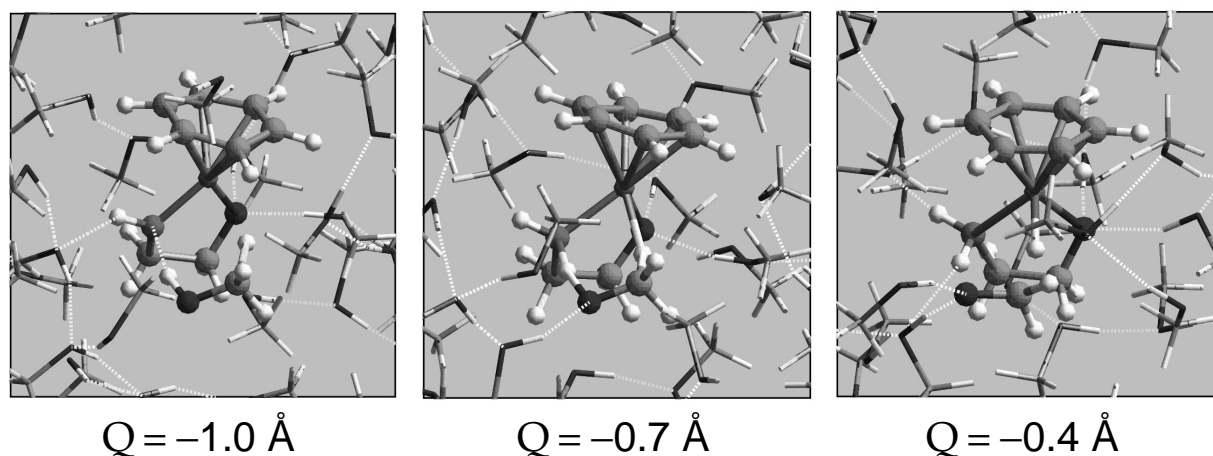


Figure 4.6: Snapshots of the solvated system along the reaction path at $Q = -1.0$, -0.7 and -0.4 Å. Ru-complex and substrate are shown as ball-stick models, solvent molecules as cylinders, and dotted lines indicate hydrogen bonds.

gas-phase transition state at $Q = -0.8$ (see Fig. 3.7). Hence, we want to stress that the associated barrier in solution is due to the coordinating solvent and not to chemical transformations.

In the gas-phase system the free-energy profile is rather flat near the transition state (Fig. 4.5). The gas-phase barriers for oxidative addition of methanol and reductive elimination of formaldehyde are 14.3 and 4.8 kcal/mol, respectively. Noyori and coworkers [33] obtained for the same system barriers of 12.2 and 4.7 kcal/mol,[§] in excellent agreement with our results, see also section 3.4.2 of the previous chapter. The free-energy profile of the solvated system differs substantially from the gas-phase free-energy profile. Whereas in the gas-phase system the free-energy profile shows a rather smooth behavior, we see a step-wise free-energy profile for the solvated system. It suggests a two-stage process, with, when converting methanol into formaldehyde, a first stage towards an intermediate state at $Q \approx -0.7$ Å with an activation barrier of 9.7 kcal/mol, followed by a second stage towards a transition state at $Q \approx 0.0$ Å with an energy of 13.0 kcal/mol. This intermediate state will be short-lived as it is not a true minimum. The activation barrier for the reverse reaction, *i.e.* converting formaldehyde into methanol is small, only 1.4 kcal/mol.

Compared to the gas-phase, the overall barriers for the oxidative addition and reductive elimination in methanol solution are reduced by 1.3 and 3.4 kcal/mol, respectively. Here it should be noted that a complete assessment of the thermochemistry of the reaction requires the inclusion of the energetics of the de-coordination and solvation of formaldehyde and methanol into solution. Yet, it is clear that the presence of the solvent has a significant effect on the en-

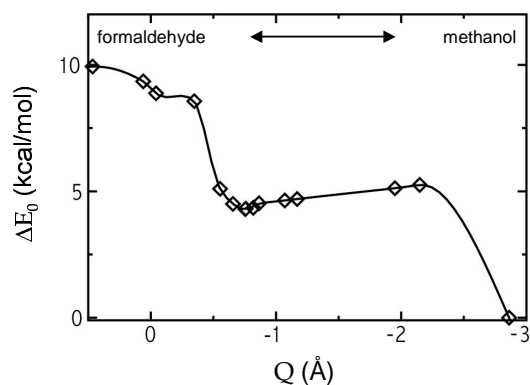


Figure 4.7: Energy profile (kcal/mol) of the concerted hydrogen transfer in the micro-solvated system. Energy values are without zero-point energy corrections and entropy contributions. Q -values are simply the difference in distance between r_{C-H} and r_{Ru-H} .

[§]B3LYP/6-311++G(d,p)-level including ZPE corrections.

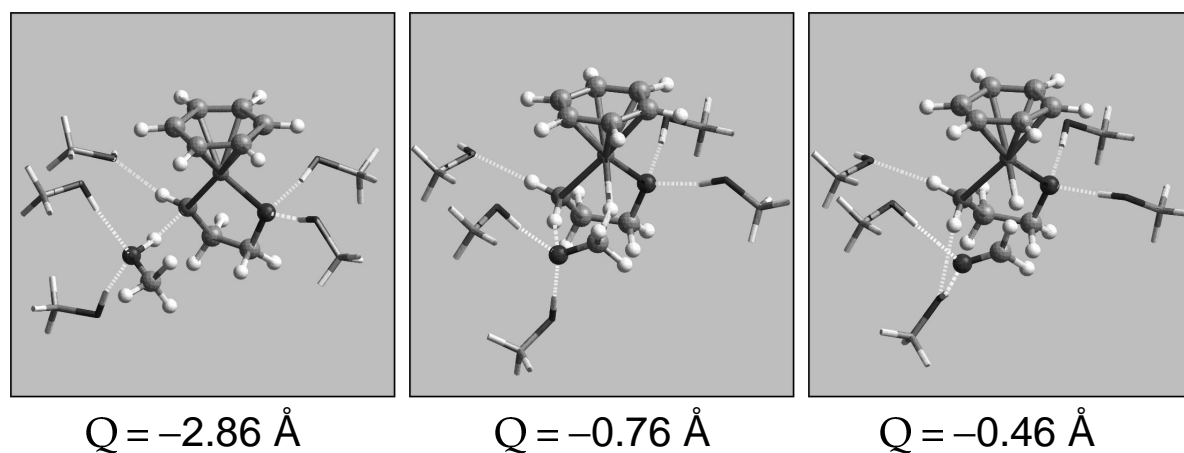


Figure 4.8: Snapshots of the micro-solvated system along the reaction path at $Q = -2.86$, -0.76 and -0.46 \AA . Ru-complex and substrate are shown as ball-stick models, solvent molecules as cylinders, and dotted lines indicate hydrogen bonds.

ergetics of the actual chemical transformation yielding a lowering of the activation barriers in both directions.

To further elucidate the role of the solvent molecules we performed calculations of a micro-solvated complex where we placed five methanol molecules at hydrogen-bonding positions around the reacting complex: two methanols near the ligand O, one methanol near the ligand NH-group and two methanols near the substrate methanol/formaldehyde. The corresponding energy profile[¶] of the concerted hydrogen transfer in the micro-solvated complex is given in Fig. 4.7, see also the snapshots in Fig. 4.8. Again we observe a stepped profile. However, it is more pronounced compared to that of the fully solvated system (Fig. 4.5). For the methanol to formaldehyde conversion we found an activation barrier of 5.3 kcal/mol for the formation of an intermediate state that appears as a local minimum at $Q = -0.76 \text{ \AA}$. This intermediate, shown in Fig. 4.8, has an energy of 4.3 kcal/mol and consists of methoxide coordinated to the Ru-complex, and is formed via proton transfer from the methanol hydroxyl group to the amide ligand. Subsequently, upon further increase of Q the hydride transfers from the methoxide C to Ru accompanied by an energy increase of 4.6 kcal/mol. From $Q \approx 0 \text{ \AA}$ and larger a third energy increase of 1.4 kcal/mol is found, associated with the de-coordination of formaldehyde from the micro-solvated ru-complex. For the reverse reaction the formation of the intermediate metal-methoxide complex is barrierless and the subsequent proton transfer yielding methanol has a small barrier of 1.0 kcal/mol.

Bond	Complex	Gas Phase	Solution
Ru–O	16- <i>e</i>	2.01	2.11
	18- <i>e</i>	2.07	2.15
Ru–H	18- <i>e</i>	1.62	1.64
	16- <i>e</i>	1.94	1.93
Ru–N	16- <i>e</i>	1.94	1.93
	18- <i>e</i>	2.21	2.20
N–H	16- <i>e</i>	1.03	1.03
	18- <i>e</i>	1.03	1.04

Table 4.2: Selected bond lengths (\AA) of the 16- and 18-electron Ru-complexes in the gas-phase and in the methanol solution. Values in solution are averaged over the respective MD simulation. Statistical errors are around 0.005 \AA .

[¶]Values are without ZPE corrections and entropy contributions.

4.4 Mechanism: Structural and Electronic Changes

The most important direct interactions of the Ru-complexes with the methanol solvent are two hydrogen bonds with the ligand oxygen and the hydrogen bond with the ligand NH-group.

The two hydrogen bonds with the ligand oxygen are relatively strong (1.6 - 1.8 Å) and do never break on the time-scale of our MD simulations. Upon solvation, the structure of the 16- and 18-electron Ru-complexes shows a small but significant change (see Table 4.2). The Ru–N, Ru–H and N–H bondlengths hardly change, but the Ru–O bond shows an increase of ≈ 0.1 Å. The latter should be attributed to the strong two-fold hydrogen bonding of the ligand oxygen that gives rise to a weakening of the Ru–O bond. In contrast, both for the 16- and the 18-electron complex the N–H bond length hardly changes when going from the gas phase to solution, indicating that the hydrogen bound to the nitrogen is not involved in hydrogen bonding.

The structural changes along the reaction path are summarized in two figures: Fig. 4.9 shows the change in distances of the substrate C–O bond and the bonds related to the proton and hydride transfer along the reaction path, both for the gas-phase reaction and the reaction in solution; and Fig. 4.10 that gives the lengths of the hydrogen bonds formed by the ligand oxygen with solvent molecules.

The electronic changes are analyzed using the method of maximally localized Wannier functions that transforms the Kohn-Sham orbitals into Wannier functions whose centers (WFC) can be assigned with a chemical meaning such as being associated with an electron bonding- or lone-pair (LP) [104, 105]. This method has proven to be a valuable tool in the investigation of the electronic charge distribution in condensed phase environment. Examples are hydrogen-bonded liquids [79,172], see also section 2.3.3. Here we will use the WFCs as a qualitative tool for describing the change in the electronic structure along the reaction path. Fig. 4.11 shows schematically the positions of the valence WFCs of the 16-electron Ru-complex, the 18-electron Ru-complex, methanol, and formaldehyde in the gas phase. The WFCs of the electrons of the semi-core 4s and 4p states of Ru, the electrons of the benzene ligand, and most of the electrons of the backbone of the aminoalcohol ligand are not shown

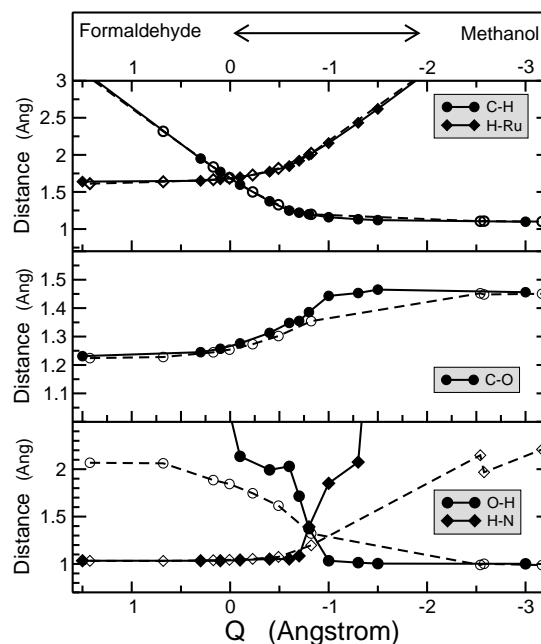


Figure 4.9: Average distances along the reaction path for the imposed substrate C to Ru hydride transfer (top), the substrate C–O bond (middle), and the substrate O to N proton transfer. Solid symbols and lines indicate results for the reaction in solution. Open symbols and dashed lines indicate gas-phase results. Statistical errors for the distances in solution are around 0.03 Å.

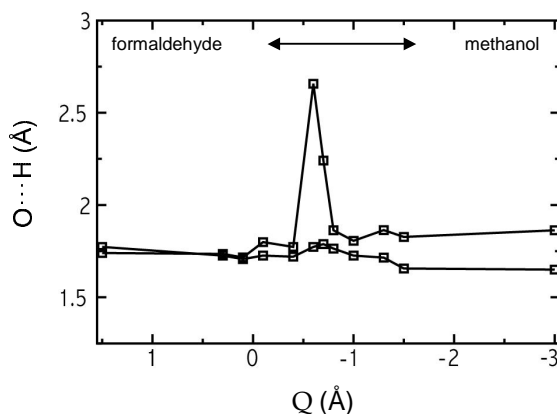


Figure 4.10: Average change in distance between the oxygen of the aminoalcohol ligand and the two hydrogen-bonded solvent molecules along the reaction path. Statistical errors are around 0.03 Å. Lines are just a guide to the eye.

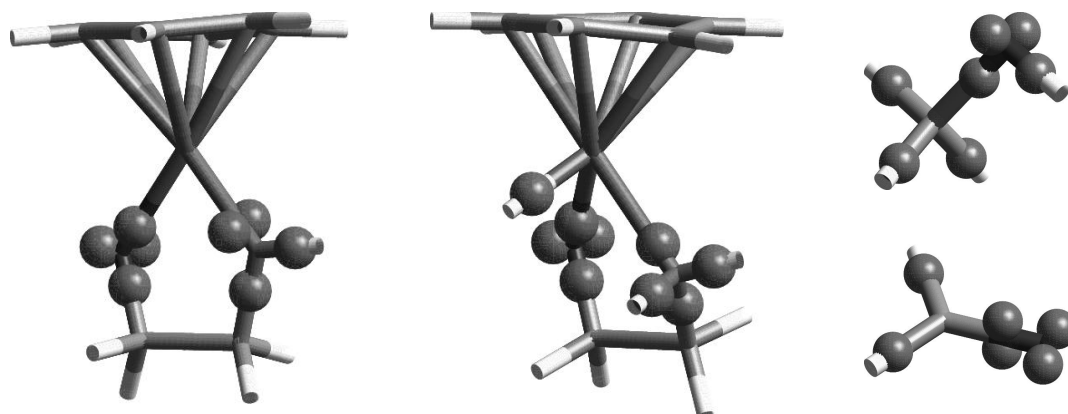


Figure 4.11: Valence Wannier functions centers (WFCs) in the gas phase of the 16-electron Ru-complex (left), 18-electron Ru-complex (middle), methanol (right, top), and formaldehyde (right, bottom). The sticks represent bonds while the balls indicate the positions of the WFCs.

as they are not involved in the reaction. Only two of the eight valence electrons of Ru are actively involved. Together with the six valence electrons of oxygen, five of nitrogen, two of the carbons in the aminoalcohol backbone, and one of the amide hydrogen lead to eight doubly occupied WFCs for the 16-electron complex. The 18-electron complex contains two extra hydrogens, hence nine WFCs. Methanol and formaldehyde possess seven and six WFCs, respectively. In Fig. 4.12 we have plotted, as function of the reaction coordinate Q , the change in position of the valence WFCs with respect to selected nuclei of the Ru-complex and the substrate in the gas phase and in the methanol solution. Fig. 4.13 shows snapshots of the solvated system including the WFCs at key stages along the reaction path.

Now we will discuss, on basis of Figs. 4.9 - 4.13, the structural and electronic changes along the reaction path when going from methanol to formaldehyde, *i.e.* along the oxidative addition pathway: $Q = -3 \text{ \AA} \rightarrow Q = 1.5 \text{ \AA}$. Here we will distinguish three stages: towards $Q = -1.0 \text{ \AA}$, from $Q = -1.0 \text{ \AA}$ to $Q = -0.6 \text{ \AA}$, and from $Q = -0.6 \text{ \AA}$ to $Q = 1.5 \text{ \AA}$. We will focus mainly on the reaction in solution and point out the important distinctions with the reaction in the gas-phase system. In the following all Q -values are in \AA .

From $Q = -3.0$ to $Q = -1.0$: Up to $Q = -1.0$ the methanol molecule is still intact both in the gas-phase and in solution. In this range the gas-phase system has the methanol hydrogen-bonded to the amide group with the hydroxyl proton showing the onset of transfer to the ligand nitrogen. In contrast, the hydroxyl group of the methanol substrate remains in solution up to $Q = -1.5$. For larger values of Q it forms a hydrogen bond with the ligand amide group. This hydrogen-bond formation is associated with a change in the nature of one of the WFCs near the nitrogen. Its nature changes from RuN-bond to lone-pair character reflected in its approach to N from 0.55 to 0.45 \AA in the region $Q = -1.5 \rightarrow Q = -1.0$ and as it is redirected and points towards the methanol hydroxyl hydrogen at $Q = -1.0$ (see snapshot). At the same time the other N WFC, still associated with the Ru-N bond, is moving away from the nitrogen.

From $Q = -1.0$ to $Q = -0.6$: In the gas-phase system there is a continuing transfer of the proton from the hydroxyl oxygen to the ligand nitrogen. However, at $Q = -0.7$ it is not yet completed as the distance to the hydroxyl oxygen is $\sim 1.4 \text{ \AA}$. In contrast, for the reaction in solution the methanol hydroxyl bond with a length of 1.03 \AA at $Q = -1.0$ is converted into a

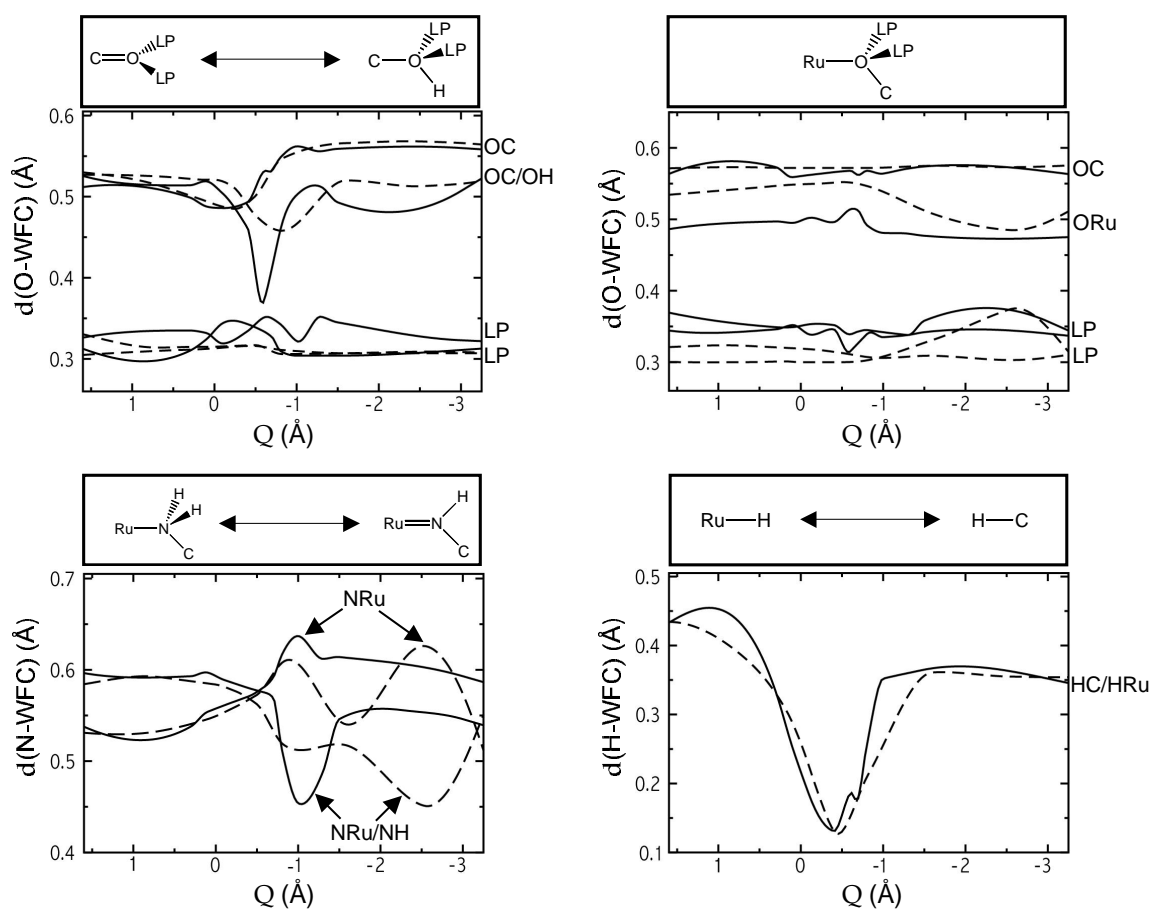


Figure 4.12: Change of the positions of the valence Wannier function centers (WFCs) with respect to selected nuclei of the Ru-complex and methanol/formaldehyde (cf. Fig. 4.11) along the reaction path in the gas-phase (dashed lines) and in the methanol solution (full lines). Data points (not shown for simplicity) for the solvated system were obtained by averaging over six configurations of the respective constraint MD simulation. Statistical errors for the solvated system are around 0.005 Å. For simplicity only two of the four WFCs associated with the nitrogen nucleus are shown, see text.

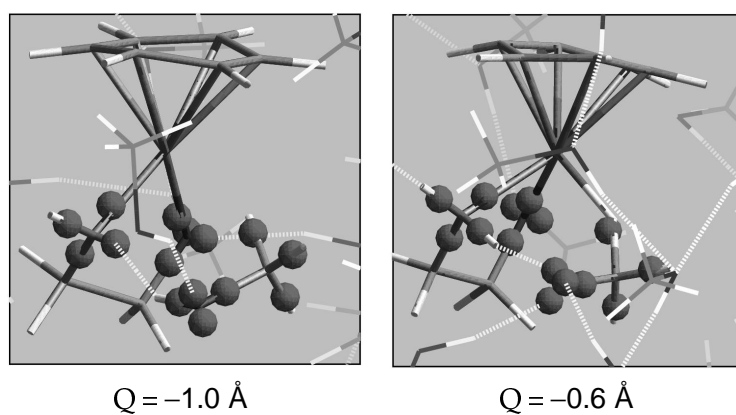


Figure 4.13: Snapshots of the solvated system at $Q = -1.0$ and -0.6 Å along the reaction path. Ru-complex and substrate are drawn as cylinders, balls indicate positions of the valence Wannier function centers, solvent molecules are drawn as sticks, and the dotted lines indicate hydrogen bonds.

Table 4.3: Molecular dipole moments of the Ru-complexes, methanol and formaldehyde in the gas phase. Experimental values are given in parentheses.

	$\mu(\text{D})$
16- <i>e</i> Ru-complex	3.35
18- <i>e</i> Ru-complex	4.31
methanol	1.73 (1.69 ^a)
formaldehyde	2.44 (2.34 ^b)

^aMicrowave study, Ref. [107].

^bMicrowave study, Ref. [177].

hydrogen bond of 1.7 Å at $Q = -0.7$. Conversely, the hydrogen bond of the ligand nitrogen with the hydroxyl hydrogen of 1.9 Å is converted into a N–H bond of 1.09 Å, that is only slightly above the gas-phase value. A little further along the oxidative addition pathway, at $Q = -0.6$, a full proton transfer has occurred converting the methanol into a methoxide and the ligand amide into an amine group (see snapshot). The N–H bond formation is reflected in the shift of the lone-pair WFC at ~ 0.45 Å from the nitrogen to ~ 0.6 Å making it a NH-bond WFC. The formation of the methoxide is further illustrated by the change in nature of the OH-bond WFC, that goes from a position at 0.5 Å to a position at 0.37 Å from the oxygen that is typical for a lone pair. In addition, the methoxide also forms strong hydrogen bonds with solvent methanol molecules with average bond lengths of 1.6 and 1.9 Å. This is reflected in the shift of the two other lone-pair WFCs of the methoxide oxygen away from the oxygen. The proton transfer is not only accompanied by local electronic changes. Also near the hydride and the ligand oxygen the electronic structure alters. The WFC of the methyl hydrogen transferring to Ru shifts towards the hydrogen indicating that it is starting to lose its CH-bond character. The WFC associated with the Ru–O bond shows a relatively sharp shift away from the oxygen at $Q = -0.6$. In the simplified picture provided by the WFCs this could be interpreted as a compensation of the shift of the WFC associated with the Ru–N bond towards the nitrogen, where, in turn, the latter is facilitated by the conversion of the nitrogen lone pair into a NH bonding pair. The shift of the RuO WFC away from the oxygen has implications for the hydrogen bonding of the ligand oxygen to solvent molecules. It is accompanied by a shift of one of the lone-pair WFC towards the oxygen destabilizing the associated hydrogen bond such that it is broken in the region near $Q = -0.6$ (see Fig. 4.10). The second solvent methanol remains strongly hydrogen bonded.

From $Q = -0.6$ to $Q = 1.5$: In the gas-phase system the proton transfer from the substrate oxygen to the ligand nitrogen is completed and a full transfer of the hydride to ruthenium takes place, converting the substrate methanol into formaldehyde. In solution, where the proton had already been transferred to the ligand nitrogen, the hydride is fully transferred to ruthenium, converting the methoxide into formaldehyde. In this process the substrate oxygen lone-pair WFC involved in the hydrogen bond with the amine group is changed into one associated with the substrate C–O bond, forming eventually the C=O bond of formaldehyde. Consequently, the hydrogen bond of the ligand amine group with the substrate oxygen breaks and is replaced by a hydrogen bond to a solvent methanol. The ligand WFC associated with the Ru–O bond decreases to a stable value. This in turn gives rise to a shift of the non-hydrogen bonded lone-pair WFC of the ligand oxygen away from the oxygen, restoring the hydrogen bond to a solvent methanol (cf. Fig. 4.10).

To quantify the change in the charge distribution of the reactive system along the reaction path in a single number we calculated the dipole moment of the reacting complex (Ru-complex + substrate) along the reaction path, assuming the electronic charge to be distributed as point charges located at the WFCs. In section 2.3.3 we saw that for liquid methanol such a

partitioning of the charges over the molecules yields a unique assignment of the WFCs over distinct molecules. Moreover, recently van Erp and Meijer showed that this methodology could give insight into the onset of chemical reactivity in a study of the aqueous solvation of ethanol and ethylene [53]. In Table 4.3 we collected the molecular dipole moments of the Ru-complexes, methanol and formaldehyde in the gas phase. Note the good agreement with experiment. The absolute gas-phase values of the Ru-complexes indicate that substantial solvent polarization effects can be expected. In connection, an *ab initio* MD study of water, a highly polarized liquid, showed that its molecular dipole moment changed from 1.9 for the gas phase monomer to 3.0 D in the liquid [79, 178]. Moreover, even the apolar ethylene molecule, with a gas-phase value of 0.5 D, yields in an aqueous surrounding instantaneous values of up to 1.0 D [53].

Fig. 4.14 shows the change of the total dipole moment of the reacting complex (Ru-complex + substrate) along the reaction path in the gas phase and in the methanol solution. In the gas phase, both the formation of the hydrogen bond between the nitrogen of the ligand and the hydroxyl hydrogen, and the hydrogen transfer lead to an increase in the total dipole moment in the order of 2-3 D. For the solvated reacting complex the total dipole moment is always higher than in the gas phase. At $Q = -3.0 \text{ \AA}$ and $Q = -1.5 \text{ \AA}$ the influence of solvation is clearly visible as the dipole moment is at least 6.5 D larger than in the gas phase. Along the solvated reaction path three maxima are visible at $Q = -1.3$, -0.6 , and $+0.1 \text{ \AA}$. At $Q = -0.6 \text{ \AA}$, *i.e.* the methoxide coordinated complex, the dipole moment is 11.7 D, a factor of two larger than in the gas phase, indicating a large polarization of the charge distribution of the complex due to the methanol solvent molecules.

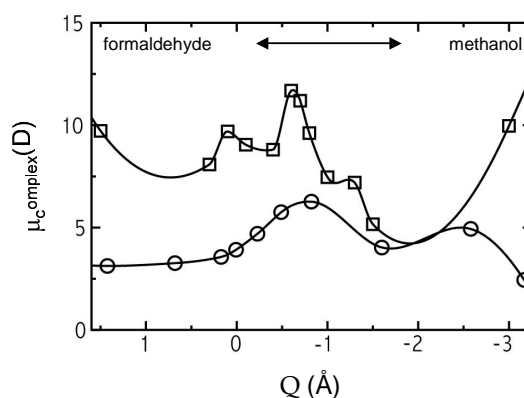


Figure 4.14: Change of the total dipole moment (Debye) of the reacting complex (Ru-complex + substrate) along the reaction path of the concerted hydrogen transfer in the gas phase (circles) and in the methanol solution (squares). Data points for the solvated system were obtained by averaging over six configurations of the respective constraint MD simulation. Statistical errors for the solvated system are around 1.0 D.

4.5 Spontaneous Reaction

As we obtained a barrier for reductive elimination of formaldehyde in the methanol solution of only 1.4 kcal/mol, we released the constraint at $Q = +0.1 \text{ \AA}$ and let the simulation run freely. Fig. 4.15 shows four snapshots of the solvated system after the constraint is released. At $t = 0 \text{ ps}$ formaldehyde approaches the 18-electron complex. The carbonyl oxygen has formed a hydrogen bond with the amine-group and with a solvent molecule. At $t = 0.69 \text{ ps}$ the hydride transfers to the carbon of the substrate. At the same time, a proton from the hydrogen-bonded solvent molecule transfers to the oxygen of the substrate. The oxygen of this solvent molecule is hydrogen-bonded to the amine-group. 0.30 ps later formaldehyde is converted to methanol, and the proton associated with the amine-group moves towards to the oxygen of the methoxide, originally the coordinating solvent molecule. However, this final proton transfer does not take place. In stead, at $t = 1.08 \text{ ps}$ the proton moves back to the amine nitrogen and another solvent molecule transfers a proton to the methoxide molecule. In fact, we let the simulation run for another 0.63 ps and found that the methoxide molecule migrates through the solution by several proton transfers, and is highly stabilized by solvent interactions. After 1.71 ps we are left with a protonated 16-electron Ru-complex and solvent-stabilized methoxide molecule,

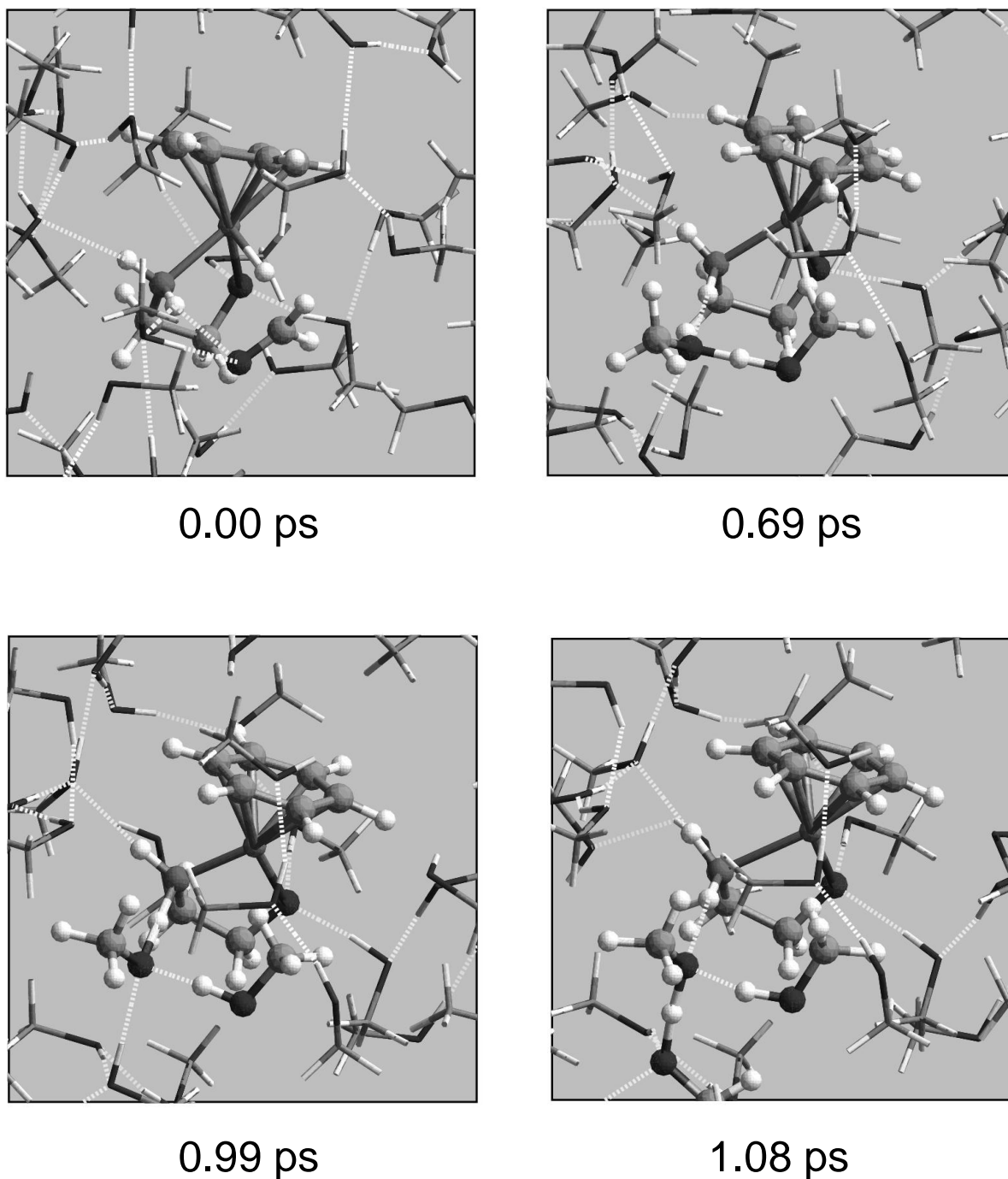


Figure 4.15: Snapshots of the solvated system after the constraint ($Q = +0.1 \text{ \AA}$) is released. Reacting molecules are shown as ball-stick models, solvent molecules as cylinders, and the dotted lines indicate hydrogen bonds.

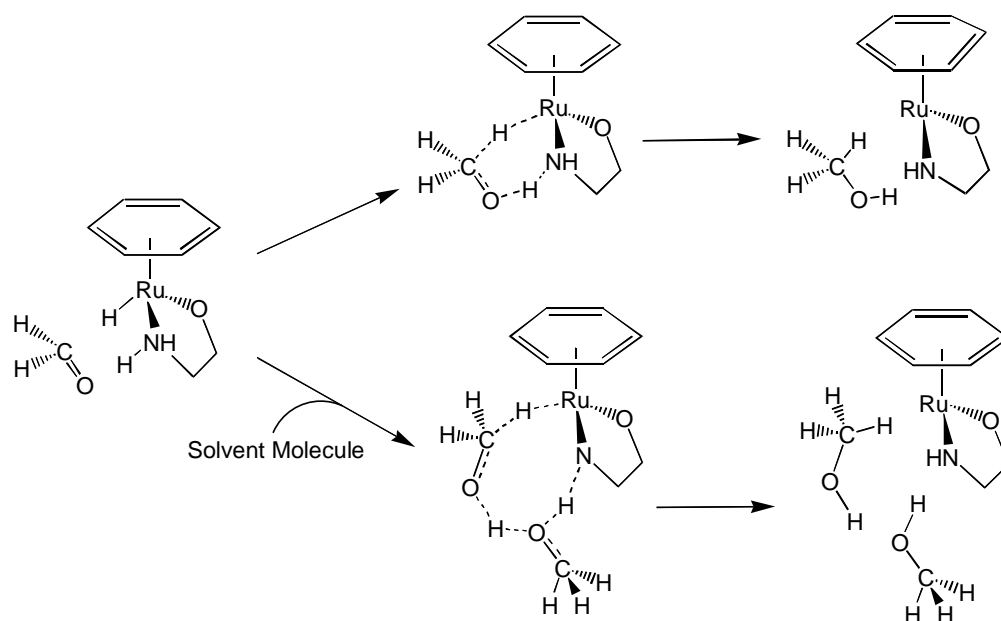


Figure 4.16: Possible (concerted) reaction pathways of the Ru-catalyzed transfer hydrogenation of ketones. Top: metal-ligand bifunctional mechanism as proposed by Noyori [155], bottom: solvent-mediated mechanism (this work).

which eventually exchange the proton to form the 16-electron Ru-complex and methanol.

Clearly, the solvent-mediated mechanism described above is different from the bifunctional mechanism as put forward by Noyori [155]. In fact, our computational results indicate that more than one concerted reaction pathway is feasible, see Fig. 4.16. Concurrent transfer of proton of the amine nitrogen and the metal-bound hydride to the coordinated ketone is still possible. However if the ketone forms a strong hydrogen bond with one of the solvent molecule, it obtains the proton from the strongly coordinated solvent molecule and not from the amine nitrogen. The deprotonated solvent molecule can be protonated directly via proton transfer from the amine group, or indirectly via another proton source in solution. This alternative solvent-mediated pathway could influence the kinetics of the overall reaction. A recent kinetic isotope study of the Ru-catalyzed transfer hydrogenation with a *N*-tosylated diamine ligand provided convincing evidence for the concurrent transfer of both hydrogens [165]. However, a distinction between the two mechanisms shown in Fig. 4.16 is not possible, since for both mechanisms the hydrogens are transferred to the substrate in a concurrent way.

4.6 Summary and Conclusions

We have performed a DFT-based *ab initio* molecular dynamics study of a full atomistic model system of the Ru-catalyzed transfer hydrogenation of formaldehyde in the gas phase, in a methanol micro-solvated system, and in a methanol liquid-solvated system. We investigated the thermodynamics, mechanism, and electronic structure along the reaction pathway. The gas-phase results are fully consistent with the results of Noyori and coworkers [33] who studied the same model system in the gas phase with DFT and MP4 computational methods. The analysis of the thermochemistry showed that solvent interactions lower the activation barrier of the oxidative addition and reductive elimination by 1.3 and 3.4 kcal/mol, respectively. The decrease for

the reductive elimination is such that the barrier is almost absent. This reinforces the assertion based on the gas-phase calculations that the hydrogen donation to the Ru-complex constitutes the rate-limiting step in transfer hydrogenation of formaldehyde.

The main distinction between the free-energy profiles of the gas-phase and solution reactions is the presence of a small plateau in the solution profile. This suggests that in solution the methanol-formaldehyde inter-conversion is a two-step process. Analysis of the changes in geometry and electronic structure clarifies the origin of this plateau and shows other distinctions between the gas-phase reaction on the one hand and the micro-solvated and solution-reaction on the other hand. In solution and for the micro-solvated system we found that when going from methanol to formaldehyde, first a proton transfers from the methanol hydroxyl group to the ligand nitrogen, converting the methanol substrate into a methoxide group. The second step consists of the hydride transfer from the methoxide carbon to ruthenium. In contrast, in the gas-phase system the proton and hydride transfer is a concerted process. The situation after the proton transfer coincides with the plateau in the reaction free-energy profile and could be considered a transient metastable state. It is stabilized by strong hydrogen bonding of the methoxide to solvent methanol molecules. The assumption of a metastable state finds support by the relatively large changes in the geometry, electronic structure, and solvent coordination upon the proton transfer. Such large changes are often an indication of the arrival in some type of stable state. The calculation of the micro-solvated system support these assertions. They show a similar two-step energy profile, where the intermediate, the deprotonated substrate, is a true local minimum.

Our calculations also provide evidence for an alternative mechanism where the proton transfer is not directly between the substrate and the ligand nitrogen but solvent mediated, *i.e.* a concerted or sequential chain of proton transfers along a chain of hydrogen-bonded solvent methanol molecules.

Acknowledgements

We are grateful to Lee Bartolotti for providing us with a program to perform the gas-phase statistical thermal analysis.

Chapter 5

Directing Rhodium Catalyzed Hydrogenation via the Substrate Polarity. A Computational Study*

Jan-Willem Handgraaf,[†] Jonathan B. Spencer,[‡] Michiel Sprik,[‡]
Jinquan Yu,[‡] and Evert Jan Meijer[†]

[†]Department of Chemical Engineering, University of Amsterdam,
Nieuwe Achtergracht 166, 1018 WV Amsterdam, The Netherlands

[‡]Department of Chemistry, University of Cambridge,
Lensfield Road, CB2 1EW, United Kingdom

Abstract

We present a density-functional-theory based computational study of the hydrogenation of functionalized alkenes using the rhodium(I)-based Wilkinson catalyst. In our study we considered two mechanistic pathways along the "dihydride route" that are distinguished by different modes of substrate coordination. We found that the coordination mode with the largest binding energy is the least favorable as its transition state is significantly higher than the pathway for the coordination mode with the lowest substrate binding energy. This can be rationalized by the fact that the high-energy coordination mode has a favorable C=C bond polarization similar to that of its transition state. Our calculations confirm experimental findings that the dihydride mechanism with the formation of the crucial rhodium(I)-dihydride complex is a viable alternative pathway to the generally accepted "unsaturated route".

*Paper in preparation.

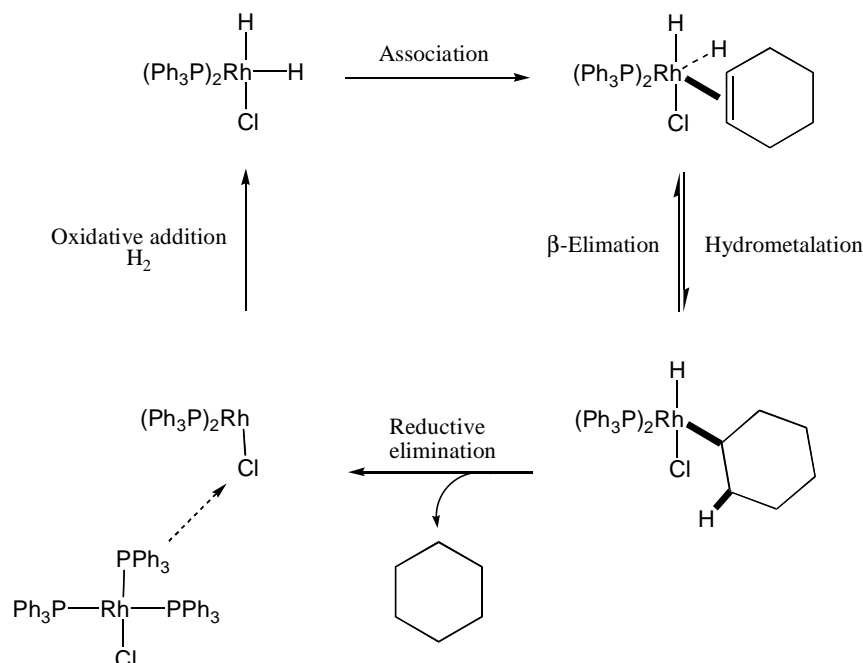


Figure 5.1: Elementary steps in the homogeneous hydrogenation with Wilkinson's catalyst (the dihydride route).

5.1 Introduction

Asymmetric homogeneous hydrogenation of pro-chiral alkenes catalyzed by transition metals is a very versatile reaction in both the laboratory and industry, providing a wide variety of biological and chemical chiral products [3, 4]. Understanding this reaction is a prerequisite for the rational design of improved catalysts. Studies have suggested that there are distinct mechanisms for hydrogenation of functionalized and non-functionalized alkenes. Detailed studies in the 1980s using Wilkinson's catalyst, $[\text{Rh}(\text{PPh}_3)_3\text{Cl}]$, revealed that the catalytic cycle of homogeneous hydrogenation of non-functionalized alkenes involves four elementary steps (Fig. 5.1) [11, 15, 179, 180]. The 14-electron, coordinatively unsaturated, *cis*-bisphosphine rhodium(I) chloride activates H_2 via oxidative addition. The resulting 16-electron hydrogenated complex is still coordinatively unsaturated and therefore can activate the alkene through interaction in a manner similar to the activation of H_2 . The intramolecular insertion of a hydride, coming from the coordinated H_2 , to the coordinated alkene (hydrometalation) is the key step and leads to the formation of the metal-alkyl complex. Kinetic measurements showed that the hydrometalation is also the rate-determining step [11], which led to the observation that the mechanism can be assigned to the so-called "dihydride route" [10, 12].

For functionalized alkenes it is commonly assumed that the mechanism is different from the one depicted in Fig. 5.1. Based on intensive kinetic studies and characterization of the stereoregulating intermediates by NMR, an "unsaturated route" for the mechanism was proposed [11, 181] (Fig. 1.3). Contrary to the dihydride route, the unsaturated route involves coordination of the functionalized alkene with the metal as a bidentate ligand *before* oxidative ad-

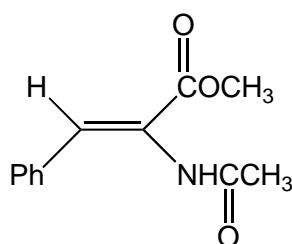
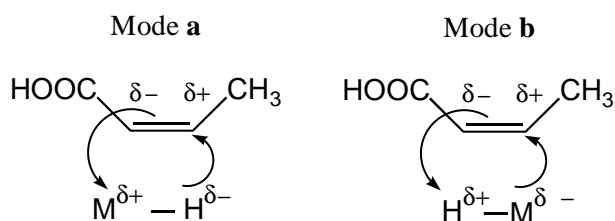
Figure 5.2: Methyl-(Z)- α -acetamidocinnamate.

Figure 5.3: Possible modes of hydrometalation.

dition of H_2 occurs. This was supported by characterization of the catalyst-substrate adduct in the hydrogenation of the pro-chiral enamide, methyl-(Z)- α -acetamidocinnamate (Fig. 5.2) [14].

The all-important question is what exactly determines the enantioselectivity of the homogeneous catalytic hydrogenation of alkenes. In the dihydride route the enantioselectivity is determined by the orientation of the coordination of the substrate to the metal hydride complex. The transfer of chirality occurs in the hydrometalation step. Recently, Yu and Spencer [182–185] found by hydrogen/deuterium substitution experiments of alkene hydrogenation by Pd and Rh compounds of a large number of substrates, that the mode of coordination is determined by the substrate polarity and the intrinsic properties of the metal. In this picture hydrometalation may occur either after coordination in mode **a** ($M^{\delta+}-H^{\delta-}$) or in mode **b** ($M^{\delta-}-H^{\delta+}$) (Fig. 5.3). There results indicated that for Pd the coordination could occur either in mode **a** or **b** suggesting that the Pd-H bond has an amphipolar nature. In contrast, for Rh the substrate coordination prior to hydrometalation was always in mode **a**.

For the unsaturated route Landis and Halpern [15] suggested, on basis of an experimental study of the model hydrogenation of a functionalized enamide, that the origin of enantioselectivity is determined by the coordination of H_2 to the substrate-metal adduct. They argue that the thermodynamically less stable adduct has a much higher reactivity for H_2 oxidative addition, referred to as an anti "lock-and-key" mechanism (Fig. 1.4). Density functional theory (DFT) calculations by Landis and Feldgus [16, 17] confirmed that the chiral product indeed arises from hydrogenation of the C=C enantioface of the enamide that binds less favorably to the catalyst. Moreover they investigated the effect of the α -substituent of the enamide on the enantioselectivity and found that for an electron-donating substituent the sense of chirality is reversed with respect to an electron-poor substituent [18]. This α -substituent effect was also found experimentally by Burk and coworkers [35].

However, the true nature of the mechanism is still a controversial subject. Recently, the low-

temperature NMR studies of Gridnev *et al.* [20,21] and Brown and coworkers [23,24] indicated that both the dihydride as the unsaturated mechanisms could be operative during the hydrogenation of a functionalized enamide.

To further clarify this subject we have performed a DFT-based computational study of the hydrogenation of several functionalized alkenes by the Wilkinson's catalyst where we focused on the substrate coordination and hydrometalation step in the dihydride route. In the following we first describe the computational methods employed, subsequently present results of the bare metal hydrides and selected substrates, *i.e.* the functionalized alkenes, and finally examine the hydrometalation step for a specific substrate.

5.2 Methods

The electronic structure calculations were computed within the Kohn-Sham formulation of DFT using gradient-corrected local functionals and scalar relativistic corrections. Using the ADF package [83] we performed geometry optimizations and transition state (TS) searches with the PW91 functional. Here PW91 refers to the LDA functional using the Vosko-Wilk-Nusair [186] parameterization of the electron-gas data of Perdew and Zunger [187], complemented with a gradient correction for exchange and correlation proposed by Perdew and Wang [44]. Scalar relativistic corrections were incorporated by way of the zero order regular approximation (ZORA) [158,188]. If necessary, spin-unrestricted calculations were performed. Molecular orbitals were expanded in an uncontracted triple- ζ Slater-type basis set augmented with $2p$ and $3d$ polarization functions for H, $3d$ and $4f$ for C, N, and O, and $5p$ and $4f$ for Rh and Pd. Cores were kept frozen.

As we are specifically interested in bond polarities a charge analysis is performed using the generalized atomic polar tensor (GAPT) method originally developed by Cioslowski [189]. Here the GAPT charge of an arbitrary atom A in a molecule is defined as

$$q^A = (1/3) \left(\frac{\partial \mu_x}{\partial x_A} + \frac{\partial \mu_y}{\partial y_A} + \frac{\partial \mu_z}{\partial z_A} \right), \quad (5.1)$$

where *e.g.* $\frac{\partial \mu_x}{\partial x_A}$ is the partial derivative of the x-component of the molecular dipole moment with respect to the x-coordinate of A. This method has the advantage that it is practically insensitive to the basis set used [190,191]. The partial derivatives were obtained from the output of a finite-difference vibrational analysis using the ADF package.

In order to study the full Wilkinson's catalyst as depicted in Fig. 5.1 we used the quantum mechanics/molecular mechanics (QM/MM)-coupling scheme of Maseras and Morokuma [192] as implemented in the ADF package [193]. In this way the Ph-groups of the PPh₃-ligands are put in the MM-region, while the rest of the system including the substrate are treated quantum mechanically. The SYBYL force field [194] was used to describe the interactions in the MM-region and a mechanical coupling was used to describe the electrostatic interactions between the QM and MM regions. This means that there is no polarization of the QM wave function, *i.e.* pure MM electrostatic coupling.

5.3 Hydrides

Hydrido metal complexes are of particular interest in chemistry as they, because of their specific structural and bonding properties, often appear as key intermediate structures in homogeneous hydrogenation reactions. Although Rh is by far the most predominant metal used in the homogeneous hydrogenation of functionalized alkenes, also Pd has been used [182–184]. In Table 5.1

Table 5.1: Selected properties of RhH and PdH and the respective dihydrides. The term symbol denotes the electronic (ground) state, r the bond length, θ the bond angle, E the binding energy, q^M the GAPT charge on the metal, and μ the molecular dipole moment.

	Term	r (Å)	θ (°)	E (eV)	q^M (e)	μ (D)
RhH ^a	³ Δ	1.561	-	-3.4	+0.250	1.71
RhH ₂ ^a	² A_2	1.542	83.0	-6.7	+0.347	2.03
PdH ^a	² Σ	1.549	-	-2.5	+0.223	1.65
PdH ₂	¹ A_1	1.533	71.6	-5.4	+0.258	1.93

^aSpin-unrestricted calculation.

we collected selected calculated properties of RhH and PdH and their respective dihydrides, and in Fig. 5.4 we plotted the molecular orbitals (MOs) with the largest contribution to the bonding for the hydride and the dihydride. As expected, the charges indicate that the metal-hydride bond is polarized as $M^{\delta+}-H^{\delta-}$ and the polarization is larger for the dihydride when compared to the hydride. Both for the hydride as the dihydride we see that the Rh-H bond is more polarized than the Pd-H bond. This is because the free Rh atom has a open-shell $4d^85s^1$ electronic configuration, whereas Pd is a closed-shell atom with a $4d^{10}$ configuration. The bonding MO of the hydride (Fig. 5.4, left) is mainly a combination of the metal d_{z^2} orbital and the hydrogen $1s$ orbital. The MOs for the dihydride are combinations of the two hydrogen $1s$ orbitals and the $d_{x^2-y^2}/d_{z^2}$ orbitals (middle) and the d_{yz} orbital (right), respectively. Note also the smaller angle θ for PdH₂ which indicates a substantial interaction between the two hydrogens, also evident from the short H-H distance of 1.79 Å.

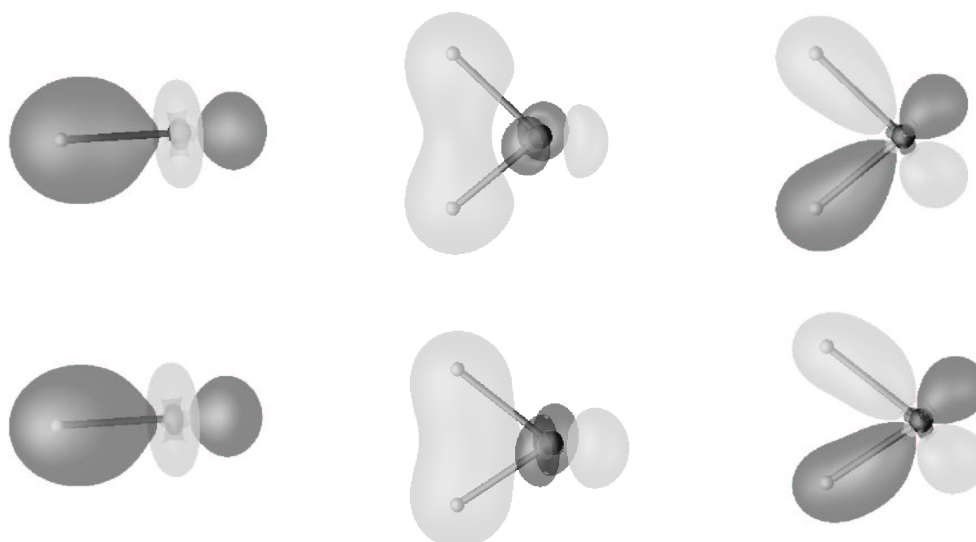


Figure 5.4: Molecular orbitals with the largest bonding character for RhH (top, left), RhH₂ (top: middle, right), PdH (bottom, left) and PdH₂ (bottom: middle, right).

Table 5.2: Selected structural and electronic properties of substrates (*Z*-configuration) with general formula $R-C_{\alpha}(H)=C_{\beta}(H)-CH_3$. Available experimental values are given in parentheses [196].

	R	$r(C_{\alpha}=C_{\beta})$ (Å)	$q^{C_{\alpha}}$ (e)	$q^{C_{\beta}}$ (e)	μ (D)
S1	CH ₃	1.338 (1.346)	-0.001	+0.003	0.29 (0.25)
S2	COOH	1.345	-0.315	+0.180	1.38
S3	Ph	1.345	-0.017	+0.010	0.42
S4	OCH ₃	1.338	+0.460	-0.229	1.45

5.4 Substrate polarity

In Table 5.2 we report selected bond lengths and charges for four typical substrates (S1–S4) with the general formula $R-C_{\alpha}(H)=C_{\beta}(H)-CH_3$ where $R=CH_3, COOH, Ph, OCH_3$. Note the good agreement with experiment for the C=C bond length and the molecular dipole moment of S1, giving confidence in the chosen computational methods. As should be, the charges indicate a zero polarization for S1. In the case of S2 the C=C bond is substantially polarized as $C_{\alpha}^{\delta-}=C_{\beta}^{\delta+}$ with a charge difference between C_{α} and C_{β} of $\sim 0.5 e$. This is easily understood as this substrate is in resonance with the corresponding vinyl acetate (Fig. 5.5). On the basis of the weak electron donating properties of the Ph-group [195] a small $C_{\alpha}^{\delta-}=C_{\beta}^{\delta+}$ -polarization is found for S3. For S4 the charges indicate a large opposite polarization with a charge difference of $\sim 0.7 e$. Note further that there seems to be a direct link between the polarization of the C=C bond and the molecular dipole moment: the larger the charge difference between C_{α} and C_{β} , the larger the dipole moment. It is stressed that these polarization effects are purely electronic in nature since the change in C=C bond length is less than 0.01 Å if the R-group is varied. Overall given a suitable transition metal catalyst, a substrate with $R=COOH$ should lead to a preference for mode **a**, whereas a substrate with $R=OCH_3$ should prefer mode **b**.

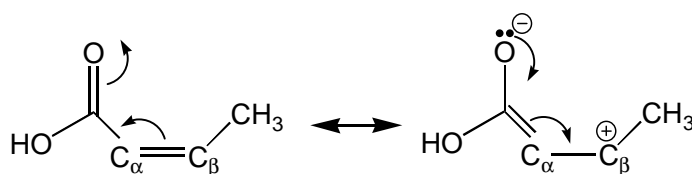


Figure 5.5: Dominant resonance structures of substrate S2 ($R=COOH$).

5.5 Hydrometalation

Fig. 5.6 shows the optimized structures of the Wilkinson's catalyst and the 16-electron hydrogenated complex that is obtained after oxidative addition of H_2 (Fig. 5.1). The former has a square-planar structure and the metal center is 'embedded' in the PPh_3 -ligands, while the latter is a distorted square pyramid with one hydrogen in an equatorial position (H_{eq}) and one in an axial position (H_{ax}). q^{Rh} of the Wilkinson's catalyst is highly negative ($-0.72 e$), even more negative than q^{Cl} . This is due to σ -donation of the PPh_3 -ligands also indicated by the three large

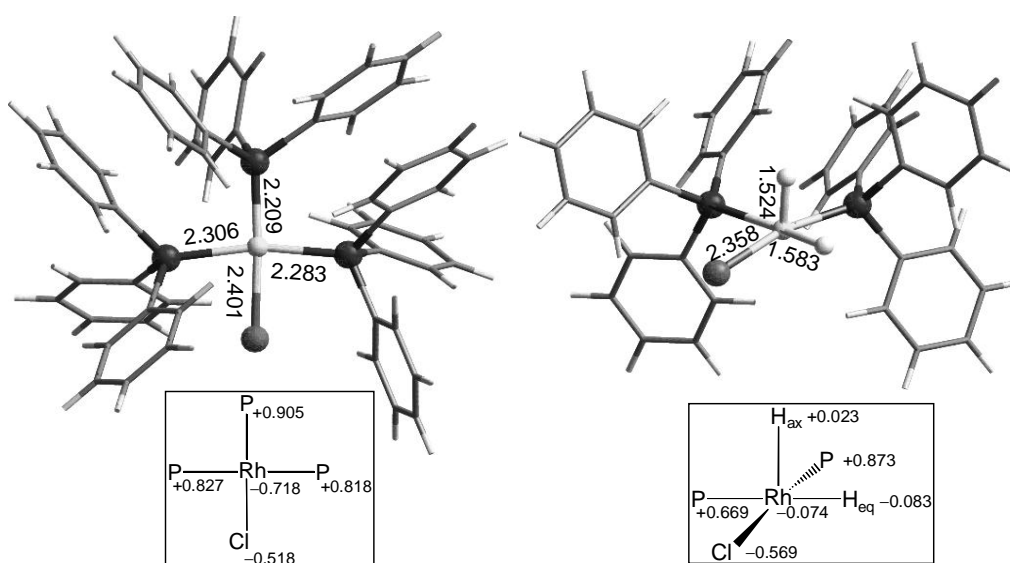


Figure 5.6: Optimized structures of the Wilkinson's catalyst (left) and the 16-electron hydrogenated complex (right). Ph-groups are drawn for clarity as cylinders. The squared boxes show the configuration around Rh and the GAP atomic charges.

positive q^P 's ranging from 0.8 till 0.9 e . If Wilkinson's catalyst is oxidized by H_2 , q^{Rh} becomes with $-0.07 e$ almost neutral in the hydrogenated complex. Note further that the Rh–H bond distances and the H–Rh–H angle are almost identical to the values reported for RhH_2 (Table 5.1). Only the Rh– H_{eq} bond is $\sim 0.04 \text{ \AA}$ longer and still has a $M^{\delta+}-H^{\delta-}$ -polarization, although much less pronounced compared to the polarization of the Rh–H bond in RhH_2 . The Rh– H_{ax} bond has now even the opposite polarization. At first sight, it seems that the hydride-metal bond in the hydrogenated complex has a too small polarization to influence the reaction pathway of the hydrogenation.

Since we are looking for a distinct effect of the polarization on the course of the reaction we choose substrate S2 with $R=COOH$ for the further computational studies. Fig. 5.7 shows the hydrometalation step for mode **a** and mode **b**, and Fig. 5.8 shows the corresponding energy

Table 5.3: Selected interatomic distances (\AA) along the potential energy surface of the hydrometalation step via mode **a** and mode **b** of the substrate with $R=COOH$.

	Rh– H_{eq}	$C_{\alpha}-C_{\beta}$	Rh– C_{α}	Rh– C_{β}	$C_{\alpha/\beta}-H_{eq}$
	1.583 ^a	1.345 ^a	–	–	–
a1	1.562	1.382	2.510	2.439	2.478
a2-TS	1.639	1.428	2.373	2.372	1.540
a3	3.400	1.523	2.155	3.189	1.096
b1	1.539	1.384	2.360	2.455	2.587
b2-TS	1.670	1.440	2.341	2.343	1.380
b3	3.318	1.541	3.115	2.123	1.093

^aInteratomic distances of isolated reactants, *i.e.* 16-electron hydrogenated complex and substrate.

profiles. Table 5.3 and 5.4 give selected structural and electronic properties, respectively.

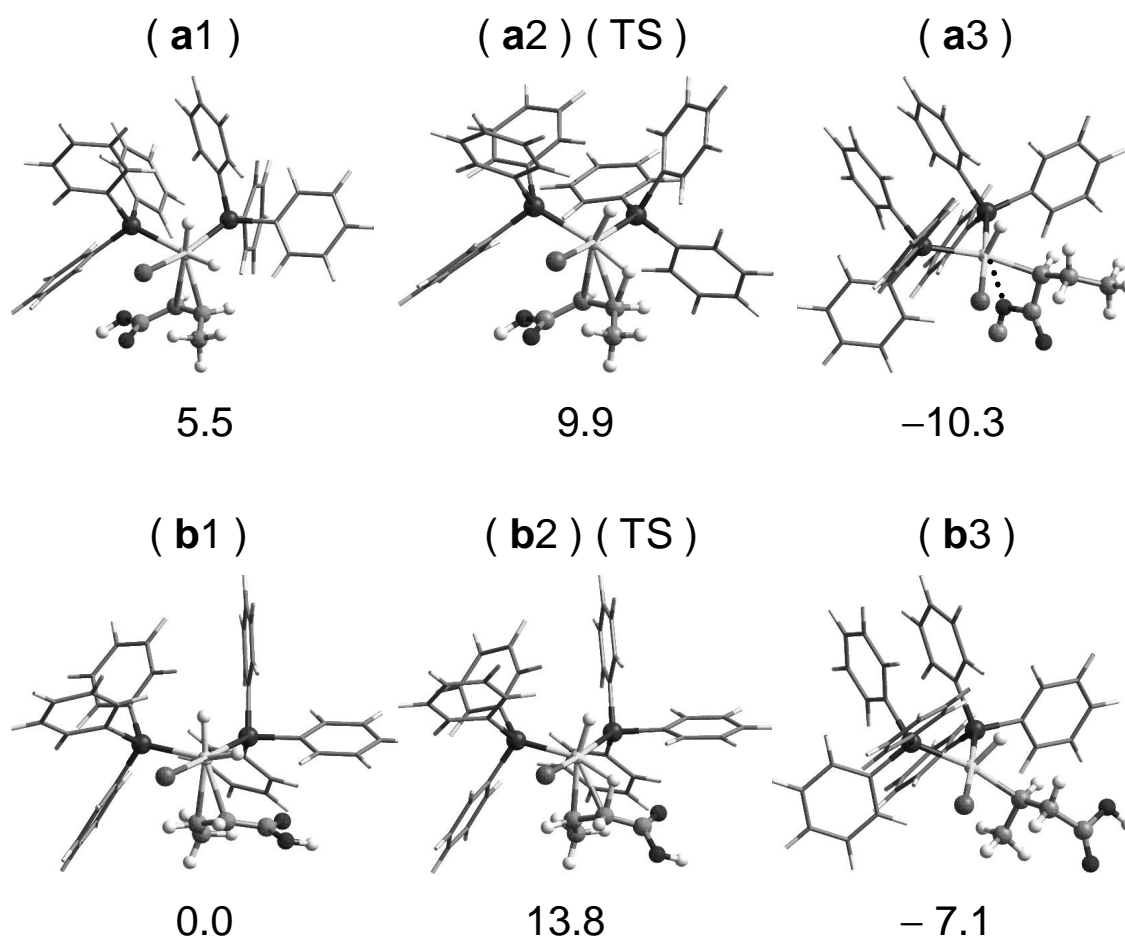


Figure 5.7: Optimized structures of the hydrometalation step via mode **a** (top) and mode **b** (bottom) for the substrate with R=COOH. For clarity the Ph-groups are drawn as cylinders. Energies (kcal/mol) are without zero-point energy corrections and entropy contributions.

For mode **a** and **b** the complexation energy of the substrate is 5.6 and 11.1 kcal/mol, respectively. The C=C bond length increases for both modes by ~ 0.04 Å, while the C=C bond polarization increases for **a1** with 31% and decreases for **b1** with 15%. For both modes the coordination of the double bond to Rh is reflected by the increase in electronic charge on Rh and associated decrease in the electronic charge on the substrate carbons. Note that also from the already electron-deficient carbon atom a significant amount of electron density is drawn. Furthermore the polarization of the substrate is significantly enhanced upon coordination in mode **a**. The 5.5 kcal/mol higher energy of mode **a** could be explained by an unfavorable charge distribution. We do see that the metal hydride loses some electron density for both modes of substrate coordination. We find no indication of an substrate induced enhancement of the polarization of

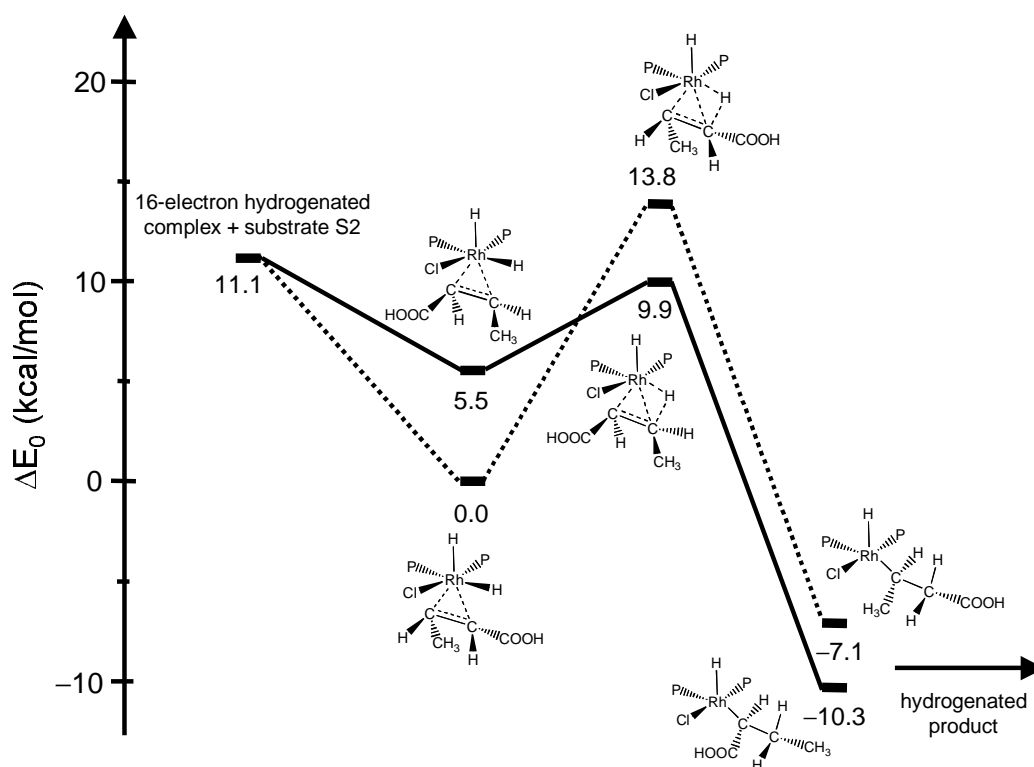


Figure 5.8: Energy profiles of the hydrometalation step via mode **a** (solid line) and mode **b** (dotted lines). Ph-groups are omitted for clarity. Energies in kcal/mol are without zero-point energy corrections and entropy contributions.

the Rh-H bond.

After complexation, the transfer of H_{eq} takes place in the transition state (TS). Our calculations show that, relative to the separated metal complex and substrate, the transfer via TS **a2** is 3.9 kcal/mol lower than the transfer via TS **b2**. The activation energy (E_a) is even 9.4 kcal/mol lower for mode **a**. For a full QM-calculation[†] using PH_3 instead of PPh_3 we find that E_a of mode **a** is 6.9 kcal/mol lower, hence the steric interactions of the PPh_3 -groups are non-negligible and responsible for approximately 25 % of the discrimination between the modes. For a similar QM-calculation using as substrate (*Z*)-1-phenylpropene (S3) instead of (*Z*)-crotonic acid (S2) E_a of mode **a** is only 2.6 kcal/mol lower. This suggests that a substrate with a relatively small C=C bond polarization is less able to discriminate effectively between the two possible modes of hydrometalation.

If we compare the structures of the two transition states we find that **b2** resembles the intermediate metal-alkyl state better than **a2**. The calculated charges show that for TS **a2** the polarization of the metal-coordinated C–C bond is now 65 % larger than the polarization of the C=C bond of the isolated substrate, whereas for TS **b2** it has almost vanished. The values of the dipole moment are, as found before for the isolated substrates, dominated by the C=C bond polarization. Interestingly, for mode **a** H_{eq} has a negative charge in the TS and is basically a hydride, whereas for mode **b** $q^{H_{eq}}$ is positive.

Fig. 5.9 shows for both transition states the MO for which the 1s atomic orbital of H_{eq} has its largest contribution. Clearly, there is a large overlap between the substrate and the metal com-

[†]We used the computational setup of section 5.2.

Table 5.4: Selected electronic properties along the potential energy surface of the hydrometalation step via mode **a** and mode **b** of the substrate with R=COOH. GAPT atomic charges are given in e and dipole moments in Debye.

	q^{Rh}	$q^{\text{H}_{\text{eq}}}$	C_{α}	C_{β}	μ
	-0.074 ^a	-0.083 ^a	-0.315 ^a	+0.180 ^a	–
a1	-0.354	+0.026	-0.279	+0.369	6.72
a2-TS	-0.328	-0.060	-0.372	+0.444	6.55
a3	-0.029	+0.017	+0.023	-0.019	7.61
b1	-0.334	+0.041	-0.180	+0.243	5.47
b2-TS	-0.307	+0.028	-0.015	+0.087	5.11
b3	-0.061	+0.052	-0.222	+0.379	7.85

^aCharges of isolated reactants, *i.e.* 16-electron hydrogenated complex and substrate.

plex for TS **a2**, which should be regarded a key factor for the more facile transfer of H_{eq} . For TS **b2** the 1s orbital mixes in with metal d-orbitals, but not with the orbitals of the substrate, hence there is not such a favorable overlap. As the TS of mode **b** is substantially higher in energy than the one for mode **a**, the hydrometalation proceeds via a mode **a** coordinated substrate. This is in accordance with the hydrogen/deuterium experiments of Spencer *et al.* [182, 183]. They suggested, at least for Pd, that the hydrometalation was guided by a favorable substrate coordination. However, our calculations for Rh suggest the opposite with the substrate coordinating predominantly via mode **b**, that is stable by 5.5 kcal/mol over mode **a**. This will have a contribution to the overall kinetics of the full reaction. This situation correspond to the anti “lock-and-key” model of Refs. [16, 17], where in the hydrogenation of a functionalized enamide the major product arises from the C=C enantioface that binds less favorably to the catalyst (see Fig. 1.4).

After the transfer the metal-alkyl complexes (**a3** and **b3**) are formed. Note that the metal-carbon bond of $\sim 2.1 \text{ \AA}$ is for both modes of coordination relatively short. However, for mode **a** the metal center forms an extra intermolecular bond of 2.76 \AA with the hydroxyl-oxygen of the substrate (Fig. 5.7, complex **a3**, dotted line). This lowers the energy of **a3** by 3.2 kcal/mol compared to **b3**. Note further that, whereas for mode **a** the C=C bond polarization has dropped to only 8 % of the initial value, for mode **b** it is 21 % larger. The next step, after formation of the alkyl-metal complex, is the rapid reductive elimination, either directly via H_{ax} of the metal complex, or via another H_2 molecule in solution, giving the saturated product, in this case butanoic acid. Oxidative addition of H_2 leads again to the 16-electron hydrogenated complex, completing the catalytic cycle. A similar reaction profile should be envisaged for pro-chiral substrates.

5.6 Discussion

Our DFT-calculations of the Wilkinson’s catalyst assisted hydrogenation of a highly polar substrate shows that the favored reaction path is via mode **a**, where in the transition state the polarization is significantly enhanced. In contrast, for an almost non-polar substrate the paths via mode **a** and **b** have a similar probability. This suggest that there is a strong influence of the substrate polarity on the course of Rh-catalyzed hydrogenation.

Hydrogen/deuterium substitution experiments showed a similar type of reaction path for the same polar substrate [182], and even for a substrate with an opposite polarity R=OCH₃ (S4 in Table 5.1) the preferred mode is still **a** in the case of Rh. This underlines the poor electron-

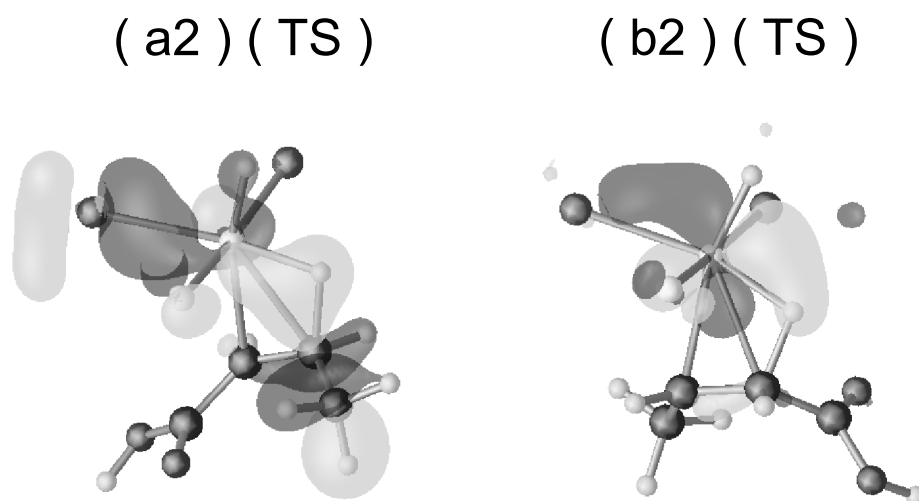


Figure 5.9: Occupied molecular orbital wherein the 1s atomic orbital of the equatorial hydrogen has its largest contribution for the TS of mode **a** (left) and the TS of mode **b** (right). Ph-groups omitted for clarity.

donating capabilities of Rh which are needed if the hydrogenation would occur via mode **b**. However, for the homogeneous catalysis with Pd these experiments showed much more variation in the product distribution. This can be traced back to our results on the bare metal hydrides where the $M^{\delta+}-H^{\delta-}$ -polarization is considerably less for Pd. Most likely Pd is able to donate electron density to the coordinating substrate, reversing the polarization to $Pd^{\delta-}-H^{\delta+}$.

Both from the low-temperature NMR experimental work of Gridnev *et al.* [20,21] and Brown and coworkers [23,24] it is evident that a Rh-dihydride complex is active during the Rh-catalyzed homogeneous hydrogenation. However, although considerable progress has been made by the latter authors, the mechanistic pathway for the hydrogenation is still as yet not clear, since the discrimination between the dihydride route and the unsaturated route is very subtle. A complicated factor to study these reactions with computer simulations could be the methanol solvent, which is normally used to conduct these experiments. By using methanol the Rh–X bond, where X is typically a halogen, is not stable in solution, and a cationic Rh-complex is formed. As we saw in the previous chapter for the Ru-catalyzed transfer hydrogenation of ketones a methanol solvent can alter the thermodynamics and the mechanism substantially, and hence the solvent should properly be accounted for. Burk *et al.* found indeed that the solvent plays an important role in the Rh-catalyzed hydrogenation, with high conversions in the case of polar protic solvents [35]. For the system we studied the solvent of choice in experiments is benzene, and solvent interactions will be less important. In contrast, Landis and Feldgus [16–18] rationalized the product distribution via the unsaturated route, but did not include any solvent interactions in their computational model.

It is evident that asymmetric catalysis is a powerful tool to synthesize a wide range of chiral compounds. However, up till now, most attention has been given to development of new chiral ligands to optimize the product distribution. This is often time-consuming and very subtle, since slight changes in the structure of the ligand could effect both the conversion and selectivity in a rather unpredictable way. In contrast, our computational study shows that the alteration of

the electronic properties of the substrate is also a possible route to optimize the product distribution. One should imagine the following. In order to obtain a high enantioselectivity for a typical asymmetric hydrogenation reaction one uses a suitable stereoregulating group which forces the desired product distribution. Of course this should from a synthetic point of view be possible, since this group has to be built in before the actual enantioselective step, and it also has to be removed after this step. However, if these problems can be overcome, one has a very direct and effective way to optimize the chiral induction, since the functionalized substrate is actively involved in the chemical transformation, while the ligands are not.

5.7 Conclusions

We have performed a DFT-based computational study and charge analysis of the homogeneous hydrogenation of functionalized alkenes, using the Rh-based Wilkinson's catalyst. Based on the dihydride mechanism our calculations showed that the product distribution, as obtained from hydrogen/deuterium substitution experiments, can be rationalized by the substrate orientation in the hydrometalation step. The charge analysis showed that the C=C bond polarization of functionalized alkenes is the key factor that lowers the activation energy of the favorable mode of hydrometalation (*i.e.* mode **a** in the case of Rh, see Fig. 5.3). In general, Rh should be viewed as an electron-deficient metal not capable of donating electron density to the coordinated substrate. This forces the hydrometalation step to take place via mode **a**.

Chapter 6

Concluding Remarks

In this final chapter we draw some general conclusions about the work presented in this thesis, and indicate the future prospects of the use of first-principles computer simulations in the field of catalysis.

Electronic Structure Calculations

The use of the gradient-corrected Becke-Lee-Yang-Parr (BLYP) density functional was guided by its former success in the study of liquid water and aqueous solvation of small solutes [171]. We showed that also for the simplest alcohol, methanol, BLYP is able to give an accurate description of the liquid phase. It is often argued in the literature that the so-called hybrid functionals such as B3LYP, which mix-in exact Hartree-Fock exchange, give more reliable energy barriers than the gradient-corrected functionals.* However, as our gas-phase study of the Ru-catalyzed transfer hydrogenation of ketones showed, we find that BLYP gives only 1-2 kcal/mol lower energy barriers compared to B3LYP, and hence, well within the general accuracy of DFT methods. More worrisome is the potential difference between DFT and perturbation methods such as the Møller-Plesset (MP) perturbation theory. Noyori and coworkers showed for a similar gas-phase study of the Ru-catalyzed transfer hydrogenation of ketones that MP4 gives in some cases for the same barrier a value that is 10 kcal/mol higher than the B3LYP-value [33]. And, although the overall energy profile is qualitatively the same for both electronic structure theories, the difference in energy barriers is not consistent. It is evident that first a convergence of these two approaches to compute the electronic structure of a system should be pursued, before one should worry a lot about different results among different density functionals.

We showed that DFT can be both a powerful and an accurate method to perform first-principles molecular dynamics simulations of liquids and solutions. However, one should keep in mind that, due to the complete neglect of dispersion forces, hydrogen bonding and/or dipole-dipole interactions should dominate the intermolecular interactions. Although dispersion forces are certainly non-negligible in the case of liquid methanol, we showed that hydrogen-bonding interactions dominate and an accurate description of the structure and dynamics of liquid methanol is attainable. In contrast, it is questionable whether a DFT-based first-principles simulation is feasible for liquid ethanol, and it would certainly fail in the case of liquid propanol, where dispersion interactions are without doubt important and must be incorporated. With the recent emergence of time-dependent DFT techniques might provide a way to incorporate dispersion forces in a first-principles simulation implicitly.

The great advantage of a first-principles simulation over a classical force-field simulation is of course the opportunity to investigate the electronic structure of the system under study.

*Hybrid functionals are not implemented in the CPMD code due to technical difficulties.

The Wannier function analysis, although qualitative in nature, proved to be a valuable tool to tackle the difficulties associated with the investigation of the electronic structure of liquid methanol of which the molecular orbitals are delocalized over the complete system (cf. Fig. 1.8). Moreover, the analysis proved to be essential in our investigation of the Ru-catalyzed transfer hydrogenation of ketones in solution. A density of states (DOS) analysis is also useful, but to be able to directly relate the influence of solvent molecules on a typical reaction one needs to know the change in position of the electrons, *i.e.* the Wannier function associated centers, along the reaction path. In addition, these centers can be used to directly calculate the average molecular dipole moment of a liquid or solute, giving an idea of the polarization of the charge distribution of a molecule due to the other molecules in the liquid. And by taking the Fourier transform of the dipole-dipole autocorrelation function one can compute the infrared spectrum of a liquid or solute [54]. Finally, we want to remark that an enhanced (static) dipole moment with respect to the gas-phase value, typically used in classical force-field simulations of liquids to account in a mean-field approach for the thermal induction effects, is an oversimplification of the large thermally driven fluctuations in the instantaneous dipole moment of solvent molecules or solutes we found in our first-principles simulations.

From Gas Phase to Solution

A computational study of a reaction both in the gas-phase and in solution has two major benefits: first the gas-phase study provides a detailed understanding of the basic chemical transformations and changes in the electronic structure along the reaction path; and second, a comparison between the gas-phase reaction and the solvated reaction directly shows the influence of the solvent. Unfortunately, in order to study a typical reaction in solution, already from the onset the reaction path should be known, and in almost all cases a constraint is needed to force the reaction to take place within a computationally feasible time-scale. Typically the chosen constraint is guided by the gas-phase reaction. However, the constraint is in general not correct since all degrees of freedom including those of the solvent molecules are implicitly involved. This is evident from the hysteresis when the reversed reaction pathway is studied by applying the same constraint values backwards, giving a somewhat different energy profile. This hysteresis effect is caused by the solvation shell that has not completely relaxed during a constraint molecular dynamics simulation, and can be quite substantial for strongly coordinating solvent molecules such as water [176]. By studying beforehand the gas-phase reaction pathway it is possible to have a constraint that mimics the actual reaction in solution very closely, and by performing sufficiently long constraint molecular dynamics simulation, one minimizes the effect of hysteresis. A way to alleviate the problems associated with the method of constraints is to use transition-path sampling [197], in which instead of constraints, one uses an algorithm that samples the true solvated transition state. This methodology needs only the initial and the final state of the reaction, and hence, prior knowledge of the reaction path is not required. In addition, it gives an estimate of the rate constant of a reaction. A drawback of this technique is that it is computationally very demanding and with the current computer resources it would require an enormous amount of CPU time to study the type of systems addressed in this thesis.

In our computational study of the Ru-catalyzed transfer hydrogenation of formaldehyde in the gas phase and in an alcohol solution the changes upon solvation were a decrease of the activation barrier in both directions and, more importantly, a significant change in the overall energy profile including, the emergence of a solvation barrier. Instead of the concerted hydride-proton transfer in the gas phase, we found a two-step process in solution. Initially, the carbonyl carbon is hydrogenated by the Ru-hydride, and subsequently, the carbonyl oxygen is protonated either by a solvent molecule or by the amine-ligand. The two-step nature of the mechanism in

solution is caused by the formation of a short-lived metal-alkoxide intermediate stabilized by two hydrogen-bonded solvent molecules. A further aspect of the reaction in solution is the formation of strong hydrogen bonds between the oxygen of the aminoalcohol ligand and two solvent molecules, making the Ru metal center more positively charged, and hence, more reactive towards a hydrogen of the methyl group of the hydrogen donor. Experiments support this observation since diamine-based ligands show no reactivity, whereas the N-monotosylated analogs show high conversions. Evidently, the oxygen of the ligand, or rather the strongly solvated oxygen, is essential to have high conversions. In summary, a protic polar solvent such as a simple alcohol or formic acid activates the amino alcohol ligand and stabilizes the metal-alkoxide intermediate in the Ru-catalyzed transfer hydrogenation of ketones. In more general terms our study gives a new perspective on the active role the solvent can have in transition metal catalyzed reactions.

First-Principles Computer Simulations

With the fundamental laws of quantum mechanics and statistical mechanics, the availability of high-performance computers, and with the growing range of sophisticated software accessible to an increasing number of scientists, the use of first-principles molecular dynamics (MD) simulations to design novel catalytic systems appears to be closer than ever. Yet the complexity of catalytic systems, especially the heterogeneous analogs, with their intriguing mechanistic interplay between substrate and catalyst, the influence of the surrounding medium including temperature effects, and the required (stereo)selectivity seems to indicate the opposite. Therefore, neither has first-principles catalyst design become a generally accepted practice nor is it complete fiction, far from any reality. The truth, it seems, is somewhere in between, with the frontier moving from fiction to fact at a steady and quite predictable pace, driven by the development of novel theoretical approaches, new algorithms, and increasingly faster hardware.

Whereas normally catalytic reactions are studied in the gas phase using standard quantum chemistry packages with a graphical user interface, the recent evolution of computer hardware (including networks) makes it feasible to study the full catalytic system including solvent and temperature effects as shown in this thesis. However, this comes at a price, since now not only one has to have fundamental knowledge of the field of quantum chemistry, but also of statistical mechanics and related thermodynamics. Moreover one has to be able to combine both methodologies. Although excellent software exists to this, from my own experience, it is quite a challenge to successfully study the full catalytic system with first-principles MD techniques. Hence, it remains to be seen if these techniques can be used in the way such as quantum chemistry packages are routinely used in both the academic world and industry.

Nowadays, except for the length scale, which should be in the pico second range, there is in principle no restriction on the type of system that can be studied using first-principles MD techniques. For example, using a hybrid QM/MM method one can expand the size of the system up to a few thousands of atoms, making it possible to study not only protein structure and dynamics, but also the associated enzymatic reactions as shown recently by Rothlisberger and coworkers [198]. Another example is the study of redox reactions using first-principles techniques. Here, using multiple electronic ground state surfaces, one for each oxidation state, one is able to swap from one surface to the other, and hence from one oxidation state to the other, by changing the electrochemical potential. Recently Sprik and coworkers illustrated this technique by an application to the redox dynamics of an aniline molecule in the gas phase [199] and in aqueous solution [200]. This opens up the way for computational voltametry and even for example the computational study of the process of corrosion on metallic surfaces. In conclusion, the restrictions on what is computationally feasible are beginning to fade, and will

be removed with the current speedup of computer hardware in the next few years, so lets wait and see what the future will give us!

Bibliography

- [1] Fluck, E.; Heumann, K. G. *Periodensystem der Elemente*; Wiley-VCH: Weinheim, 2002.
- [2] Beck, G. *Synlett* **2002**, 837-850.
- [3] Ojima, I. *Catalytic Asymmetric Synthesis*; VCH: New York, 1993.
- [4] Noyori, R. *Asymmetric Catalysis in Organic Synthesis*; Wiley: New York, 1994.
- [5] Noyori, R.; Hashiguchi, S. *Acc. Chem. Res.* **1997**, *30*, 97-102.
- [6] Osborn, J. A.; Jardine, F. H.; Young, J. F.; Wilkinson, G. *J. Chem. Soc. A* **1966**, 1711.
- [7] Knowles, W. S. *Angew. Chem. Int. Ed.* **2002**, *41*, 1998-2007.
- [8] Knowles, W. S.; Sabacky, M. J. *J. Chem. Soc., Chem. Commun.* **1968**, 1445.
- [9] Halpern, J.; Wong, C. S. *J. Chem. Soc., Chem. Commun.* **1973**, 629.
- [10] Halpern, J.; Okamoto, T.; Zakhariiev, A. *J. Mol. Catal.* **1976**, *2*, 65-68.
- [11] Halpern, J. *Inorg. Chim. Acta* **1981**, *50*, 11-19.
- [12] Dawans, F.; Morel, D. *J. Mol. Catal.* **1977**, *3*, 403-415.
- [13] Halpern, J. Asymmetric Catalytic Hydrogenation: Mechanism and Origin of Enantioselectivity. In *Asymmetric Synthesis*, Vol. 5; Morrison, J. D., Ed.; Academic Press: New York, 1985; Chapter 2.
- [14] Chan, A. S. C.; Pluth, J. J.; Halpern, J. *Inorg. Chim. Acta* **1979**, *37*, L477-L479.
- [15] Landis, C. R.; Halpern, J. *J. Am. Chem. Soc.* **1987**, *109*, 1746-1754.
- [16] Landis, C. R.; Feldgus, S. *Angew. Chem. Int. Ed.* **2000**, *39*, 2863-2866.
- [17] Feldgus, S.; Landis, C. R. *J. Am. Chem. Soc.* **2000**, *122*, 12714-12727.
- [18] Feldgus, S.; Landis, C. R. *Organometallics* **2001**, *20*, 2374-2386.
- [19] Burk, M. J.; Casy, G.; Johnson, N. B. *J. Org. Chem.* **1998**, *63*, 6084-6085.
- [20] Gridnev, I. D.; Higashi, N.; Asakura, K.; Imamoto, T. *J. Am. Chem. Soc.* **2000**, *122*, 7183-7194.
- [21] Gridnev, I. D.; Higashi, N.; Imamoto, T. *J. Am. Chem. Soc.* **2000**, *122*, 10486-10487.
- [22] Ramsden, J. A.; Claridge, T. D. W.; Brown, J. M. *J. Chem. Soc., Chem. Commun.* **1995**, 2469-2471.
- [23] Adams, N. J.; Bargon, J.; Brown, J. M.; Farrington, E. J.; Galardon, E.; Giernoth, R.; Heinrich, H.; John, B. D.; Maeda, K. *Pure Appl. Chem.* **2001**, *73*, 343-346.
- [24] Heinrich, H.; Giernoth, R.; Bargon, J.; Brown, J. M. *Chem. Commun.* **2001**, 1296-1297.
- [25] Gridnev, I. D.; Imamoto, T. *Organometallics* **2001**, *20*, 545-549.
- [26] Gridnev, I. D.; Higashi, N.; Imamoto, T. *Organometallics* **2001**, *20*, 4542-4553.
- [27] Zassinovich, G.; Mestroni, G.; Gladiali, S. *Chem. Rev.* **1992**, *92*, 1051-1069.
- [28] Noyori, R. *Adv. Synth. Catal.* **2003**, *345*, 15-32.
- [29] Noyori, R.; Ohkuma, T. *Angew. Chem. Int. Ed.* **2001**, *40*, 40-73.
- [30] Wilds, A. L. *Org. React.* **1944**, *2*, 178-223.

- [31] Alanso, D. A.; Brandt, P.; Nordin, S. J. M.; Andersson, P. G. J. *Am. Chem. Soc.* **1999**, *121*, 9580-9588.
- [32] Petra, D. G. I.; Reek, J. N. H.; Handgraaf, J.-W.; Meijer, E. J.; Dierkes, P.; Kamer, P. C. J.; Brussee, J.; Schoemaker, H. E.; van Leeuwen, P. W. N. M. *Chem. Eur. J.* **2000**, *6*, 2818-2829.
- [33] Yamakawa, M.; Ito, H.; Noyori, R. *J. Am. Chem. Soc.* **2000**, *122*, 1466-1478.
- [34] Guiral, V.; Delbecq, F.; Sautet, P. *Organometallics* **2001**, *20*, 2207-2214.
- [35] Burk, M. J.; Kalberg, C. S.; Pizzano, A. J. *Am. Chem. Soc.* **1998**, *120*, 4345-4353.
- [36] Born, M.; Oppenheimer, J. R. *Annln. Phys.* **1927**, *84*, 457.
- [37] McWeeny, R. *Methods of Molecular Quantum Mechanics*; Academic Press: London, 2 ed.; 1992.
- [38] Hohenberg, P.; Kohn, W. *Phys. Rev.* **1964**, *136*, B864-B871.
- [39] Parr, R. G.; Yang, W. T. *Density-Functional Theory of Atoms and Molecules*; Oxford University Press: New York, 1989.
- [40] Kohn, W.; Sham, L. J. *Phys. Rev.* **1965**, *140*, A1133-A1138.
- [41] Gill, P. M. W. Density Functional Theory (DFT), Hartree-Fock (HF), and the Self-consistent Field. In *Encyclopedia of Computational Chemistry*; von Ragué Schleyer, P., Ed.; Wiley: New York, 1998.
- [42] Becke, A. D. *Phys. Rev. A* **1988**, *38*, 3098-3100.
- [43] Lee, C. T.; Yang, W. T.; Parr, R. G. *Phys. Rev. B* **1988**, *37*, 785-789.
- [44] Perdew, J. P.; Chevary, J. A.; Vosko, S. H.; Jackson, K. A.; Pederson, M. R.; Singh, D. J.; Fiolhais, C. L. *Phys. Rev. B* **1992**, *46*, 6671-6687; Erratum, *Phys. Rev. B.* **1993**, *48*, 4978.
- [45] Hu, C.-H.; Chong, D. P. Density Functional Applications. In *Encyclopedia of Computational Chemistry*; von Ragué Schleyer, P., Ed.; Wiley: New York, 1998.
- [46] Koch, W.; Hertwig, R. H. Density Functional Theory Applications to Transition Metal Problems. In *Encyclopedia of Computational Chemistry*; von Ragué Schleyer, P., Ed.; Wiley: New York, 1998.
- [47] Allen, M. P.; Tildesley, D. J. *Computer Simulation of Liquids*; Clarendon Press: Oxford, 2001.
- [48] Frenkel, D.; Smit, B. *Understanding Molecular Simulation*; Academic Press: San Diego, 2002.
- [49] Swope, W. C.; Andersen, H. C.; Berens, P. H.; Wilson, K. R. *J. Chem. Phys.* **1982**, *76*, 637-649.
- [50] Marx, D.; Hutter, J. Ab initio molecular dynamics: Theory and Implementation. In *Modern Methods and Algorithms of Quantum Chemistry*, Vol. 1; Grotendorst, J., Ed.; John von Neumann Institute for Computing: Jülich, 2000.
- [51] Car, R.; Parrinello, M. *Phys. Rev. Lett.* **1985**, *55*, 2471-2474.
- [52] van Erp, T. S.; Meijer, E. J. *Chem. Phys. Lett.* **2001**, *333*, 290-296.
- [53] van Erp, T. S.; Meijer, E. J. *J. Chem. Phys.* **2003**, *118*, 8831-8840.
- [54] Gaigeot, M.-P.; Sprik, M., submitted for publication in *J. Chem. Phys.*
- [55] Bachelet, G. B.; Hamann, D. R.; Schlüter, M. *Phys. Rev. B* **1982**, *26*, 4199-4228.
- [56] Vanderbilt, D. *Phys. Rev. B* **1985**, *32*, 8412-8415.
- [57] Troullier, N.; Martins, J. L. *Phys. Rev. B* **1991**, *43*, 1993-2006.
- [58] <http://molsim.chem.uva.nl/cluster/>.
- [59] <http://www.sara.nl/>.
- [60] <http://www.cpmo.org/>.
- [61] <http://www.scm.com/>.
- [62] <http://www.fulvic.com/>.
- [63] <http://www.opendx.org/>.

- [64] <http://public.kitware.com/VTK/>.
- [65] <http://www.opengl.org/>.
- [66] Ensing, B. *Chemistry in water, First Principles Computer Simulations*, Thesis, Free University Amsterdam, Department of Theoretical Chemistry, 2003.
- [67] Images were rendered with gOpenMol (<http://www.csc.fi/gopenmol/>).
- [68] Geometry of fulvic acid was optimized with ADF and images were rendered with OpenDx.
- [69] Petra, D. G. I. *Asymmetric Transfer Hydrogenation of Ketones*, Thesis, University of Amsterdam, Institute of Molecular Chemistry, 1999.
- [70] Yamaguchi, T.; Hidaka, K.; Soper, A. K. *Mol. Phys.* **1999**, *96*, 1159-1168; Erratum, *Mol. Phys.* **1999**, *97*, 603-604.
- [71] Adya, A. K.; Bianchi, L.; Wormald, C. J. *J. Chem. Phys.* **2000**, *112*, 4231-4241.
- [72] Haughney, M.; Ferrario, M.; McDonald, I. R. *J. Phys. Chem.* **1987**, *91*, 4934-4940.
- [73] Bianchi, L.; Kalugin, O. N.; Adya, A. K.; Wormald, C. J. *Mol. Simulation* **2000**, *25*, 321-338.
- [74] Tu, Y.; Laaksonen, A. *Phys. Rev. E* **2001**, *64*, 026703.
- [75] Martín, M. E.; Sánchez, M. L.; del Valle, F. J. O.; Aguilar, M. A. *J. Chem. Phys.* **2002**, *116*, 1613-1620.
- [76] Tsuchida, E.; Kanada, Y.; Tsukada, M. *Chem. Phys. Lett.* **1999**, *311*, 236-240.
- [77] Laasonen, K.; Sprik, M.; Parrinello, M.; Car, R. *J. Chem. Phys.* **1993**, *99*, 9080-9089.
- [78] Sprik, M.; Hutter, J.; Parrinello, M. *J. Chem. Phys.* **1996**, *105*, 1142-1152.
- [79] Silvestrelli, P. L.; Parrinello, M. *J. Chem. Phys.* **1999**, *111*, 3572-3580.
- [80] Marx, D.; Sprik, M.; Parrinello, M. *Chem. Phys. Lett.* **1997**, *273*, 360-366.
- [81] Raugei, S.; Klein, M. L. *J. Chem. Phys.* **2002**, *116*, 196-202.
- [82] Hutter, J.; Alavi, A.; Deutsch, T.; Bernasconi, M.; Goedecker, S.; Marx, D.; Tuckerman, M.; Parrinello, M. "CPMD, version 3.4", MPI für Festkörperforschung and IBM Zurich Research Laboratory, 1995-1999.
- [83] te Velde, G.; Baerends, E. J.; et al., "ADF, version 2000", Theoretical Chemistry, Vrije Universiteit, Amsterdam, 2000.
- [84] M6, O.; Y6ñez, M.; Elguero, J. *J. Chem. Phys.* **1997**, *107*, 3592-3601.
- [85] Martyna, G. J.; Tuckerman, M. E. *J. Chem. Phys.* **1999**, *110*, 2810-2821.
- [86] Schütz, M.; Brdarski, S.; Widmark, P.-O.; Lindh, R.; Karlstr6m, G. *J. Chem. Phys.* **1997**, *107*, 4597-4605.
- [87] González, L.; M6, O.; Y6ñez, M. *J. Chem. Phys.* **1998**, *109*, 139-150.
- [88] Lovas, F. J.; Belov, S. P.; Tretyakov, M. Y.; Stahl, W.; Suenram, R. D. *J. Mol. Spectrosc.* **1995**, *170*, 478-492.
- [89] Lovas, F. J.; Hartwig, H. *J. Mol. Spectrosc.* **1997**, *185*, 98-109.
- [90] Mooij, W. T. M.; van Duijneveldt, F. B.; van Duijneveldt-van de Rijdt, J. G. C. M.; van Eijck, B. P. *J. Phys. Chem. A* **1999**, *103*, 9872-9882.
- [91] Kristy6n, S.; Pulay, P. *Chem. Phys. Lett.* **1994**, *229*, 175-180.
- [92] Meijer, E. J.; Sprik, M. *J. Chem. Phys.* **1996**, *105*, 8684-8689.
- [93] Riddick, J. A.; Bunger, W. B.; Sakano, T. K. *Organic solvents: physical properties and methods of purification*; Wiley: New York, 1986.
- [94] Nos6, S. *J. Chem. Phys.* **1984**, *81*, 511-519.
- [95] Guillot, B.; Guissani, Y. *J. Chem. Phys.* **1998**, *108*, 10162-10174.
- [96] Shimanouchi, T. *Tables of molecular vibrational frequencies consolidated*; National Bureau of Standards: Washington, 1972.

- [97] Bertie, J. E.; Zhang, S. L.; Eysel, H. H.; Baluja, S.; Ahmed, M. K. *Appl. Spectrosc.* **1993**, *47*, 1100-1114.
- [98] Bouř, P. *Chem. Phys. Lett.* **2002**, *365*, 82-88.
- [99] Garberoglio, G.; Vallauri, R. *J. Chem. Phys.* **2001**, *115*, 395-401.
- [100] Hansen, J. P.; McDonald, I. R. *Theory of Simple Liquids*; Academic Press: London, 2 ed.; 1986.
- [101] Ludwig, R.; Zeidler, M. D. *Mol. Phys.* **1994**, *82*, 313-323.
- [102] Lock, A. J.; Woutersen, S.; Bakker, H. J. *J. Phys. Chem. A* **2001**, *105*, 1238-1243.
- [103] Hurle, R. L.; Woolf, L. A. *Aust. J. Chem.* **1980**, *33*, 1947-1952.
- [104] Marzari, N.; Vanderbilt, D. *Phys. Rev. B* **1997**, *56*, 12847-12865.
- [105] Silvestrelli, P. L.; Marzari, N.; Vanderbilt, D.; Parrinello, M. *Solid State Commun.* **1998**, *107*, 7-11.
- [106] Cornell, W. D.; Cieplak, P.; Bayly, C. I.; Gould, I. R.; Merz, K. M.; Ferguson, D. M.; Spellmeyer, D. C.; Fox, T.; Caldwell, J. W.; Kollmann, P. A. *J. Am. Chem. Soc.* **1995**, *117*, 5179-5197.
- [107] Ivash, E. V.; Dennison, D. M. *J. Chem. Phys.* **1953**, *21*, 1804.
- [108] Hünenberger, P. H.; van Gunsteren, W. F. *J. Chem. Phys.* **1998**, *108*, 6117-6134.
- [109] Saiz, L.; Guàrdia, E.; Padró, J.-A. *J. Chem. Phys.* **2000**, *113*, 2814-2822.
- [110] Resta, R.; Sorella, S. *Phys. Rev. Lett.* **1999**, *82*, 370-373.
- [111] Silvestrelli, P. L.; Bernasconi, M.; Parrinello, M. *Chem. Phys. Lett.* **1997**, *277*, 478-482.
- [112] Skaf, M. S.; Fonseca, T.; Ladanyi, B. M. *J. Chem. Phys.* **1993**, *98*, 8929-8945.
- [113] Oster, G.; Kirkwood, J. G. *J. Chem. Phys.* **1943**, *11*, 175-178.
- [114] Svishchev, I. M.; Kusalik, P. G. *J. Chem. Phys.* **1994**, *100*, 5165-5171.
- [115] Kusalik, P. G.; Mandy, M. E.; Svishchev, I. M. *J. Chem. Phys.* **1994**, *100*, 7654-7664.
- [116] Hashiguchi, S.; Fujii, A.; Takehara, J.; Ikariya, T.; Noyori, R. *J. Am. Chem. Soc.* **1995**, *117*, 7562-7563.
- [117] Yang, H.; Alvarez, M.; Lugan, N.; Mathieu, R. *J. Chem. Soc., Chem. Commun.* **1995**, 1721-1722.
- [118] Fujii, A.; Hashiguchi, S.; Uematsu, N.; Ikariya, T.; Noyori, R. *J. Am. Chem. Soc.* **1996**, *118*, 2521-2522.
- [119] Gao, J.-X.; Ikariya, T.; Noyori, R. *Organometallics* **1996**, *15*, 1087-1089.
- [120] Jiang, Q. Z.; Plew, D. V.; Murtuza, S.; Zhang, X. M. *Tetrahedron Lett.* **1996**, *37*, 797-800.
- [121] Takehara, J.; Hashiguchi, S.; Fujii, A.; Inoue, S.; Ikariya, T.; Noyori, R. *Chem. Commun.* **1996**, 233-234.
- [122] Haack, K.-J.; Hashiguchi, S.; Fujii, A.; Ikariya, T.; Noyori, R. *Angew. Chem. Int. Ed. Engl.* **1997**, *36*, 285-288.
- [123] Hashiguchi, S.; Fujii, A.; Haack, K.-J.; Matsumura, K.; Ikariya, T.; Noyori, R. *Angew. Chem. Int. Ed. Engl.* **1997**, *36*, 288-290.
- [124] ter Halle, R.; Schulz, E.; Lemaire, M. *Synlett* **1997**, 1257-1258.
- [125] Matsumura, K.; Hashiguchi, S.; Ikariya, T.; Noyori, R. *J. Am. Chem. Soc.* **1997**, *119*, 8738-8739.
- [126] Palmer, M.; Walsgrove, T.; Wills, M. *J. Org. Chem.* **1997**, *62*, 5226-5228.
- [127] Alonso, D. A.; Guijarro, D.; Pinho, P.; Temme, O.; Andersson, P. G. *J. Org. Chem.* **1998**, *63*, 2749-2751.
- [128] Jiang, Y. T.; Jiang, Q. Z.; Zhang, X. M. *J. Am. Chem. Soc.* **1998**, *120*, 3817-3818.

- [129] Schwink, L.; Ireland, T.; Püntener, K.; Knochel, P. *Tetrahedron: Asymmetry* **1998**, *9*, 1143-1163.
- [130] Aranyos, A.; Csjernyik, G.; Szabó, K. J.; Bäckvall, J.-E. *Chem. Commun.* **1999**, 351-352.
- [131] Braunstein, P.; Fryzuk, M. D.; Naud, F.; Rettig, S. J. *J. Chem. Soc., Dalton Trans.* **1999**, 589-594.
- [132] Alonso, D. A.; Nordin, S. J. M.; Roth, P.; Tarnai, T.; Andersson, P. G.; Thommen, M.; Pittelkow, U. *J. Org. Chem.* **2000**, *65*, 3116-3122.
- [133] Braunstein, P.; Naud, F.; Graiff, C.; Tiripicchio, A. *Chem. Commun.* **2000**, 897-898.
- [134] Ohkuma, T.; Ishii, D.; Takeno, H.; Noyori, R. *J. Am. Chem. Soc.* **2000**, *122*, 6510-6511.
- [135] Quirnbach, M.; Holz, J.; Tararov, V. I.; Börner, A. *Tetrahedron* **2000**, *56*, 775-780.
- [136] Braunstein, P.; Naud, F.; Rettig, S. J. *New J. Chem.* **2001**, *25*, 32-39.
- [137] Everaere, K.; Mortreux, A.; Bulliard, M.; Brussee, J.; van der Gen, A.; Nowogrocki, G.; Carpentier, J.-F. *Eur. J. Org. Chem.* **2001**, 275-291.
- [138] Gamez, P.; Fache, F.; Mangeney, P.; Lemaire, M. *Tetrahedron Lett.* **1993**, *34*, 6897-6898.
- [139] Gamez, P.; Fache, F.; Lemaire, M. *Tetrahedron: Asymmetry* **1995**, *6*, 705-718.
- [140] Gamez, P.; Dunjic, B.; Lemaire, M. *J. Org. Chem.* **1996**, *61*, 5196-5197.
- [141] Nishibayashi, Y.; Singh, J. D.; Arikawa, Y.; Uemura, S.; Hidai, M. *J. Organomet. Chem.* **1997**, *531*, 13-18.
- [142] Bernard, M.; Guiral, V.; Delbecq, F.; Fache, F.; Sautet, P.; Lemaire, M. *J. Am. Chem. Soc.* **1998**, *120*, 1441-1446.
- [143] de Bellefon, C.; Tanchoux, N. *Tetrahedron: Asymmetry* **1998**, *9*, 3677-3686.
- [144] Mashima, K.; Abe, T.; Tani, K. *Chem. Lett.* **1998**, 1199-1200.
- [145] Mashima, K.; Abe, T.; Tani, K. *Chem. Lett.* **1998**, 1201-1202.
- [146] Mao, J. M.; Baker, D. C. *Org. Lett.* **1999**, *1*, 841-843.
- [147] Murata, K.; Ikariya, T.; Noyori, R. *J. Org. Chem.* **1999**, *64*, 2186-2187.
- [148] Polborn, K.; Severin, K. *Eur. J. Inorg. Chem.* **2000**, 1687-1692.
- [149] Zassinovich, G.; Bettella, R.; Mestroni, G.; Bresciani-Pahor, N.; Geremia, S.; Randaccio, L. *J. Organomet. Chem.* **1989**, *370*, 187-202.
- [150] Müller, D.; Umbricht, G.; Weber, B.; Pfaltz, A. *Helv. Chim. Acta* **1991**, *74*, 232-240.
- [151] ter Halle, R.; Bréhéret, A.; Schulz, E.; Pinel, C.; Lemaire, M. *Tetrahedron: Asymmetry* **1997**, *8*, 2101-2108.
- [152] Inoue, S.; Nomura, K.; Hashiguchi, S.; Noyori, R.; Izawa, Y. *Chem. Lett.* **1997**, 957-958.
- [153] Petra, D. G. I.; Kamer, P. C. J.; Spek, A. L.; Schoemaker, H. E.; van Leeuwen, P. W. N. M. *J. Org. Chem.* **2000**, *65*, 3010-3017.
- [154] Guiral, V.; Delbecq, F.; Sautet, P. *Organometallics* **2000**, *19*, 1589-1598.
- [155] Noyori, R.; Yamakawa, M.; Hashiguchi, S. *J. Org. Chem.* **2001**, *66*, 7931-7944.
- [156] Nishide, K.; Node, M. *Chirality* **2002**, *14*, 759-767.
- [157] Gladiali, S.; Pinna, L.; Delogu, G.; Martin, S. D.; Zassinovich, G.; Mestroni, G. *Tetrahedron: Asymmetry* **1990**, *1*, 635-648.
- [158] van Lenthe, E.; Ehlers, A.; Baerends, E. J. *J. Chem. Phys.* **1999**, *110*, 8943-8953.
- [159] Braunstein, P.; Naud, F. *Angew. Chem. Int. Ed.* **2001**, *40*, 680-699.
- [160] Hamprecht, F. A.; Cohen, A. J.; Tozer, D. J.; Handy, N. C. *J. Chem. Phys.* **1998**, *109*, 6264-6271.
- [161] Singh, U. C.; Kollman, P. A. *J. Comp. Chem.* **1984**, *5*, 129-145.
- [162] Yamakawa, M.; Yamada, I.; Noyori, R. *Angew. Chem. Int. Ed.* **2001**, *40*, 2818-2821.

- [163] Everaere, K.; Mortreux, A.; Carpentier, J.-F. *Adv. Synth. Catal.* **2003**, *345*, 67-77.
- [164] Handgraaf, J.-W.; Reek, J. N. H.; Meijer, E. J. *Organometallics* **2003**, *22*, 3150-3157.
- [165] Casey, C. P.; Johnson, J. B. *J. Org. Chem.* **2003**, *68*, 1998-2001.
- [166] Reichardt, C. *Solvents and Solvent Effects in Organic Chemistry*; VCH: Weinheim, 2 ed.; 1990.
- [167] Meijer, E. J.; Sprik, M. J. *Am. Chem. Soc.* **1998**, *120*, 6345-6355.
- [168] Carloni, P.; Sprik, M.; Andreoni, W. *J. Phys. Chem. B* **2000**, *104*, 823-835.
- [169] Ensing, B.; Buda, F.; Blöchl, P.; Baerends, E. J. *Angew. Chem. Int. Ed.* **2001**, *40*, 2893-2895.
- [170] Tuckerman, M. E.; Marx, D.; Parrinello, M. *Nature* **2002**, *417*, 925-929.
- [171] Sprik, M. J. *Phys.: Condens. Matter* **2000**, *12*, A161-A163.
- [172] Handgraaf, J.-W.; van Erp, T. S.; Meijer, E. J. *Chem. Phys. Lett.* **2003**, *367*, 617-624.
- [173] Kozelka, J. Molecular Modeling of Transition Metal Adducts with Nucleic Acids and their Constituents. In *Metals Ions in Biological Systems*, Vol. 33; Sigel, A.; Sigel, H., Eds.; M. Dekker Publishing: New York, 1996.
- [174] Carter, E. A.; Ciccotti, G.; Hynes, J. T.; Kapral, R. *Chem. Phys. Lett.* **1989**, *156*, 472-477.
- [175] Atkins, P. W. *Physical Chemistry*; Oxford University Press: Oxford, 6 ed.; 1998.
- [176] Ensing, B.; Meijer, E. J.; Blöchl, P. E.; Baerends, E. J. *J. Phys. Chem. A* **2001**, *105*, 3300-3310.
- [177] McClellan, A. L. *Tables of Experimental Dipole Moments*; W. H. Freeman and Company: San Francisco, 1963.
- [178] Silvestrelli, P. L.; Parrinello, M. *Phys. Rev. Lett.* **1999**, *82*, 3308-3311; Erratum, *Phys. Rev. Lett.* **1999**, *82*, 5415.
- [179] Brown, J. M.; Evans, P. L.; Lucy, A. R. *J. Chem. Soc., Perkin Trans. II* **1987**, *2*, 1589-1596.
- [180] Koga, N.; Morokuma, K. *Chem. Rev.* **1991**, *91*, 823-842.
- [181] Ando, D.; Bevan, C.; Brown, J. M.; Price, D. W. *J. Chem. Soc., Chem. Commun.* **1992**, 592-594.
- [182] Yu, J.; Spencer, J. B. *J. Am. Chem. Soc.* **1997**, *119*, 5257-5258.
- [183] Yu, J.; Spencer, J. B. *Tetrahedron* **1998**, *54*, 15821-15832.
- [184] Yu, J.; Whitney, P.-S.; Spencer, J. B. *J. Mol. Catal. A: Chemical* **1999**, *146*, 199-210.
- [185] Yu, J. *Mechanistic Investigation into Catalytic Hydrogenation*, Thesis, University of Cambridge, University Chemical Laboratory, 2000.
- [186] Vosko, S. H.; Wilk, L.; Nusair, M. *Can. J. Phys.* **1980**, *58*, 1200.
- [187] Perdew, J. P.; Zunger, A. *Phys. Rev. B* **1981**, *23*, 5048-5079.
- [188] van Lenthe, E.; van Leeuwen, R.; Baerends, E. J.; Snijders, J. G. *Int. J. Quantum Chem.* **1996**, *57*, 281-293.
- [189] Cioslowski, J. *J. Am. Chem. Soc.* **1989**, *111*, 8333-8336.
- [190] Cioslowski, J.; Hamilton, T.; Scuseria, G.; Hess, B. A.; Hu, J.; Schaad, L. J.; Dupuis, M. *J. Am. Chem. Soc.* **1990**, *112*, 4183-4186.
- [191] Wiberg, K. B.; Rablen, P. R. *J. Comp. Chem.* **1993**, *14*, 1504-1518.
- [192] Maseras, F.; Morokuma, K. *J. Comp. Chem.* **1995**, *16*, 1170-1179.
- [193] Woo, T. K.; Cavallo, L.; Ziegler, T. *Theor. Chem. Acc.* **1998**, *100*, 307-313.
- [194] Clark, M.; Cramer, R. D.; van Opdenbosch, N. *J. Comp. Chem.* **1989**, *10*, 982-1012.
- [195] Carey, F. A.; Sundberg, R. J. *Advanced Organic Chemistry, Part A: Structure and Mechanisms*; Kluwer Academic/Plenum Publishers: New York, 4 ed.; 2000.
- [196] Lide, D. A., Ed.; *Handbook of Chemistry and Physics*; CRC press: Boca Raton and New York, 78 ed.; 1997.
- [197] Dellago, C.; Bolhuis, P. G.; Csajka, F. S.; Chandler, D. *J. Chem. Phys.* **1998**, *108*, 1964-1977.

-
- [198] Sulpizi, M.; Laio, A.; VandeVondele, J.; Cattaneo, A.; Rothlisberger, U.; Carloni, P. *Proteins: Structure, Function, and Genetics* **2003**, *52*, 212-224.
- [199] Tavernelli, I.; Vuilleumier, R.; Sprik, M. *Phys. Rev. Lett.* **2002**, *88*, 213002.
- [200] Tavernelli, I.; Sprik, M. *et al.* (to be published).

Summary

This thesis deals with a computational study of homogeneous transition metal catalyzed hydrogenation reactions in the gas-phase and in solution, on an atomistic level, using first-principles (or *ab initio*) techniques. Here first-principles denotes without prior knowledge of the interactions between the atoms. This in contrast to classical computational studies that use predetermined force fields describing the atomic interactions. These force fields are based on experimental data or high-level first-principles calculations of small molecular clusters in the gas phase. There are two reasons why we have to derive the interactions from first-principles: first, force fields do not include bond formation and breaking and as we are interested in reactions we need a method that can handle this; and second, transition metals cannot be accurately parameterized by force fields due to the special properties of the metal d-orbitals. These orbitals are very flexible and are able to adopt a wide variety of different hybridizations depending on the metal and the ligand(s) in question. The first-principles interactions are derived from electronic structure calculations using density functional theory (DFT). The reason why we use DFT is that is relatively inexpensive in terms of CPU[†] time compared to other electronic structure methods, while still maintaining a satisfactory level of accuracy with respect to structure and energetics. Here, "relatively inexpensive" means that we still have to perform large-scale calculations on parallel supercomputers, and even then the calculations may take many months. In our case we choose the Becke-Lee-Yang-Parr (BLYP) generalized gradient corrected density functional which has shown to give an accurate description of liquid water and small solutes in aqueous environment. The Car-Parrinello technique was used to perform the first-principles molecular dynamics (MD) simulations. This technique efficiently unifies DFT with MD by introducing a fictitious kinetic energy for the orbital degrees of freedom that follow the much slower dynamics of the nuclei "on-the-flight", reducing the computational effort by a factor of roughly ten compared to other first-principles MD techniques. The smaller part of the calculations presented in this thesis were performed with the atomic orbital based ADF package, whereas the major part were done with the plane-wave based CPMD program.

Chapter 2 gives the results of a first-principles MD simulation of liquid methanol, *i.e.* the solvent of choice for the computational study in solution. A prior study of liquid methanol was needed as we were not sure whether DFT could describe accurately the properties of this liquid as current density functionals do not account for dispersion interactions that could be important for methanol with its hydrophobic methyl group. Moreover, also from a fundamental point of view our study could prove interesting since there is much debate in the literature concerning the microscopic structure and related properties of liquid methanol. In first instance the numerical accuracy of the CPMD program was validated against the state-of-the-art ADF package. Using the methanol dimer as test case we find that bond lengths differ by not more than 0.02 Å whereas complexation energies are within 1 kJ/mol, indicating an excellent accuracy for the numerical methods employed in CPMD. To quantify the effect of the neglect of dispersion we compared the bindings energies of several different geometrical configurations

[†] Abbreviation for central processing unit.

of the dimer against MP2 literature data. From this we concluded that although the effect of dispersion is non-negligible, it is small compared to the magnitude of the hydrogen-bonding interaction, hence making it possible to study liquid methanol with DFT-BLYP based MD. For our study of the liquid at ambient conditions we considered a 32- (small) and 64-molecule (large) system. In this way we could quantify the effect of the finite-system size. We first investigated the structure of the liquid. Both the peak positions and peak heights of the computed hydrogen-bonding atom-atom radial distribution functions of the small and large system agreed closely with recent neutron diffraction (ND) experiments, although the small system tend to underestimate the peak heights somewhat. Depending on the definition of integration we computed for the number of hydrogen-bonded neighbors values of 1.6 to 2.0, again in close agreement with the ND data. Secondly, we looked at the short-time dynamics of the liquid by calculating the Fourier transform of velocity auto-correlation function, *i.e.* the power spectrum. In addition we also computed the power spectrum of one methanol molecule in the gas phase. All frequency modes in the obtained spectra are approximately 10 % underestimated, a known feature of BLYP. Compared to the gas-phase we see that the O–H stretching mode is in the liquid broadened and shifts to red by approximately 200 cm^{-1} , whereas the O–H bending mode is blue-shifted by approximately 70 cm^{-1} . At 650 cm^{-1} a broad band appears in the spectrum of the liquid that is not seen in the monomer spectrum. This mode is associated with the O–H torsion coupling with the intermolecular motions. Finally, we looked at the electronic properties of the liquid. To quantify the charge distribution we used the Wannier function analysis, which is a method that transforms the set of Kohn-Sham orbitals into localized Wannier functions and the associated centers (WFCs) that in turn may be assigned to common chemical meaning such as being associated with a bonding or lone pair. Again we compare the liquid with the gas-phase monomer. We find that there is small but significant shift of 0.03 \AA for the WFC associated with the O–H bond towards the oxygen atom. This is a manifestation of the hydrogen bonding and the induced polarization among the dipolar methanol molecules. To quantify the change in charge distribution in a single number we calculated the molecular dipole moment by assuming the electronic charge to be distributed as point charges located on the WFCs. In this way we find for the gas-phase monomer a value of 1.73 Debye and for the liquid 2.59 Debye, *i.e.* an enhancement of approximately 50 % and, due to thermal motion, there is a significant variation ranging from 1.7 to 3.5 Debye. In connection, the popular AMBER force field uses a static value of 2.2 Debye for the liquid, somewhat lower than our value and a simplification of the thermally induced variations. Another important electronic property of a liquid is its relative permittivity, commonly used to describe in an averaged manner solvent effects in quantum chemistry packages. From our first-principles simulation we obtain a value of 33, identical to the experimental value, indicating that we accurately describe the polarization of liquid methanol.

Having established that we can accurately describe liquid methanol using DFT-BLYP based MD, we focused our attention on the transition metal catalyzed transfer hydrogenation of ketones, one of the key transformations in synthetic chemistry to create chiral centers in molecules. Chapter 3 gives the results of a DFT-based computational study of the ruthenium and iridium catalyzed transfer hydrogenation of ketones in the gas phase using the BLYP functional.[‡] In general these catalysts consist of a transition metal, a stabilizing ligand, usually an arene, and a chiral ligand that enforces a high enantioselective outcome of the reaction. In experiments ruthenium (Ru) is the predominantly used metal, but also rhodium (Rh) and iridium (Ir) are

[‡]We are aware that currently better density functionals are available than BLYP. However, since we already used it in our first-principles MD study of liquid methanol we used it in the gas-phase study in order to be able to make a direct comparison between the gas-phase reaction and the reaction in solution (chapter 4). In connection, we found from the gas-phase study that the computed structures and energy barriers were in close agreement with B3LYP literature data of a similar gas-phase study.

used, and even catalysts with rare-earth metals were found to be active. Based on experimental well-performing catalysts we modeled the stabilizing ligand with benzene (Ru catalyst) and 1,5-cyclooctadienyl (Ir catalyst). For the chiral ligand we used the N,O-chelating aminoethanol ligand and for the transfer hydrogenation we considered a symmetric model reaction with methanol being the hydrogen donor and formaldehyde representing the hydrogen acceptor. The reason why we commenced with a gas-phase study and not straight with a study in solution is that we had to validate whether the CPMD program was able to accurately describe the structure and energetics of these metal complexes. Moreover, from the literature we knew that there was a possible difference in mechanism between the Ru- and Ir-catalyzed transfer hydrogenation which had not been clarified by other researchers.

The numerical accuracy of CPMD was validated against the ADF package by performing calculations on the metal hexacarbonyls. Both for structure and energetics excellent agreement was obtained, indicating state-of-the-art accuracy for the numerical methods employed in CPMD. The results of the comparison between the Ru- and Ir-catalyzed transfer hydrogenation were divided in three parts. First we looked at the bare metal compounds and the possible substrate coordinations. From our calculations we found that the ligand-coordination is much stronger in the Ru compound compared to the Ir analog. Initial coordination of the hydrogen donor or acceptor leads for the Ir complex to an elongation of the Ir–O bond and even a complete cleavage of this bond, whereas the Ru–O bond remains unchanged. These observations showed that the metal-oxygen bond has in the case of the Ir compound an intermolecular nature, while for the Ru compound this bond is strong and has substantial σ -character. In the second part of the results we looked at the formation the metal-alkoxide complexes. These complexes are possible important intermediates and obtained via proton transfer from the hydroxyl group to the nitrogen ligand in the methanol-coordinated complex. We found that for both the Ru- and Ir-complex the formation proceeds with negligible barriers, forming very stable methoxide-complexes. In fact, these complexes are the most stable on the potential energy surface, indicating that they are certainly formed and important intermediates or reservoirs of inactive catalyst in the catalytic cycle. In the final part of this gas-phase computational study we examined three different proposed reaction mechanisms of the transfer hydrogenation in order to elucidate which is the energetically most favorable. In close agreement with other, recently published computational gas-phase studies, we found that the mechanism of the Ru-catalyzed transfer hydrogenation takes place via a concerted transfer of the Ru-hydride and the proton bound to the ligand nitrogen, *i.e.* the metal-ligand bifunctional mechanism as proposed by Noyori. In contrast, our calculations showed that the Ir-catalyzed transfer hydrogenation favors direct transfer of an α -hydrogen of methoxide to the substrate, both coordinated with their oxygen to the Ir metal center, similar to the Meerwein-Ponndorf-Verley reduction. These findings are depicted schematically in Fig. 1. A direct consequence is that the formation of the very stable Ru-methoxide complex lies on a non-productive route, however, the formation takes place and is important for the overall kinetics of the catalytic cycle. Experimentally this fundamental difference between the mechanism of the Ru- and Ir-catalyzed transfer hydrogenation is also found, since for the Ir-catalyzed transfer the enantioselective outcome is dominated by the choice of hydrogen donor, whereas for the Ru-catalyzed transfer the choice of hydrogen donor has no influence on the enantioselectivity.

Now that we investigated both liquid methanol and the Ru-catalyzed transfer hydrogenation of ketones in the gas phase, we could study the transfer hydrogenation in solution, of which the results are given in chapter 4. Again we modeled the Ru-catalyst with the Ru-benzene-aminoethanol compound, and looked at the symmetric interconversion of methanol and formaldehyde. As the gas-phase barrier for the oxidative addition of methanol is more than 10 kcal/mol, it is classified as a rare event on the time scale of first-principles MD, typically ten

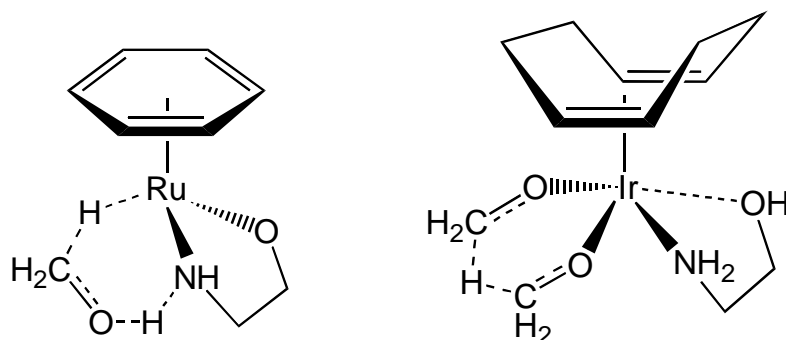


Figure 1: Schematic representation of the transition state structures of the Ru- (left) and Ir-catalyzed (right) transfer hydrogenation of ketones in the gas phase.

picoseconds. Hence, we had to use some trick to still be able to study the reaction in solution. This was done by using the method of constraints, where one imposes a gradual change of a suitable reaction coordinate, forcing the reaction to occur. In this way we performed 12 constraint MD simulations along the reaction path. To quantify the role of the methanol solvent we directly compared the gas-phase reaction with the reaction in solution. In first instance we looked at the thermochemistry. In contrast to the broad energy profile of the gas-phase reaction we find for the reaction in solution a two-step profile including the emergence of a clear solvation barrier. The two-step nature is caused by the formation of a short-lived metal-alkoxide complex.[§] It is formed via proton transfer from the hydroxyl group of methanol to the amide ligand, or vice versa, via proton transfer from the amine ligand to formaldehyde, and highly stabilized by two hydrogen-bonded solvent molecules. The barriers for oxidative addition and reductive elimination are reduced in solution by 1.3 and 3.4 kcal/mol compared to the gas phase. The existence of the metal-alkoxide complex was confirmed via a study of a micro-solvated system where we placed five methanol solvent molecules at crucial positions around the reacting complex. Secondly, we investigated the mechanistic aspects of the reaction by looking at the structural and electronic changes along the reaction path. For the latter we used, as in chapter 2, the Wannier function analysis. For the gas-phase reaction we find that the proton and the hydride are transferred in a concerted and gradual manner. In contrast, in solution, as soon as the substrate coordinates to the Ru-compound, the transfers occurs rather quickly and without substantial barriers in both directions. The Wannier analysis showed that along the oxidative addition pathway one of the WFCs associated with the Ru–N bond transforms into a nitrogen lone pair, forming with the incoming proton a new N–H bond. For the substrate we find that the O–H bond WFC shifts to oxygen at a distance typical for a lone-pair, a clear indication of the formation of the metal-alkoxide complex.

As the barrier for reductive elimination is reduced to only 1.4 kcal/mol in solution we decided to release the constraint at the formaldehyde coordinated Ru-complex and see what happened. We find that after 0.69 ps the hydride transfers to formaldehyde, while at the same time the oxygen of the substrate receives a proton from a coordinated solvent molecule, and *not* from the amine ligand. This solvent-mediated mechanism is clearly different from the metal-ligand

[§]This complex should not be confused with the previously mentioned metal-alkoxide complex that is bound to the metal center via the oxygen of the ligand, while this one is coordinated to the metal via the hydride.

bifunctional mechanism as proposed by Noyori. Very likely both mechanisms are operational during the Ru-catalyzed transfer hydrogenation of ketones.

Chapter 5, not directly related to the previous chapters, describes the results of a computational study of the homogeneous hydrogenation of functionalized alkenes using the Rh-based Wilkinson's catalyst $[\text{Rh}(\text{PPh}_3)_3\text{Cl}]$. This versatile reaction is predominantly used in industry and academia for the synthesis of chiral compounds, similar to the transfer hydrogenation. However, differently from the transfer hydrogenation, the hydrogen source in the catalytic hydrogenation is molecular hydrogen. Obviously, from an experimental point of view this is not the ideal hydrogen source since the reaction cannot be operated at ambient pressure. Concerning the mechanism there is quite some controversy in the current literature. Basically, there is argument about the order in which the reaction takes place. According to "the unsaturated route" first the catalyst-substrate adduct is formed that thereupon reacts in the enantioselective step with molecular hydrogen. In "the dihydride route" the order is reversed. First the catalyst is oxidized by molecular hydrogen to form an active complex that in turn reacts in the enantioselective step, *i.e.* the hydrometalation step, with the substrate. Based on experimental evidence, Yu and Spencer proposed in the 1990s a model where they could rationalize the enantioselective outcome by the two possible modes of coordination in the hydrometalation step of dihydride route, see Fig. 2. Moreover, they proposed that the mode can be directed via the polarization of the C=C double bond of well-chosen substrates. This chapter is a computational backup of their findings. We used the gradient corrected Perdew-Wang (PW91) density functional for all our calculations, which were performed with the ADF package. A charge analysis was performed with the generalized atomic polar tensor (GAPT) method, originally developed by Cioslowski.

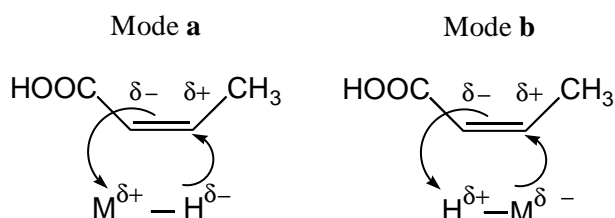


Figure 2: Possible modes of hydrometalation.

The results were divided in three parts. In first instance we looked at the bare hydrido-metal complexes of rhodium and palladium, the most commonly used transition metals in the catalytic hydrogenation, providing us with insight in the electronic properties of the metal-hydride bond. Our results showed that the Rh-H is strongly polarized as $\text{M}^{\delta+}-\text{H}^{\delta-}$, whereas the Pd-H shows the same polarization direction, but substantially less. Next we investigated the properties of four different substrates with the general formula $\text{R}-\text{C}_\alpha(\text{H})=\text{C}_\beta(\text{H})-\text{CH}_3$ where $\text{R}=\text{CH}_3$, COOH, Ph, OCH₃. The charge analysis reproduced the correct C=C bond polarizations as expected from chemical intuition. From these substrates we choose the one with $\text{R}=\text{COOH}$ having a large C=C bond polarization for the further studies, since a large polarization would possibly give a substantial directing effect on the course of the hydrogenation. To this end we computed the reaction pathway of the hydrometalation step for the two possible modes of coordination.

We find that the initial coordination of the activated Rh complex and substrate is more favorably by 5.5 kcal/mol for mode **b**. In contrast, the activation energy for mode **a** is 9.4 kcal/mol lower than for mode **b** due to a favorable charge overlap in the transition state. Somewhat contradictory to the model of Yu and Spencer, these results indicate that substrate coordination will predominantly occur via mode **b**. However, it is evident that the key-factor that lowers the activation energy of the favorable mode of hydrometalation, in this case mode **a**, is the C=C bond polarization. This shows that the concept of bond polarization is a potentially strong enantioselecting tool in the Rh-catalyzed hydrogenation.

In conclusion, for the homogeneous transition metal catalyzed hydrogenation reactions as discussed in this thesis, an atomistic model of the solvent is necessary for a correct reproduction of all the chemical transformations. Our computational study gives furthermore a new perspective of the active role a solvent can have in transition metal catalyzed reactions.

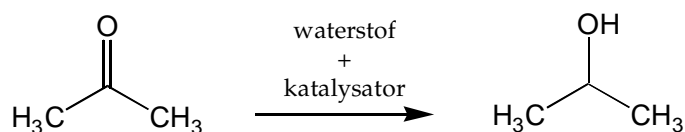
Samenvatting voor Iedereen

De samenvatting in het nederlands is traditioneel vaak de direct vertaling van de engelstalige "Summary". Om toch het werk waaruit dit proefschrift is voortgekomen voor een breder publiek toegankelijk te maken, zal ik hier zoveel mogelijk de computer en chemische terminologie weglaten, niet te gedetailleerd zijn, en (hopelijk) in meer simpele termen de bevindingen van dit werk uitleggen. Graag verwijs ik de lezer met meer expertise in dit veld naar de "Summary".

Dit proefschrift beschrijft een theoretische studie van metaal gekatalyseerde reacties dit met behulp van computer berekeningen. Hierbij is vooral onderzocht wat de invloed van het oplosmiddel is waarin de reactie plaats vindt. Normaal gesproken wordt in een scheikundig laboratorium een reactie gedaan door de reagerende stoffen te mengen, vaak in een oplosmiddel, en eventueel de temperatuur te verhogen. Vervolgens vindt de reactie plaats wat enige tijd kan duren, en uiteindelijk worden (na afkoeling) de producten gescheiden van het oplosmiddel en verder gezuiverd. Nu is het technisch vaak moeilijk om tijdens de reactie te kijken wat er gebeurt. Dit komt omdat belangrijke intermediairen over het algemeen instabiel zijn en dus niet in grote concentraties in oplossing zullen voorkomen. Dit maakt dat deze intermediairen moeilijk te detecteren zijn. Uiteraard heeft men wel een goed idee hoe de reactie zal plaatsvinden en welke producten je kunt verwachten, maar dit doet geen afbreuk aan het feit dat het om fundamentele redenen belangrijk is om precies te weten hoe een reactie verloopt. Een manier om het reactie-verloop in detail te bestuderen is het nabootsen of simuleren van de reactie met behulp van geschikte computer programma's en apparatuur.

De reacties bestudeerd in dit werk zijn zogenaamde hydrogenatie reacties waarbij waterstof reageert met een onverzadigde verbinding tot het verzadigde product. Een voorbeeld is de omzetting van een keton tot een alcohol, zie Figuur 1, waarbij de reactie wordt versneld onder invloed van een geschikte katalysator. Deze katalysatoren hebben meestal als reactief centrum een metaal atoom, net zoals katalysatoren in de levende natuur, *i.e.* enzymen. De belangrijkste toepassing van hydrogenatie reacties in de scheikunde is de synthese van chirale[¶] verbindingen. Voor dit type verbindingen bestaan er twee verschillende ruimtelijke oriëntaties die elkaars spiegelbeeld zijn, en die je net als je linker- en rechterhand niet over elkaar heen kan leggen. Nu gaat het erom om tijdens de synthese slechts één van de twee te synthetiseren. In de levende natuur, waarin enzym reacties zeer selectief kunnen zijn, is dit geen probleem. Dit in tegenstelling tot chirale synthese in het laboratorium wat nogal complex bleek te zijn. Een doorbraak vond plaats in de jaren 70 van de vorige eeuw. In die tijd werd een synthese route ontwikkeld voor L-DOPA, een chirale verbinding die als medicijn kan dienen tegen de ziekte van Parkinson. Dit onderzoek werd in 2001 beloond met de Nobel Prijs voor de Scheikunde. In de afgelopen 30 jaar zijn talloze andere chirale verbindingen gesynthetiseerd in het laboratorium met behulp van hydrogenatie reacties en dit zal door steeds beter synthese methoden alleen nog maar toenemen

[¶]Chiraal is afkomstig van het Griekse *cheir*, hand.



Figuur 1: Schematische voorstelling van de hydrogenatie reactie van aceton tot het corresponderende alcohol.

Computer berekeningen werden tot voor kort hoofdzakelijk gebruikt voor het bestuderen van reacties in de gas fase. Ofschoon dit zeer informatief en nuttig is, kan men zich voorstellen dat dit enigszins naast de werkelijkheid is, gezien het feit dat sterk coördinerende oplosmiddelen wel degelijk een invloed zullen hebben op het reactie-verloop. Een belangrijke rede waarom pas sinds een jaar of tien reacties in het oplosmiddel kunnen worden bestudeerd met behulp van computer simulaties, is omdat daarvoor de computers simpelweg niet snel genoeg waren. Tegenwoordig, met de steeds snellere processors en communicatie, is zo een studie in oplossing wel mogelijk. Desalniettemin zijn het soort berekeningen zoals beschreven in dit proefschrift nog steeds erg tijdrovend; een typische berekening duurt al gauw enkele weken op een aan elkaar geschakelde set van snelle computers. De noodzaak voor zoveel computer kracht is inherent aan de berekening zelf. De krachten tussen de deeltjes worden namelijk berekend via de kwantum mechanica, en wel een speciale vorm van de kwantum mechanica, de dichtheids-functionaal-theorie. Moleculen bestaan uit atomen, en atomen op hun beurt uit kernen en elektronen. De dichtheids-functionaal-theorie beschrijft de eigenschappen van moleculen, of een systeem van moleculen zoals in dit werk. Deze eigenschappen zijn afhankelijk van de dichtheid van de elektronen in het te onderzoeken systeem. In andere woorden: zij worden bepaald door de ruimtelijke verdeling van de elektronen in het systeem. Deze gedetailleerde theorie is nodig voor het simuleren van reacties, waarbij bindingen tussen de atomen worden verbroken en gemaakt.

Zoals de titel van mijn proefschrift zegt, omvat dit onderzoek een computationele studie van de metaal gekatalyseerde hydrogenatie in de gas fase en in oplossing. Meer specifiek heb ik vooral gekeken naar de ruthenium gekatalyseerde transfer hydrogenatie van ketonen, zie Figuur 1. Door de gas-fase reactie te vergelijken met de reactie in oplossing kon er direct worden bepaald wat nu precies de invloed is van het oplosmiddel, in dit de geval het meest simpele alcohol, methyl alcohol. Samengevat werden twee belangrijke verschillen ontdekt tussen de gas-fase reactie en de reactie in oplossing. Ten eerste bevatte het energie profiel in oplossing een plateau halverwege de reactie die er niet is in de gas fase. Dit plateau correspondeert met een kort-levend intermediair wat sterk is gestabiliseerd door waterstofbrug-vormende oplosmiddel moleculen. Ten tweede bleek dat niet alleen het gangbare reactie mechanisme operationeel is, zoals gevonden via gas-fase berekeningen, maar ook een mechanisme waarbij proton^{||} transfers plaatsvinden langs een keten van oplosmiddel moleculen.

Als laatste wil ik iets zeggen over het "fysieke werk" voor de totstandkoming van dit proefschrift. Het komt erop neer dat je letterlijk vier jaar achter een PC zit, waarbij het werk voornamelijk bestaat uit het valideren van de numerieke nauwkeurigheid van de gebruikte computer programma's, het inzetten en controleren van berekeningen en het schrijven van artikelen voor vakbladen. Verder het lezen van vakliteratuur, het discussiëren over je werk met begeleiders en collega's, het gaan naar congressen in het binnen- en buitenland voor het presenteren

^{||}Waterstof atoom zonder elektron.

van je werk, en ook het zelf begeleiden van studenten. En, uiteindelijk dit proefschrift te schrijven en te promoveren. Al met al best leuk denk!

Curriculum Vitae

Jan-Willem Handgraaf was born on 15 June 1976 in Alkmaar, the Netherlands. He grew up in the small village Akersloot, 9 km to the south of Alkmaar, where he went to primary school. After finishing High School in 1994 he went to the Free University in Amsterdam to commence with a study in chemistry. Although halfway he was sure to finish his study doing a major in organic chemistry, some interesting introductory courses in theoretical chemistry made him choose for the latter. There, in the group of Prof. Evert Jan Baerends under supervision of Célia Fonseca Guerra, he compared and qualified methods to calculate atomic charges in molecules. This proved to be only the onset of more extensive studies and after four more years of research performed in the group of Prof. Baerends, finally led to a quite extensive publication, which is to appear shortly. As one can imagine Jan-Willem Handgraaf could not do nothing in the mean time, and hence, after graduating in 1999 he moved to the other university in Amsterdam to start his Ph.D. project in the Computational Physics & Chemistry group of Prof. Berend Smit under supervision of Evert Jan Meijer. In collaboration with Joost Reek from the Homogeneous Catalysis group of the University of Amsterdam he started a computational project investigating homogeneous transition metal catalyzed hydrogenation reactions with the computer, in first instance in the gas phase. After learning about the Car-Parrinello technique to perform first-principles simulations during a CECAM course in Lyon (France) he was able to incorporate solvent molecules implicitly, making it possible to study these type of reactions in solution. As a side-project, in collaboration with Prof. Francesco Zerbetto from the University of Bologna (Italy), he studied the chirality transmission during these reactions. In September 2003 he started as a post-doc in the group of Prof. Zerbetto where he works on something completely different, *i.e.* the interaction between polymers and clay using dissipative particle dynamics computational techniques.

Publications

- Petra, D. G. I.; Reek, J. N. H.; Handgraaf, J.-W.; Meijer, E. J.; Dierkes, P.; Kamer, P. C. J.; Brussee, J.; Schoemaker, H. E.; van Leeuwen, P. W. N. M., "Chiral Induction Effects in Ruthenium(II) Amino Alcohol Catalysed Asymmetric Transfer Hydrogenation of Ketones: An Experimental and Theoretical Approach", *Chem. Eur. J.* **2000**, *6*, 2818-2829.
- Handgraaf, J.-W.; van Erp, T. S.; Meijer, E. J., "Ab initio molecular dynamics study of liquid methanol", *Chem. Phys. Lett.* **2003**, *367*, 617-624.
- Handgraaf, J.-W.; Reek, J. N. H.; Meijer, E. J., "Iridium(I) versus Ruthenium(II). A Computational study on the Transition Metal Catalyzed Transfer Hydrogenation of Ketones", *Organometallics* **2003**, *22*, 3150-3157.
- Guerra, C. F.; Handgraaf, J.-W.; Baerends, E. J.; Bickelhaupt, F. M., "Voronoi Deformation Density (VDD) Charges: A New Scheme for Analyzing the Effect of the Chemical Bond Formation on the Electron Density" (accepted for publication in *Journal of Computational Chemistry*).
- Reek, J. N. H.; Handgraaf, J.-W.; Bellarosa, L.; Zerbetto, F., "In Silico Prove of Chirality Transmission in Ruthenium Catalyzed Transfer Hydrogenation of Acetophenone" (in preparation).
- Handgraaf, J.-W.; Meijer, E. J., "Structural, Dynamic and Electronic Properties of Liquid Methanol from First Principles" (in preparation).
- Handgraaf, J.-W.; Meijer, E. J., "Ab Initio Simulation of Ruthenium Catalyzed Transfer Hydrogenation of Ketones in Methanol Solution" (in preparation).
- Handgraaf, J.-W.; Spencer J. B.; Sprik M.; Yu J.; Meijer E. J., "Directing Rhodium(I) Catalyzed Hydrogenation via the Substrate Polarity. A Computational Study" (in preparation).

Acknowledgments

For the realization of this thesis I am indebted to a great many people. In first instance I would like to thank Berend Smit for giving me the opportunity to start a Ph.D. project in his group. Secondly, I would like to acknowledge my supervisor Evert Jan Meijer for his guidance during the project. Thirdly, I would like to thank all the people who further contributed to the scientific work: Joost Reek for the very useful input concerning the experimental aspects of homogeneous catalysis; Michiel Sprik for getting me involved in the Car-Parrinello technique and giving me the opportunity to visit his group in Cambridge; and Jonathan Spencer and Jinquan Yu for their contribution to the work on the rhodium catalyzed hydrogenation.

Furthermore, I would like to thank Titus van Erp who, practically at the same time as I started his Ph.D. project, also in the field of chemistry in solution. In fact, we were at that time the only two in this field in our group, hence our nickname "the quantum boys". Also I am indebted to Jochem Wichers Hoeth and Gooitzen Zwanenburg for their help in getting me familiar with Linux, which certainly in the beginning of my Ph.D. project was quite a struggle. For discussions about my work many thanks also go to my colleagues at ITS. And of course not only for the discussions, but also for the nice evenings involving Belgian beer and movies. For proofreading parts of the manuscript I would like to thank David Dubbeldam, Abdon Pijpelink and Gadi Rothenberg. Paul Griffiths is acknowledged for corrections to the English. And finally, I would like to thank Saskia, my father, mother and sister for having to put up with me during the writing of this thesis, which was not always easy, I can imagine.